INFORMATION TO USERS

This manuscript has been reproduced from the microfilm master. UMI films the text directly from the original or copy submitted. Thus, some thesis and dissertation copies are in typewriter face, while others may be from any type of computer printer.

The quality of this reproduction is dependent upon the quality of the copy submitted. Broken or indistinct print, colored or poor quality illustrations and photographs, print bleedthrough, substandard margins, and improper alignment can adversely affect reproduction.

In the unlikely event that the author did not send UMI a complete manuscript and there are missing pages, these will be noted. Also, if unauthorized copyright material had to be removed, a note will indicate the deletion.

Oversize materials (e.g., maps, drawings, charts) are reproduced by sectioning the original, beginning at the upper left-hand corner and continuing from left to right in equal sections with small overlaps.

Photographs included in the original manuscript have been reproduced xerographically in this copy. Higher quality 6" x 9" black and white photographic prints are available for any photographs or illustrations appearing in this copy for an additional charge. Contact UMI directly to order.

Bell & Howell Information and Learning
300 North Zeeb Road, Ann Arbor, MI 48106-1346 USA
800-521-0600

Effect of Vacuum Level on the Vacuum-Assisted Resin Transfer Molding Process

Ali Al Omari

A Thesis

in

The Department

of

Mechanical Engineering

Presented in Partial Fulfillment of the Requirements

for the Degree of Master of Applied Science at

Concordia University

Montreal, Quebec, Canada

April 1999

ABSTRACT

Effect of Vacuum Level on the Vacuum-Assisted Resin Transfer Molding Process

Ali Al Omari

Liquid composite molding (LCM) processes have become increasingly popular during the past five decades for the production of complex composite parts. Resin transfer molding (RTM) and structural reaction injection molding (SRIM) are the most widely used LCM processes. These two processes have the potential to become major mass production techniques for manufacturing light weight, high strength polymer composite parts with a complicated geometry.

In the RTM process, two types of flow occur simultaneously, i.e. the macro-flow and the micro-flow. At low flow velocity, the micro-flow is ahead of the macro-flow due to capillary effect. On the other hand, at high flow velocity, the filling process is dominated by the applied pressure, as a result, the macro-flow is ahead of the micro-flow. This flow nature complicates the mold filling process, and may lead to potential problems such as dry spots and voids. Due to the fact that the physical and mechanical properties, as well as the finish of the final product are strongly affected by voids and dry spots, the mold filling stage is one of the key issues in the RTM process.

The influence of vacuum level, fluid type and preform on the mold filling phase of the resin transfer molding process was experimentally investigated for a flat mold with unidirectional flow. Permeability of M8610 mat and woven roving preform was measured using different liquids and vacuum levels. Effects of vacuum levels and liquid type was

studied. The wetting out process of different preforms was experimentally investigated. Finally, experimental verification of a constant inlet-pressure boundary condition scale relation was conducted.

The resin-mat system clearly showed the effect of macro-flow and micro-flow competition on the preform wet-out. Experimental results revealed that an average dimensionless pressure difference $\left(\frac{\Delta P_{avg.}}{\frac{1}{2}\rho \overline{V}^2} \right)$ of about (1×10^9) was required to get good wet-out in the resin-mat system in the Reynolds number range of ($0.06 \leq Re \leq 0.11$).

The constant inlet-pressure scale relation was experimentally verified. Effect of the vacuum level, fluid type and preform on the measured permeabilities of OCF-M8610 fiberglass mat and Bay Mills style 302 woven roving fiberglass was discussed. Finally, general observations noticed during experiments were reported and discussed.

ACKNOWLEDGMENTS

I would like to thank my supervisors, Professor S.V. Hoa and Dr. X.R Xiao for their guidance and support during the course of this study. Special thanks to Professor Hoa for his fruitful suggestions and feedback during thesis writing stage. The financial support of CIDA/JUST/Concordia program is gratefully acknowledged. The help and kindness of Mr. John Elliott during the experimental part is highly appreciated.

I'm so grateful to my parents for their love, concern, encouragement and support through out my thesis stages. I'm deeply indebted to my wife and my daughter for their love, patience and support; without which I could not have finished this work. I would like to express my appreciation to my sisters and brothers for their love, concern and continuous encouragement. Finally, I would like to thank many true friends for their concern and support.

To my parents,

my wife Khuloud,

my little daughter Tuga,

and my sisters and brothers

TABLE OF CONTENTS

LIST OF FIGURES

LIST OF TABLES

LIST OF SYMBOLS

A	specimen cross-sectional area
g	gravity acceleration
H	fluid height
K	permeability
$K_{avg.}$	Preform average permeability
K_{ij}	permeability tensor
$(K_t)_i$	transient permeability at time (t_i)
ℓ	characteristic length of the mold
L	the specimen (preform) length in the streamwise direction
L_d	preform length obtained from the flow front profiles drawing
L_i	location of the flow front at time (T_i or t_i)
L_{i-1}	location of the flow front at time (T_{i-1})
L_{T1}	location of pressure transducer #1
m_f	preform mass
P	pressure
P_O	fluid inlet pressure
$P_{VAC.}$	vacuum pressure used
P_{1i}	pressure transducer #1 reading at time (t_i)
P_{2i}	pressure transducer #2 reading at time (t_i)
ΔP	the pressure difference over the specimen
$\Delta P_{avg.}$	The average pressure difference required to get good wet-out

$\frac{\partial P}{\partial x}, \frac{\partial P}{\partial y}, \frac{\partial P}{\partial z}$	pressure gradient in x,y,z directions, respectively
$\frac{dP}{dx}$	pressure gradient in the fluid flow direction in unidirectional flow
q	fluid velocity
$\overline{q}_i$	average velocity in the time interval (i)
$q(t)$	flow front velocity at time (t)
Q	volumetric flow rate
Re	Reynolds number
S_F	scale factor
t	time
t_i	time at which transient permeability is being calculated
t_f	lead final thickness
$T_{filling}$	filling time
T_i	time at the end of the time interval (i)
T_{i-1}	time at the beginning of the time interval (i)
t_{T1}	time at which flow front reaches pressure transducer #1
t_{T2}	time at which flow front reaches pressure transducer #2
u, v, w	fluid average velocities in x,y,z directions, respectively
V_f	fiber volume fraction
V_T	cavity total volume
$\overline{V}$	average filling velocity
W	preform width

μ	fluid viscosity
ρ	fluid mass density
ρ_f	preform mass density
θ	contact angle between liquid and solid

CHAPTER 1

INTRODUCTION

1.1 General

Liquid composite molding (LCM) processes have become increasingly popular during the past fifteen years for the production of complex composite parts. Once used primarily by the commodities industry to make parts ranging from bath tubs to computer housings, these processes have evolved and are currently being investigated for use in the fabrication of structural parts for automobiles and commercial and military aircrafts. The two most widely used LCM processes are resin transfer molding (RTM) and structural reaction injection molding (SRIM). These two processes have the potential to become major mass production techniques for manufacturing light weight, high strength polymer composite parts with a complicated geometry. RTM resins are pumped into the mold at a much slower rate than SRIM resins due to their higher viscosities and lower reactivities. The mold filling pressure of RTM is often several times less than that of SRIM in the industry. Since our work is closer to the RTM process regarding the fluid viscosities and the mold filling pressure, this process is explained in details in the following sections.

The resin transfer molding (RTM) process has many advantages over other composite manufacturing processes such as hand lay up, spray up, and autoclave. Some of the RTM advantages are:

- Design flexibility.
- Low start up cost.
- Faster than conventional techniques.
- High quality surface finish.
- Very tight dimensional tolerances.
- Lower labor cost/part than other processes.
- Low wastage.
- Excellent part reproducibility.
- Possibility of adding filler additives to get better properties.
- Higher fiber volume fraction.
- Better environmental compliance than hand lay up and spray up techniques

1.2 Overview of the Resin Transfer Molding Process

The RTM process generally includes four phases. The first phase is *fiber preforming*, in which reinforcing fibers are arranged and combined (possibly with inserts and cores) into a skeleton of the actual part in order to satisfy microstructural and geometric requirements. The preform is then loaded into the mold and the mold is closed. The second phase, *mold filling*, begins when the mold is closed and the resin enters the mold cavity through one or several injection ports. This resin should impregnate the

preform thoroughly, while the air is expelled through properly positioned air vents. Once the mold is filled by the resin, the phase of *curing* starts. Ideally, this phase should not start before completely filling the mold cavity. *Part removal* is the final phase that takes place after the curing phase. The RTM process is illustrated in Figure 1.1.

During the mold filing process, resin is forced to flow into the pore spaces among the filaments of a fiber tow (the micropores), and the pore spaces formed between the fiber tows (the macropores). At a macroscopic level, the impregnation of the fiber tows by the resin is usually modeled as a flow through a porous medium. This flow is governed by Darcy's law, which states that the volumetric flow rate (Q) through a constant area specimen is proportional to the cross section area (A), and the pressure difference over the specimen (ΔP); and inversely proportional to the length of the specimen in the streamwise direction (L) and the fluid viscosity (μ):

$$Q = -K\frac{A}{\mu}\frac{\Delta P}{L} \tag{1.1}$$

Darcy's law can be generalized and written in three-dimensional form to represent the actual state in the mold filling process of the anisotropic porous media used in the manufacturing of composite materials. Darcy's law can be written in a matrix form as:

$$\begin{pmatrix} u \\ v \\ w \end{pmatrix} = -\frac{1}{\mu}\begin{pmatrix} K_{xx} & K_{xy} & K_{xz} \\ K_{yx} & K_{yy} & K_{yz} \\ K_{zx} & K_{zy} & K_{zz} \end{pmatrix}\begin{pmatrix} \frac{\partial P}{\partial x} \\ \frac{\partial P}{\partial y} \\ \frac{\partial P}{\partial z} \end{pmatrix} \tag{1.2}$$

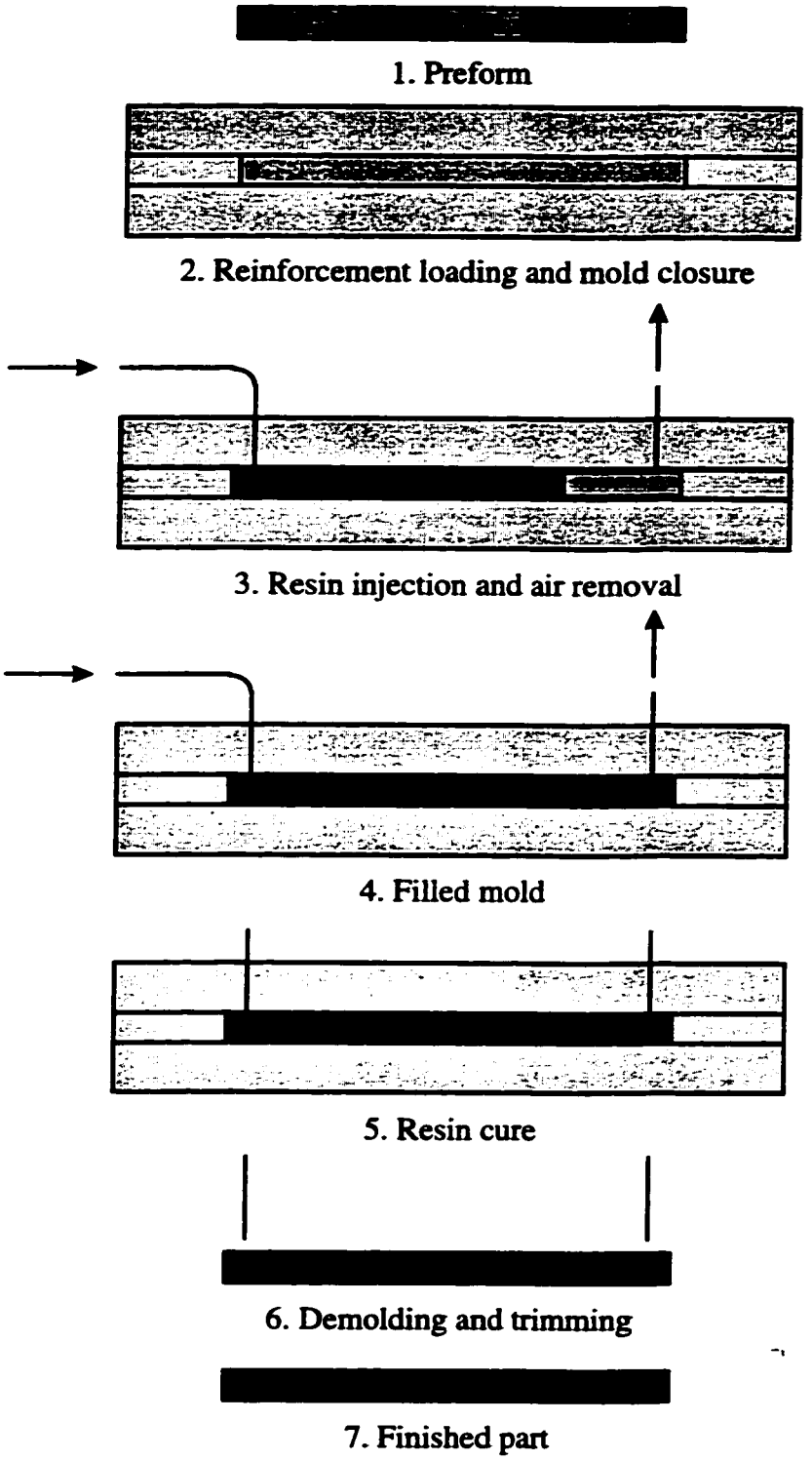

Fig. 1.1 - Schematic diagram of the RTM process

where:

$u, v, w =$ fluid average velocities in x, y, z directions, respectively.

$\mu =$ the fluid viscocity.

$K_{ij} =$ the permeability tensor.

$\frac{\partial P}{\partial x}, \frac{\partial P}{\partial y}, \frac{\partial P}{\partial z} =$ pressure gradients in x, y, z directions, respectively.

Since most mold filling processes in anisotropic porous media deal with parts which have a shell-like geometry (i.e. the thickness being smaller than the other dimensions of the part), this allows us to ignore the flow in the thickness direction and model the flow using the two-dimensional form of the Darcy's model. As the edge injection strategy was used in our experimental work, and the thickness dimension is much less than the other two dimensions; the one-dimensional form of the Darcy's law is used to model the filling process. The Darcy's one-dimensional model is given as:

$$q = -\frac{K}{\mu}\frac{dP}{dx} \tag{1.3}$$

where:

$q =$ the fluid velocity (m / s)

$K =$ the permeability of the porous medium (m^2)

$\mu =$ the fluid viscosity (Pa_s)

$\frac{dP}{dx} =$ the pressure gradient (Pa / m)

Due to the fact that the mold filling process has two distinct scales: microscopic and macroscopic, the nonuniformity of macro-flow and micro-flow is believed to be the main reason for void formation. The physical and mechanical properties as well as the finish of the product are strongly affected by the presence of voids, as a result, this problem is the most crucial one in the RTM process. The manufacturing of high-

performance, low void content parts depends on both the infusion of resin into the preform, and the adhesion between the resin and the fibers. The infusion process is complicated by the microflow. On the other hand, the mechanism of adhesion is complex and depends largely on the chemical composition of the fiber and resin, including any sizing used to enhance bonding. However, wetting of the fiber surface by the resin is a prerequisite for good adhesion because of the short-range nature of inter-molecular forces.

Whereas Darcy's law can describe the global resin front movement through the fiber preform, it does not provide the detailed information of the microflow inside the fiber tows themselves. The microflow is driven by both the injection pressure and the capillary force, while the macroflow is only driven by the injection pressure. This is due to the fact that the capillary force in the macropores can be neglected compared to that in the micropores because of the macropore large size. As a result, the capillary pressure should be taken into consideration when studying the microflow part.

The natural wet-out of an arbitrary surface by any liquid occurs only if the contact angle between the surface and the contacting liquid is less than 90°. Assume that a liquid is radially approaching a tow of fibers [1], at the point of first contact the contact is tangential between fibers. As the liquid wets the fibers a concave meniscus is formed and the wetting front starts to move inward to minimize the surface energy. The liquid continues to move inward until the equilibrium is achieved and no pressure differential exists across the liquid surface, at which the flow ceases. This process is illustrated in Figure (1.2) below. The only way natural wetting can continue is if the liquid front touches another fiber prior to reaching the equilibrium position. It is to be expected that in

organized reinforcements there will be regions that are naturally wet-out by the radial flow in the absence of any external pressure. On the other hand, other areas in the tow require additional driving pressures to permit full wet-out.

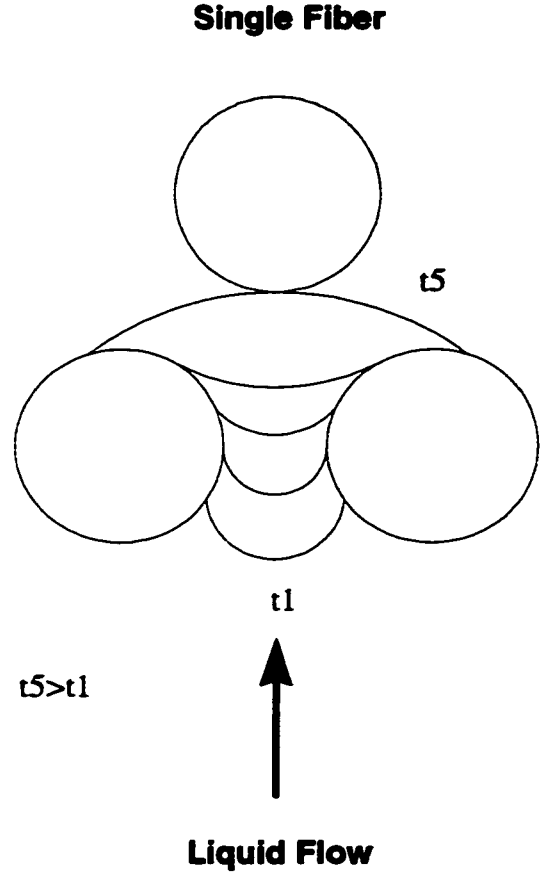

Figure 1.2 - Stages in the wetting-out process of a bundle of fibers by capillary action.

1.3 Materials for RTM Composites

1.3.1 Resins

A resin system selection is primarily based on the performance requirements of the product. In general, resin systems that are most suitable for the RTM process have a long pot life (at least 2 hours), low viscosity at the temperature used to transfer the resin (1000 mPa.s or less), a short gel time at the curing temperature (less than 1 hour), and low levels of out gases and volatiles. A long pot life allows the resin system to completely fill large complex parts with high fiber volume fraction before gelation. The low viscosity is desirable because it permits the liquid to fill all areas of the mold. Moreover, good fiber wet-out can be achieved at low resin viscosity. Finally, low outgassing and volatility help minimize void formation in the product. Commonly used RTM resins are: polyesters, vinylesters, phenolics, methacrylate, and epoxy.

Resin modifiers are added to the resin for many purposes, some of which are: decreasing the cost, preventing problems of shrinkage in curing of the resins, imparting flame retardance, giving a particular color to the product, inhibiting the curing of the resin, and accelerating the curing of the resin. Calcium carbonate, clay, glass microspheres, talc, and alumina trihydrate are some powdered inorganic materials which are commonly used fillers. The main purpose for adding these fillers to resin is to lower the cost since the fillers are much cheaper than resins and reinforcements. Some fillers are called *low-profile additives*, and they are used to help prevent shrinkage in curing of resins. They are very important in polyester resin formulations. Other fillers may impart flame retardation, especially if they contain water molecules (hydrated), chlorine, bromine, or iodine. However, fillers may affect the resin's ability to transfer forces to the

reinforcements. So, fillers are avoided in high-performance applications. Colorants, pigments, and dyes may be added to most resin systems. These colorants do not appreciably affect the composite's properties since they are added in small amounts. Some pigments, such as carbon black and titanium dioxide, absorb ultraviolet light and prevent or reduce ultra-violet degradation of the resin. On the other hand, some colorants are sensitive to environmental factors and change colors or otherwise breakdown, which decreases the composite's resistance to the environment. Also colorants often affect the cure rate.

Other non-filler materials, that are added in small concentrations, include: inhibitors (which are used to extend shelf life), accelerators(which are used to speed up the cure of the resin system), ultra-violet light absorbers, and flame retardant additives. These non-filler materials have minor effects on the composite's properties.

1.3.2 Reinforcements

Reinforcements for composites can be fibers, particles, whiskers. Each type has its own applications. The most common reinforcements are fibers, which have the most influence on composite's properties. Fibers are available in many oriented forms such as strand, tow, roving, tape, yarn, woven fabric, braiding and mat.

The predominant fiber materials are glass, graphite, boron, aramid, and ceramic, the first two being the most common. Graphite provides the best property performance with respect to its weight, and used in applications such as aerospace parts, in which reduced weight and high performance are dominant factors. However, it is more costly

than glass and aramid. Glass is often used in parts with lower cost and property performance requirements, such as automobile, industrial, and consumer products.

1.4 Process Variables in RTM

The Resin Transfer Molding process involves many variables that are linked to the design of the part produced, the selection of the constituent materials, and the design of the mold and molding process. Some of these variables are interdependent and some have more marked effects than others. The major process variables that may affect the RTM process include:

- Reinforcement used (type of cloth and fiber, surface treatment, orientation, ply stack sequence, temperature, and fiber volume fraction).
- Resin characteristics (viscosity and reaction kinetics).
- Mold geometry, thermal characteristics and temperature.
- Injection pressure.
- Mold cavity evacuation (vacuum assistance).
- Ambient conditions.

The effect of process variables on the filling process can be studied by monitoring the progression of the flow front. Optimization of parameters such as injection pressure, flow rate, gate locations, preform lay up, etc. may be done by monitoring the filling process to achieve acceptable flow pattern, so that problems such as dry spots and void formation can be avoided or at least reduced.

CHAPTER 2

LITERATURE REVIEW

2.1 Introduction

The flow of viscous fluids through porous media has been studied for more than a century. This problem has been studied by those interested in geological problems [2,3], heat transfer [4], and composite manufacturing [8,12,13,15-21]. Porous media are generally used as reinforcing materials, filters, and a way to improve heat transfer. Each application involves different combinations of fiber diameter, fiber volume fraction, and Reynolds number. Composites typically consist of fibers with diameters at the order of microns, with dense fiber volume fractions ranging from 40% to 70%, and creeping flows, i.e., Re less than 0.1 [5]. Henry Darcy (1856) studied the horizontal flow of an incompressible Newtonian fluid through a porous medium, and assumed that the flow rate of Newtonian fluids through saturated porous media is proportional to the pressure drop across the medium. The constant of proportionality is a function of the permeability of the porous medium. Researchers in the geological field have extended Darcy's law to two and three dimensional cases, that relate the fluid velocity to the pressure gradient in

the direction of the flow. Recently, this law has been adopted for processing of composite materials.

Resin Transfer Molding (RTM) is one of the newly developed processes used in manufacturing composite parts and structures. RTM has always offered the potential for improving quality of a part as well as constructing parts with more complexity. RTM is currently being used to manufacture complex tubular shapes, truck parts, components in the recreation industry, automotive, aerospace, medical field, industrial as well as a wide range of other components for the FRP industry.

In the resin transfer molding (RTM) manufacturing process, two types of flow occur simultaneously, i.e., the micro-flow and the macro-flow. The macro-flow of the mold filling involves distribution of the fluid through the mold cavity, and the micro-flow involves penetration of the resin into fiber bundles. Whereas, the macro-flow is between the fiber bundles, the micro-flow is among the fibers in the bundles. This flow nature complicates the mold filling process, and may lead to potential problems such as dry spots and voids. As a result the mold filling stage is one of the key issues in the RTM process. Experimental study of the mold filling in RTM process has been performed by many investigators for different purposes, some of which are: introducing and verification of a new sensing technique, permeability measurement, experimental verification of a numerical simulation of the mold filling process, and experimental study of the process variables in the RTM process.

2.2 Introducing and Verification of a New Sensing Technique

Several sensing techniques have been utilized in the molding process. The sensors used in these sensing techniques are classified into two categories: embedded and non-embedded sensors.

2.2.1 Embedded sensing techniques:

Embedded sensing techniques utilize sensors which are located within the mold structure. These sensors are used to monitor flow front movement, pressure distribution, and resin cure kinetics through the mold cavity. Pressure sensors, such as pressure transducers, have been used to determine pressure distribution during molding as well as temporal flow front location. Resulting pressure profiles have been utilized for the determination of the embedded fibrous preforms permeabilities.

Diallo, et al. [6] proposed a technique for the observation of flow front into multilayer glass fiber preforms. The technique uses electrical wires placed between the layers to detect the arrival of the aqueous corn syrup solution used in their experiments to fill the cavity. As the aqueous corn syrup arrives at each wire end, the electrical contact is established through the liquid and the computer records this status through digital based logic (a value 0 is recorded if no fluid is detected and the value switches to 1 when fluid is detected). The fluid is recorded as well as the time to provide the flow front location and velocity. Time associated to a recorded position is obtained by using the system clock of the computer. This technique is called the electrical conductivity technique. They used this technique to investigate the effect of the through-thickness inhomogeneities on the flow front profile in the thickness direction. They found that this technique is elegant for

investigating the impregnation of multi-layers with variable in-plane porosity, and it is well adapted for thick parts.

Kikuchi, et al. [7] investigated the embedded electronic flow sensors technique that has been proposed and initially investigated by Walsh at the U.S. Army Materials Technology Laboratory. This technique was found to be applicable for the monitoring of fluid flow propagation during relatively slow molding processes, such as resin transfer molding and slow injection molding. The embedded electronic sensors concept is based on the positioning of electrically conductive wires within the mold cavity to form an orthogonal grid pattern with non intersecting grid junctions. The region between adjacent grid layers is a sensing gap. Initially all the electrical circuits are opened since there is no fluid with some degree of conductivity inside the mold cavity to complete them. When the fluid enters the sensing gap, electrical circuits are completed by the addition of the finite electrical resistance associated with the fluid. Temporal fluid flow propagation can be monitored by monitoring the resistance at each of the sensing gaps within the mold cavity. Furthermore, since the fluid resistivity changes with the fluid rheological state , temporal fluid rheological properties, such as viscosity and degree of cure, can also be monitored using this technique.

Kranbuehl, et al. [8,9] used dielectric sensors to monitor flow and cure processes. Dielectric sensors have been used to monitor molding process. These sensors are based on resin dielectric properties that change with viscosity and/or degree of cure. Dielectric sensors have been used to monitor cure and flow processes through measured local changes in resin capacitance. These changes in resin capacitance are due to changes in stored electrical charges in the material during processing.

Weitzenbock, et al. [10] addressed the problem of fluid flow through thick stacks of reinforcement material in RTM process. They introduced the thermistor method to detect the flow front position within the cavity. They outlined the thermistor concept and its experimental verification for measurement of the flow front within a stack of fiber mats. Thermistors are sufficiently robust, available in very small sizes (1.5 mm in diameter) and produce distinctly different signals under heat and when cooled by the advancing flow. The thermistors are initially heated with a power input of about 20 mW each. This is enough to raise the surface temperature sufficiently to experience a large enough temperature and resistance change to give a distinct voltage jump when the fluid reaches the thermistor. The heated thermistor has no noticeable influence on the surrounding fluid. Calculations have shown that the heated zone is in the range of a few μm. To detect the flow front, thermistors are placed at different locations through the depth and width of the mold lay-up. Experiments were carried out to assess the reliability and accuracy of the flow measurement technique, the results were quite encouraging.

Trochu, et al. [11] suggested a method that allows the measurement of the flow front position at selected points within the cavity of the mold. This method employs thermistors to detect when the flow front has reached a location of interest. They used this method to detect the shape of the flow front in the thickness direction.

Ahn, et al. [12] described an experimental technique for detecting the position of the fluid front inside the cavity of the mold. This technique utilizes embedded optical fibers. This is accomplished by removing short segments (<2mm) of the cladding from the optical fiber. The optical fiber containing several such bare spots is embedded inside the preform. Laser light is transmitted through the optical fiber, and the light intensity at

the end of the optical fiber is recorded. When the fluid reaches a bare spot, there is a significant and sudden drop in the transmitted light intensity. From the observed changes in the light intensity, the rate of fluid front movement can be deduced. By embedding a three-dimensional fiber optic sensor grid through the preform, the three-dimensional flow of the fluid can be monitored. The validity of this technique was checked out by comparing its results with a flow visualization technique results, and good agreement was found between the results of these techniques.

Frequency dependent electromagnetic sensors (FDEMS) are more recently developed sensors applied to molding process. FDEMS technique has been used by many investigators, some of them are: Kranbuehl, et al. [13,14], Hart, et al. [15], Loos, et al. [16], and others. Loos, et al. [16] found that the FDEMS technique is capable of monitoring fluid flow front propagation during injection process along with the changes in fluid properties during the cure cycle. FDEMS has been used to monitor the molecular activity of the fluid flow through detecting the change in the fluid electrical capacitance, conductance, dipolar relaxation time and permittivity. By measuring both the capacitance and conductance of the fluid, fluid permittivity can be calculated. Fluid ionic mobility or conductivity as well as the fluid dipolar relaxation time may be then determined using the fluid permittivity value. Fluid conductivity and fluid dipolar relaxation time are related to the fluid viscosity, reaction rate, and degree of cure at a given time and location within the mold cavity. Flow front movement may be monitored with FDEMS sensors by noting when initial and dramatic changes in fluid conductivity occur.

2.2.2 Non-embedded sensing techniques:

The earliest type of non-embedded sensing technique applied to molding process utilized video-camera monitoring and recording of fluid flow front propagation within transparent molds. Bruschke, M., and Advani, S. [17] used a video-camera visualization technique to verify their proposed numerical simulation model that was based on the finite element/control volume method. Their model was proposed to predict the flow of a viscous fluid through a fiber network. Experiments were performed in a flat rectangular mold using a Newtonian fluid. They found that their model was able to predict flow front movement in relatively complex geometries in anisotropic media. Pollard, M., [18] used a glass-top mold to visualize the flow of the liquid through various fiber mats, and to determine the corresponding permeabilities. Flow profiles were videotaped using a video-camera. Their experiments indicated that the same resin and processing conditions that will be used to fabricate the composite should be utilized for the permeability measurement experiments. Trochu, et al. [19] developed a numerical model based on nonconforming finite elements to simulate the resin transfer molding process. This model was verified by comparing the calculated solutions with experimental data obtained by monitoring the resin front progression through the transparent cover of the mold and recording it on a videotape. Gauvin, R., and Trochu, F. [20] compared the resin front positions and pressure distributions obtained with the computer program of Li and Gauvin [21] with experimental results on mold filling. The resin front progression was observed through the transparent cover of the mold , and the experiments were recorded on a videotape. Chan, et al. [22] developed a procedure for determining the general anisotropic in-plane permeability of fiber preforms from constant flow rate mold filling

experiments. The procedure was based on the application of Darcy's law to a two-dimensional in-plane flow situation. The changes in flow front position and inlet pressure with mold filling time were experimentally obtained, and the in-plane permeabilities were calculated using parameters obtained from two linear plots. The flow front position is recorded through a clear polycarbonate mold by a video recording system with built-in timer. Loos, et al. [16] developed a simulation model that can be used to simulate the infiltration of resin into a fibrous preform. They verified their model by conducting flow visualization tests in a transparent mold using a video-camera. Ahn, et al. [12] measured the in-plane principal permeabilities of a woven fabric and chopped strand mat by monitoring the in-plane spread of the corn oil with a video-camera. Gauvin, et al. [23] used a digital camera to record the flow front shape and successive positions for a permeability measurement and a mold filling model verification.

A similar approach using a photo camera to follow the progress of the fluid permeating the preform was employed by Lekakou, et al. [24]. In their experiments the progress of the flow front of the permeating fluid at the top the mold was tracked with a 35 mm camera fitted with a wide-angle lens. The camera was mounted on a tripod and placed directly above the mold assembly. Two techniques of measuring the in-plane permeability of the reinforcement were considered by those investigators. The first one involves rectilinear flow of a model fluid, whereas the second technique involves radial flow of the fluid injected from a central gate. By measuring the orientation and value of the major and minor axes of the progressing elliptical flow front from the camera photos, the direction and value of the principal permeabilities of the textile could be derived simultaneously. Um, M., and Lee, W. [25] carried out an experimental verification for a

numerical simulation model. They performed mold filling tests to evaluate the validity of the numerical results. Pictures of the fluid flow front were taken with a camera at an arbitrary time interval, so as to obtain the location of the fluid flow front at each time step.

Video-camera monitoring technique is more efficient than just using a photo camera, since the video-camera provides a continuous recording for the whole filling process. In the work done so far, all the investigators used a visualization technique to monitor in-plane propagation of fluid flow front through rectangular transparent molds. Investigators deal with such case as a two dimensional problem assuming that the thickness is too small with respect to other dimensions. Although few investigators studied the case of rectangular cavities with obstacles [7,12,13], the problem was dealt with as a two-dimensional case.

2.3 Permeability Studies

Darcy's law is the most commonly used model for flow prediction through porous media. Since the permeability value is needed for accurate prediction of the flow behaviour during the filling process, the permeability of the preform is an important consideration in the design of the RTM process. Most commercial preforms, such as fabrics and mats, are planar in form; and therefore the permeability for such preforms is characterized by an in-plane permeability tensor (i.e., second order tensor), and a first order tensor which is in the direction normal to the preform plane. Practically investigators deal with the preform as a two-dimensional case, assuming that the preform thickness is too small with respect to the other dimensions. The components of the second

order permeability tensor may be obtained from in-plane radial flow experiments using the two-dimensional form of Darcy's law. There is, however, scarcity of through-thickness permeability measurement studies.

Pollard, M. [18] measured the permeabilities of various fiber mats using the visualization technique. Fiber mat permeabilities were found to be sensitive to Reynolds number and fluid used as well as porosity, fiber weave and preforming technique. They recommended that permeability experiments should be performed at the processing conditions that will be used to fabricate the composite, and if possible, with the same resin rather than an oil.

Chan, et al. [22] also used the visualization technique to determine the in-plane permeabilities of different fiber preforms from constant flow rate mold filling experiments . Their procedure was based on the application of Darcy's law to a two-dimensional in-plane flow situation, and experimental data on changes in flow front position and inlet pressure with mold filling time. Experimental data for a commercial fabric confirmed the applicability of their procedure.

Lekakou, et al. [24] measured the in-plane permeability of the preform using two techniques. The first one involves rectilinear flow of a liquid, whereas the second involves radial flow of a liquid injected from a central gate. They found that the permeability of the woven cloths is sensitive to porosity, speed of permeation and state of wetting of cloths. Small variation in preform compression was found to have a significant change in the measured permeability. As a result, the measurement of the degree of compression of fibrous preforms during the processing of composites is absolutely essential in the determination of permeability. The dependence of the apparent

permeability on the permeation speed caused discrepancies between permeability measurements obtained from rectilinear and radial flow mode experiments. Somehow, wet clothes were found to have a higher permeability than dry ones.

Ahn, et al. [12] presented an experimental technique that can be used to measure the three principal permeabilities of fiber preforms made of continuous or short fibers. This technique utilizes embedded optical fibers to detect the fluid flow front through the preform. Using the point injection strategy, expressions were derived for calculating the permeabilities from the three-dimensional measurement of the liquid flow front. Good agreement between embedded fiber optic technique results and those obtained using pressure drop and flow visualization techniques were found.

Wu, et al. [26] measured the trans-plane fluid permeability of various fiber reinforcements using the unidirectional flow method, from which the measured injection pressure and flow rate together with a one-dimensional Darcy's law were used to calculate the trans-plane permeability.

2.4 Experimental Verification of Numerical Simulation

The analysis of fluid flow in the mold cavity is a very important task in designing the RTM process. Numerical analysis of mold filling process in the RTM process has been performed by many investigators. Several numerical methods have been developed for the simulation of the resin flow.

Trochu, et al. [19] developed a computer program based on non-confirming finite elements that can follow the successive positions of the resin front through orthotropic preforms and inside molds of arbitrary shape. They used the visualization technique to

verify their numerical model of the mold filling process. They found good agreement between calculated and experimental flow fronts.

Um, M., and Lee, W. [25] performed a numerical simulation of the mold filling process during RTM using the boundary element method (BEM). They verified their method by comparing their numerical results with the experiment results obtained from observing the filling process visually using a camera. They found excellent agreement between the calculation and their experiments.

Bruschke, M., and Advani, S. [17] presented a numerical simulation to predict the flow of a viscous fluid through a fiber network. This simulation was based on the finite element/ control volume method. The visualization technique was used to verify their numerical simulation. They noticed that although they were able to predict flow front movement in relatively complex geometry shapes in an isotropic media, they should further understand the interactions between the fluid and the porous medium.

2.5 Molding Process Variables Investigations:

The major factors that may affect the molding process include resin characteristics (viscosity and reaction kinetics), reinforcements (its type, orientation, surface treatment, ply stacking sequence, volume fraction), mold (its geometry, thermal characteristics and temperature), injection pressure, mold cavity evacuation (vacuum assistance), and ambient conditions. Some of these factors are interdependent and some have more obvious effects than others.

Rudd, et al. [27] carried a theoretical and experimental study of the effect of several of the process variables on the cycle times achieved in a plaque molding facility.

Fiber volume fraction, injection pressure, resin preheat and preform preheat were examined in their work. Their investigation was based on the use of heated molds and hot setting polyester resins, a combination which has been demonstrated to possess good potential for the achievement of short cycle times, owing to the reduction of resin viscosity and reduced fill times. The fiber volume fraction of the molding has a very important effect on the mechanical properties of the final part. However, changes in the fiber volume fraction can also have an influence on the molding process. It was found that the cavity fill time reduces significantly as the fiber volume fraction reduces owing to the higher permeability of the preform at the reduced fiber volume fraction. The choice of injection pressure is a matter for debate among investigators. Whereas some investigators prefer using low injection pressures to improve the process of wetting out the fibers by the fluid, others prefer high injection pressures to expel trapped air. Neither of these points of view appears to be backed by experimental data. Rudd found that the resin supply pressure affects the cavity fill time to a greater extent than the overall cycle time. The resin preheat temperature was varied in their work using a heater jacket fitted to the resin pot with on/off control. Moldings were produced at resin preheat temperatures of 20°C and 55°C. The use of a preheated resin system was found to be beneficial in reducing the overall cycle time, although the effect was shown to be not significant as that of preform preheat.

Stabler et al. [28] studied the effects of the injection pressure, the filling time, the initial bubble content of the resin, the vibration frequency of the mold during filling, and the application and the amount of mold releasing agent on void formation. They found that injection pressure and filling time did not affect void formation, whereas good

surface waxing, low initial bubble content, and vibration at 10Hz reduced voids significantly.

The influence of vacuum on the quality of RTM laminates has raised a lot of interest recently. Lundstrom, et al. [29] studied the influence of vacuum assistance on the void formation in RTM. They conducted their experiments in a flat mold with edge injection (unidirectional flow from one side to the other) in which the vacuum level could be varied from atmospheric pressure to about 1 kPa. The void volume fraction was determined with optical microscopy and image analysis. It was found that the most of the voids were concentrated at a small area close to the flow front. The void content and the size of the region with voids were also found to decrease with increasing vacuum. A simple theory based on the ideal gas law was suggested to explain the positive influence of the vacuum.

Hayward, J. and Harris, B. [30] discussed the effects of four of the major process variables in the production of GRP moldings. The variation in resin injection pressure, mold temperature, resin viscosity and the use of vacuum assistance were discussed. They found that mechanical properties and porosity levels of moldings had been improved significantly with vacuum assistance, compared with those moldings produced without vacuum. It was noticed that regardless of the reinforcement type (i.e., woven or non-woven), resin type and viscosity; vacuum assistance greatly improved the wetting of the fibers within a molding, giving plates a semi-transparent appearance. The effect of vacuum assistance was found not to be equivalent to an increase in resin injection pressure. The improvement in appearance was noticed to be coupled with an improvement in mechanical properties. A marked improvement in the strengths of the

plates molded with vacuum assistance was noticed from tension, flexural and short-beam shear tests. Image analysis of the microstructure of the test plates showed that there was a substantial reduction in porosity. The mean levels of porosity were found to be 0.15% for the plates molded with vacuum assistance, whereas the porosity levels was found to be 1% for the plates molded without the vacuum assistance. A marked trend for the porosity level to increase towards the plate edges when no vacuum is applied was noticed, while the porosity is uniformly distributed when the vacuum is used. It was found that as the porosity level increases the strength of the piate decreases. Variations in injection pressure was found to have no effect on the quality of moldings. Mold temperature variation was noticed to have no effect on the quality of the moldings other than by way of resin cure differences. No resin viscosity was found to be ideal for all RTM operations. A wide range of resin viscosity (100 mPa.s to 3500 mPa.s) was successfully used. Selection of a suitable resin viscosity for a particular molding was found to be dependent on the fiber volume fraction.

Lundstrom, et al. [31] extended their investigation started in [29] to include several new processing variables. They conducted their experimental work using the same mold and injection strategy used in their last study. The voids were found concentrated in a narrow region close to the ventilation side of the mold. Void volume fraction in this region was almost constant and dropped over a short distance to basically no voids in the rest of the laminate. The vacuum assistance technique was found to be beneficial both for the magnitude of the void content and for the extent of the void region. They found that the void content with the highest vacuum level (about 1kPa absolute pressure) was practically negligible. Increasing the cure pressure and the flushing time was found to be

beneficial in getting lower void content. On the other hand, increasing the processing temperature gave a higher total void content.

Vacuum studies, done so far, examined the effect of vacuum on the RTM process by applying a vacuum pressure to a mold cavity being filled by positive pressure injection. In this work, the effect of vacuum assistance was studied by filling the mold cavity using vacuum pressure only, rather than using a combination of positive and vacuum pressure filling.

2.6 Scale Relations for Mold Filling Simulation in RTM

The use of models to facilitate design and testing of engineering systems is often very beneficial. Experimentation on models which are correctly designed, constructed and used can significantly reduce the likelihood of committing costly mistakes. Filling process in resin transfer molding, like other types of fluid flow, may be experimentally simulated using small scale model tests. Scale relations of the RTM mold filling process under isothermal conditions were derived by Xiao, et al. [32] for constant inlet resin flow rate boundary conditions. They verified their scale relations by scale experiments and by simplified mold filling simulation developed by Cai [33]. They also derived a scale relations for constant inlet pressure boundary condition from Cai's approach. Whereas the constant inlet resin flow rate scale relations were verified experimentally and analytically, the constant inlet pressure scale relations have not yet been experimentally verified. As a result, an experimental verification of these scale relations was one of the main objectives of conducting this work.

2.7 Scope and Objectives of the Present Work

Resin Transfer Molding is one of a family of processes which includes simple gravity or vacuum impregnation and structural reaction injection molding. The feature that is shared by each process in this family is the introduction of a liquid resin into a closed mold under forcing pressure gradient. The applied pressure difference may be created by applying a vacuum to the mold (vacuum impregnation), an external source at elevated pressure such as gravity feed or more usually a positive displacement pump or pressure vessel. Most of the work done so far utilized a positive displacement pump or pressure vessel to create the forcing pressure gradient. The vacuum impregnation technique with gravity feed was used in this work.

The manufacturing of a high-performance, low void content part depends on both the infusion of resin into the preform, and the adhesion between the resin and fibers. The infusion of resin consists of two simultaneous flows: macroscopic flow which is characterized by permeability, and microscopic flow that is related to fiber wet-out. These two kinds of flow are of great importance due to the fact that they determine the product properties. The two simultaneous flows; bulk mold filling and tow wetting during the resin injection step; often result in air entrapment in the composite part which results in degradation of part mechanical properties. Voids may occur both in the resin matrix and within the fiber bundles. Flow advances more rapidly among the fiber bundles than within the bundles themselves. Due to this flow nature, voids are formed within the bundles. On the other hand, the adhesion is complex and is depending largely on the chemical composition of the fiber and the resin, including any sizing used to enhance bonding. However, wetting of the fiber surface by the fluid is a prerequisite for good

adhesion because of the short-range nature of intermolecular forces [34]. An acceptable flow pattern can be obtained by optimizing the process parameters such as injection pressure, liquid flow rate, gate location, preform lay up, etc.. As a result, problems such as dry spots and void formation can be avoided or at least reduced.

A variety of theoretical models [35] have been proposed to predict permeability as a function of structure. While these models work well for predicting the resistance to flow through idealized particle and fiber beds, there are considerable discrepancies between the model prediction and experimental data for flow through real fiber beds, i.e. fabrics typically used in RTM. These discrepancies are due to the non-uniformities associated with the fiber packing, bundle size, fiber alignment and fiber volume fraction. Until more accurate models are developed that take in to account the stochastic nature of these materials, fabric permeabilities must be determined experimentally. Previous experimental studies of fabric permeability have used idealized Newtonian fluids such as corn syrup, silicone oil, corn oil, tap water, and DOP oil. The first investigators to use an actual resin system were perhaps Adams et al. [36] when they measured the in-plane permeabilities of woven fabrics. In this work two idealized Newtonian fluids (10W30 and 20W50 motor oils) and one real resin (Vinyl Ester) were used to measure the permeability of two types of reinforcements.

The objectives of this work are:

- Experimental study of the effects of vacuum level, fluid type and preform on the mold filling phase (cavity pressure, flow pattern, flow velocity and filling time) of the Resin Transfer Molding Process.
- Experimental measurements of the average and transient permeabilities of M8610 fiberglass mat and woven roving fiberglass using different fluids and vacuum levels, and to study the effect of vacuum level and fluid type on the measured permeabilities.
- Experimental study of the wetting-out process.
- Experimental verification of a constant inlet-pressure boundary condition scale relations derived by Xiao, et. al. [32] from a simplified mold filling simulation model developed by Cai [33].

2.8 Thesis Overview

Chapter 3 explains the experimental details, i.e. tooling, fluids, reinforcement types, experimental set-up and experimentation. In chapter 4, a sample calculation is shown in details, results are presented and discussed. General conclusions about the work done are presented in chapter 5 together with an outlook for future work.

CHAPTER 3

EXPERIMENTAL DETAILS

3.1 Introduction

The mold filling experimental set-up was constructed at the Concordia Center for Composites (CONCOM) Manufacturing Laboratory to study the effects of the vacuum level on the mold filing aspects of the Liquid Transfer Molding process. The permeabilities of M8610 fiberglass mat and woven roving fiberglass were measured, and the effect of vacuum level on the measured permeability was studied. A constant inlet pressure boundary condition scale relation was verified experimentally.

3.2 Tooling

Two molds were used in the experimental work. One of them is a part of the 2-D mold filling simulation set-up built at the CONCOM manufacturing laboratory and was used to conduct the motor oil experiments, and the second was manufactured to be used for the resin experiments. The mold used for motor oil experiments consists of a 24"×24"×2" (60cm×60cm×5cm) aluminum base and acrylic top (Figure 3.1 and Figure 3.2) separated by a rubber spacer with 10.5"×5" (26.25cm×12.5cm) cavity dimensions (Figure 3.3). However, one quarter of this mold was used to conduct the motor oil experiments. Lead pieces were placed between the upper and lower mold plates to determine the thickness of the cavity. The aluminum base has 18 ports for pressure

measurements and 3 ports for resin injection. On the other hand, the acrylic top has 5 ports to be used as vents or connected to the vacuum pump.

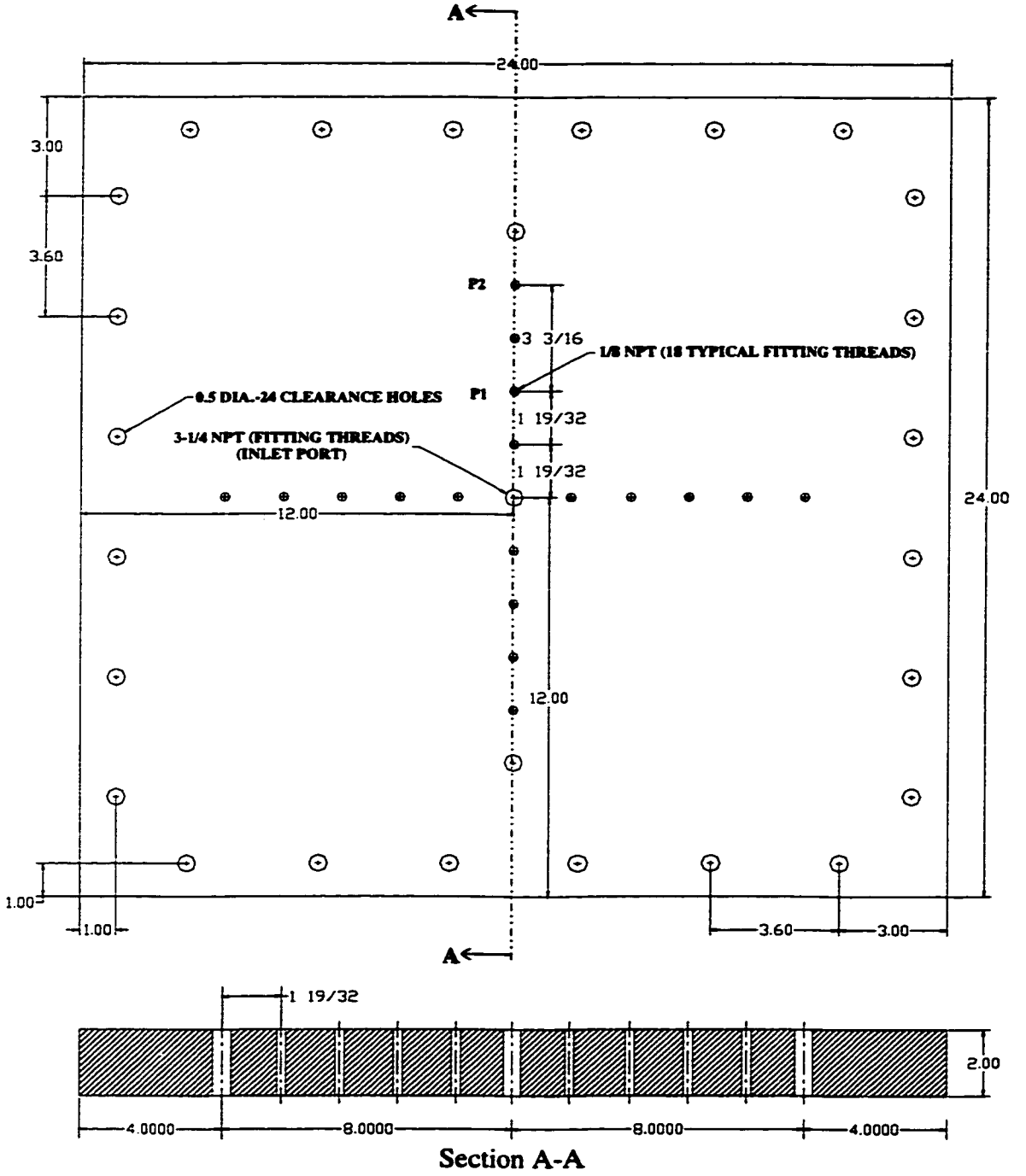

Figure 3.1 - Aluminum base of the motor oil mold (Dimensions are in inches).

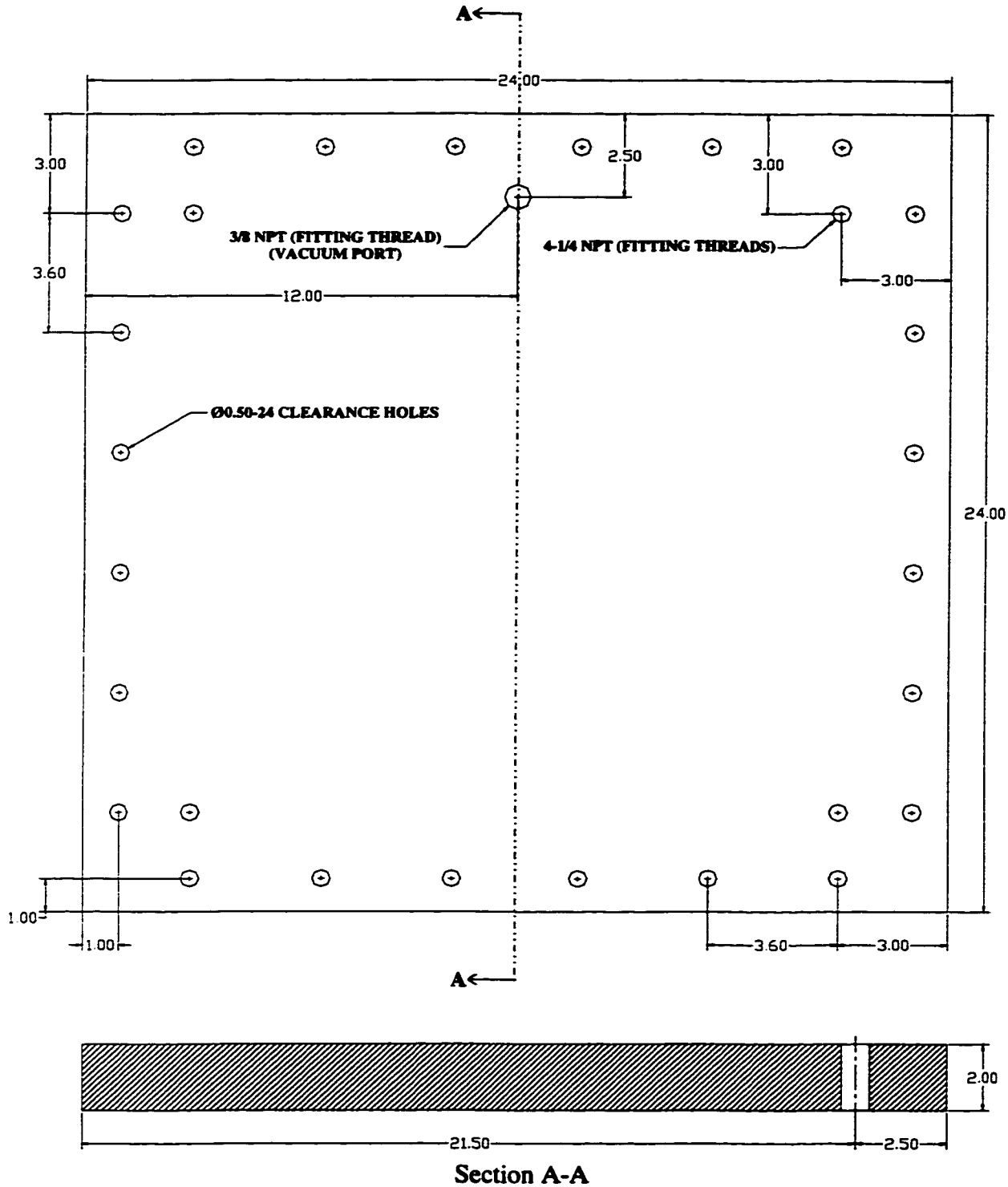

Section A-A

Figure 3.2 - Acrylic top of the motor oil mold (Dimensions are in inches).

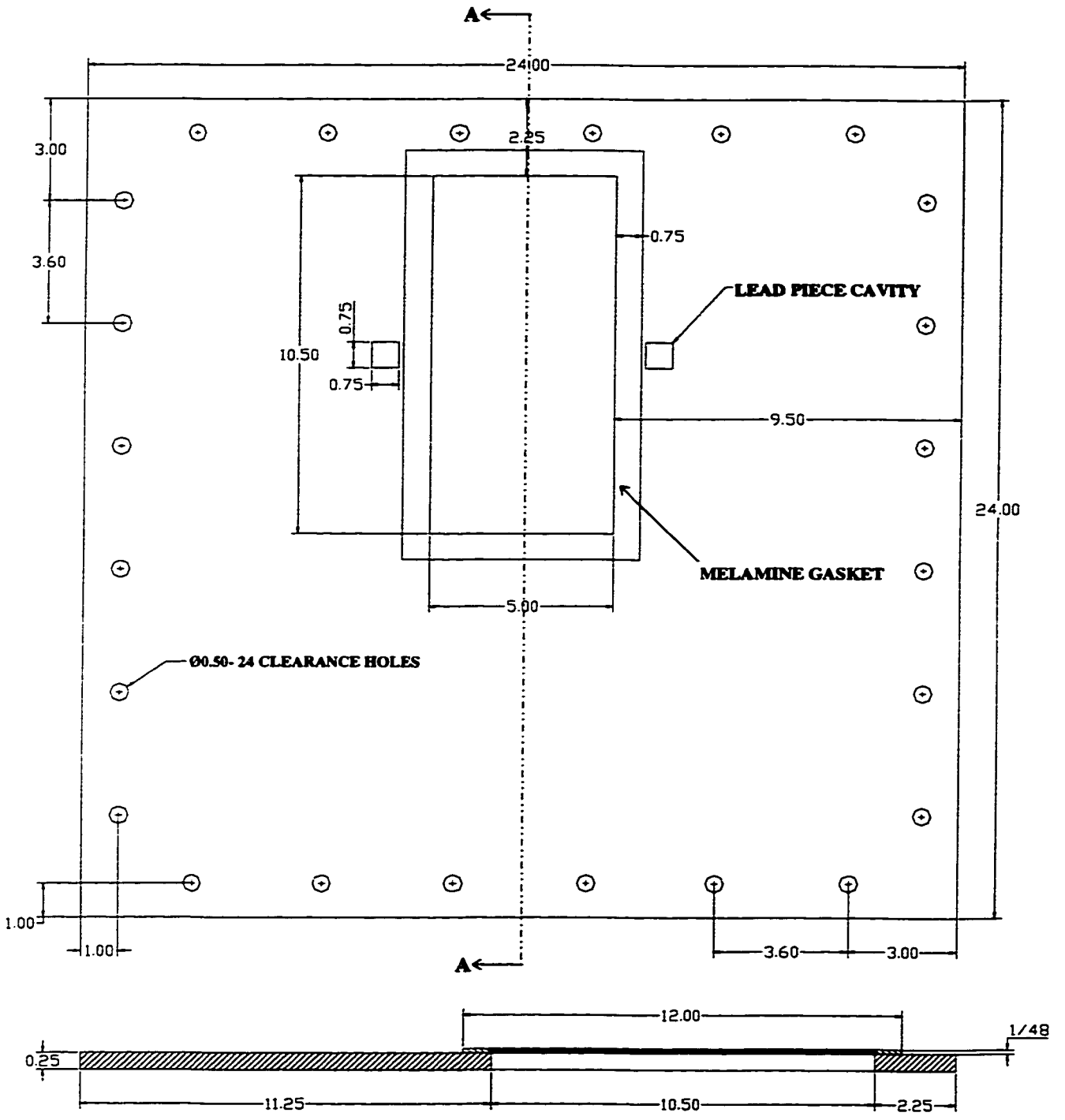

Section A-A

Figure 3.3 - Rubber spacer of the motor oil mold (Dimensions are in inches).

Figure (3.4) shows a photograph of the resin mold plates, which consists of 18"×13"×1" (45cm×32.5cm×2.5cm) aluminum base and acrylic top (Figure 3.5 and Figure 3.6) separated by a rubber spacer with 10.5"×5" (26.25cm×12.5cm) cavity dimensions (Figure 3.7). The aluminum base has 6 ports for pressure transducers and one port for resin injection, whereas the acrylic top has one port to be connected to the vacuum pump.

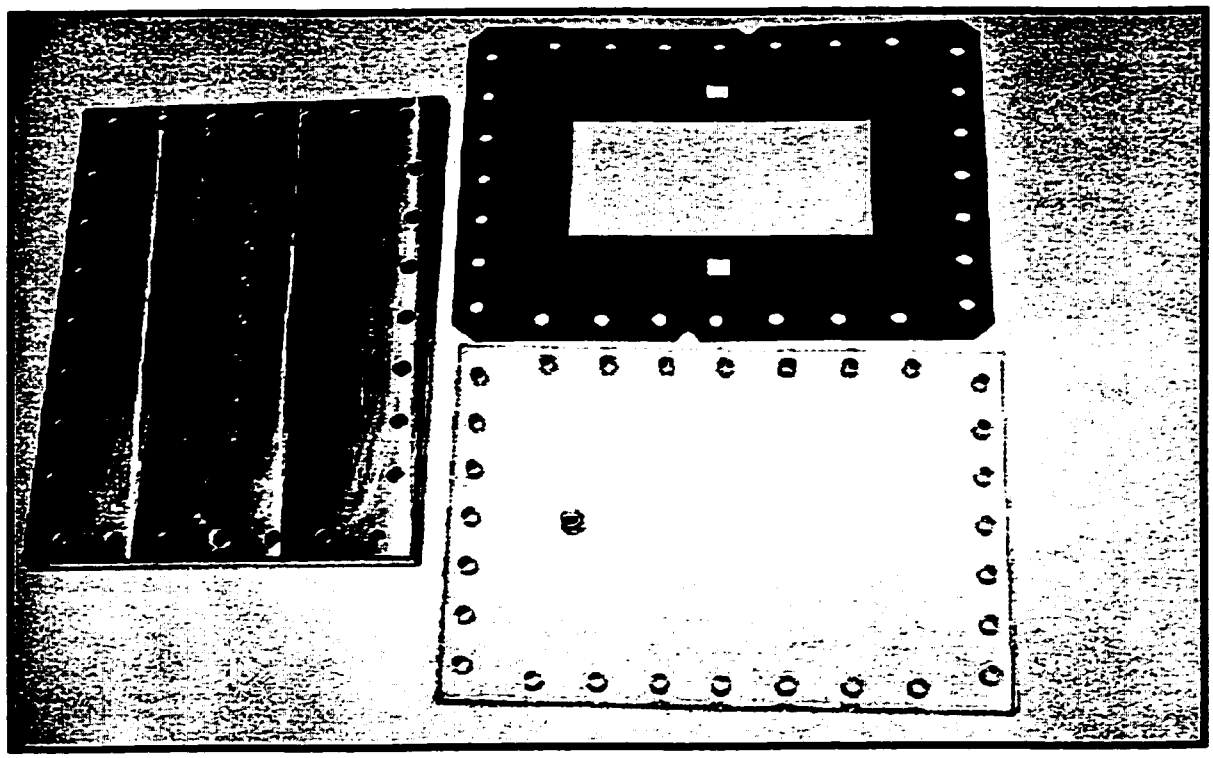

Figure 3.4 - Photograph of the resin mold plates.

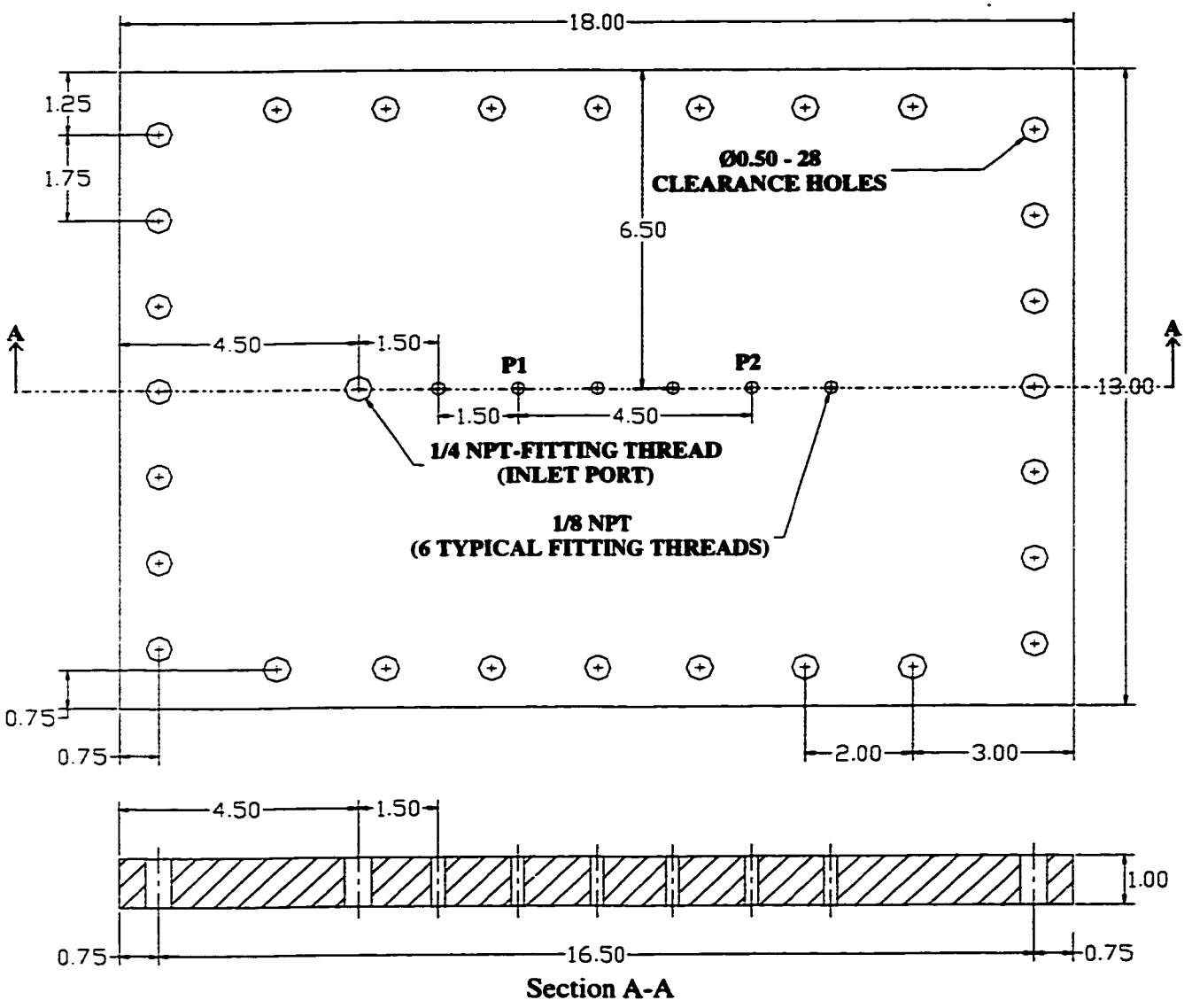

Figure 3.5 - Aluminum base of the resin mold (Dimensions are in inches).

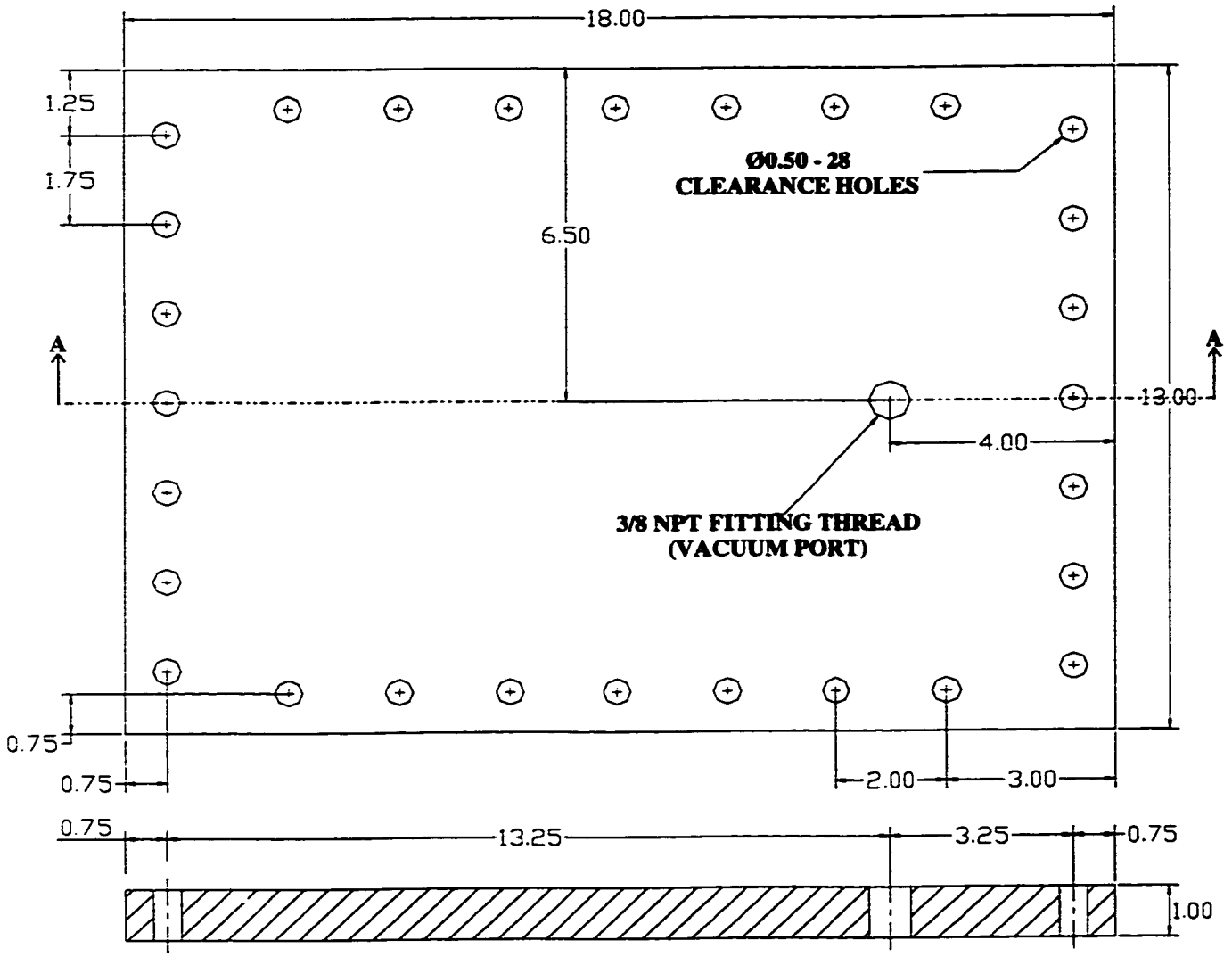

Section A-A

Figure 3.6 - Acrylic top of the resin mold (Dimensions are in inches).

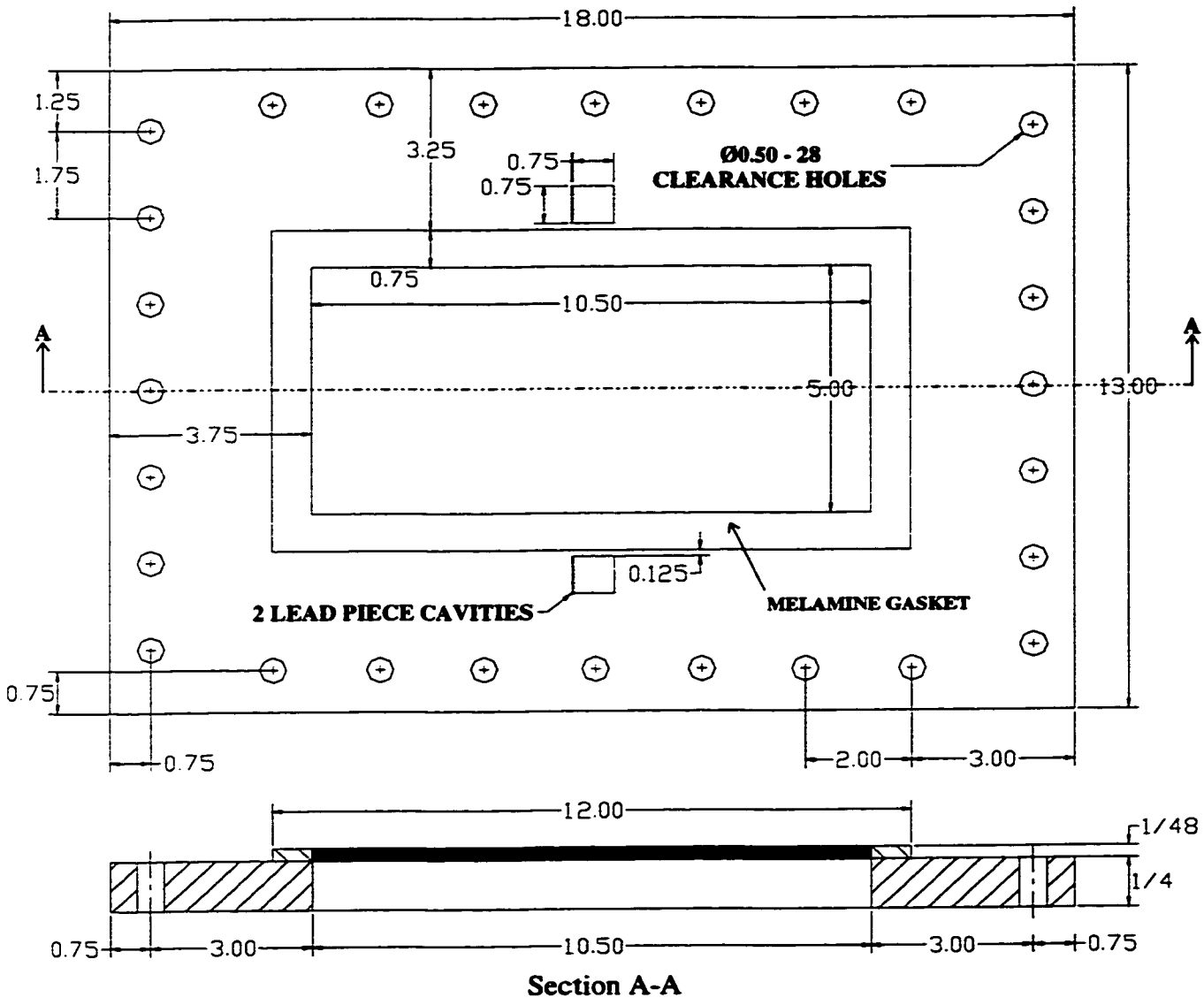

Section A-A

Figure 3.7 - Rubber spacer of the resin mold (Dimensions are in inches).

3.3 Reinforcements

Two commonly used fabrics in liquid molding (LM) processes were selected to conduct the experimental work: Owens/Corning Fiberglass (OCF) M8610 chopped strand fiberglass mat with a nominal surface density of 450 g/m^2, and Bay Mills style 302 plain weave woven roving fiberglass with a nominal surface density of 815 g/m^2.

3.4 Fluids

Three types of fluids were used to impregnate the preform; two of them were used as model fluids and the third was a real resin. Table (3.1) below shows the different types of fluids and their nominal viscosities.

Table 3.1 - Fluids used in the experimental work.

Fluid Type	**Nominal Viscosity (μ) at 20°C (mPa.s)**
DERAKANE ™ 411-350 Vinyl Ester Resin (from DOW Chemical Company)	650
MOTORMASTER NUGOLD 10W30 Motor Oil	150
MOTORMASTER SUPREME 20W50 Motor Oil	440

3.5 Data Acquisition

Two pressure transducers were used to measure the pressure at two different locations along the cavity center line. A FLUKE 2286A data logging system was used to scan and sample the pressure transducers signals values once every second, convert them to pressure readings, and record them as a function of mold filling time. The data was

stored on a floppy disk. The fluid flow front progression was monitored through the transparent acrylic mold top plate, by recording the filling process using a video camera. The built-in timer of the video camera was synchronized with the data logging system clock so that the relationship between the flow front location and the pressure reading could be obtained. The flow front profiles were obtained later from the video recording with the aid of a video projector.

3.6 Experimental Set-up

The experimental set-up used in our work is shown schematically in Figure (3.8). A clear acrylic top mold was designed and built to observe the flow front progression through the preform. A Hi8 Sony video camera, connected to a TV monitor, was mounted above the mold so that the filling process could be videotaped. The fluid was introduced into the cavity from the fluid container located above the mold. A valve located before the inlet port was used to control the start of the filling process. A vacuum pump was used to get the forcing pressure gradient required to fill the cavity with the fluid used. A vacuum gauge was used to read the vacuum pressure. The vacuum level required was obtained by adjusting the release valve located on the vacuum line. Two pressure transducers (P1 and P2 in Figures 3.1 and 3.5) were mounted on the bottom of the aluminum base mold to measure the pressure at two locations along the center line of the cavity. The distance between the pressure transducers was 8.1cm in the motor oil mold, while the distance was 11.43cm in the resin mold. The signals from the pressure transducers were transmitted to the data logging system, converted to pressure readings

and saved as a function of time on a floppy disk in the data logging system drive. A photograph of the experimental set-up is shown in Figure (3.9).

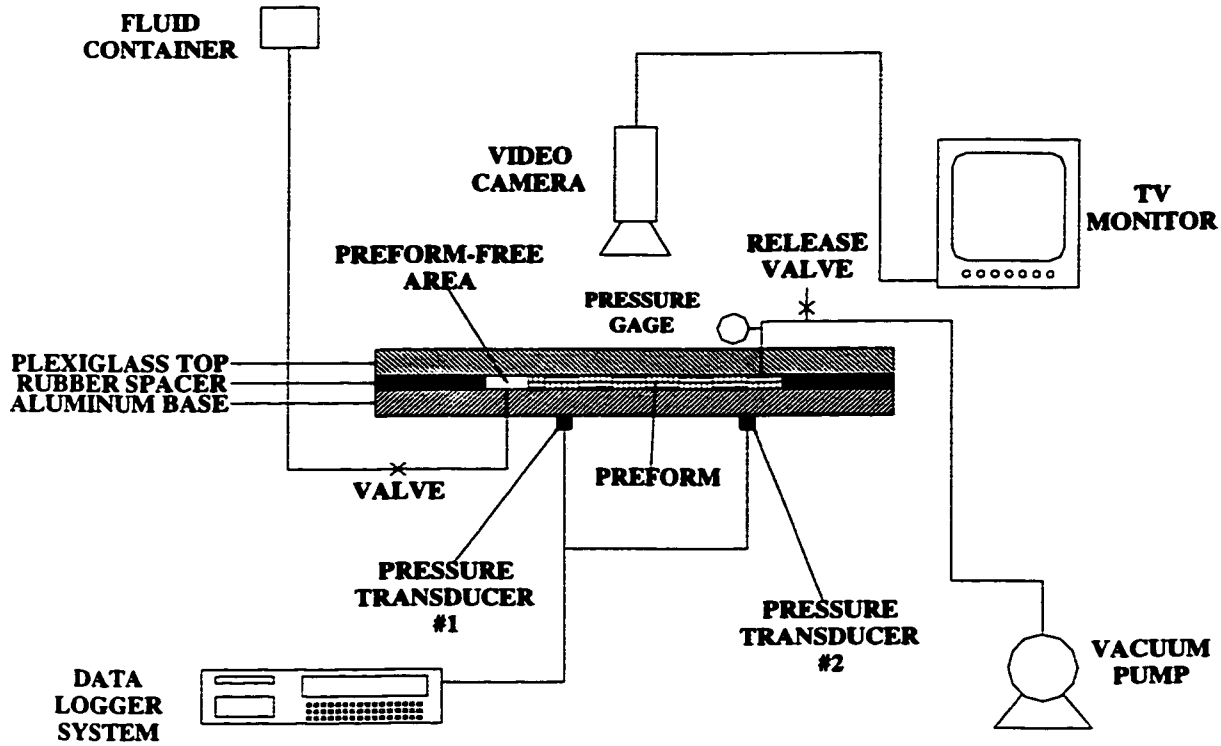

Figure 3.8 - Schematic diagram of the experimental set-up.

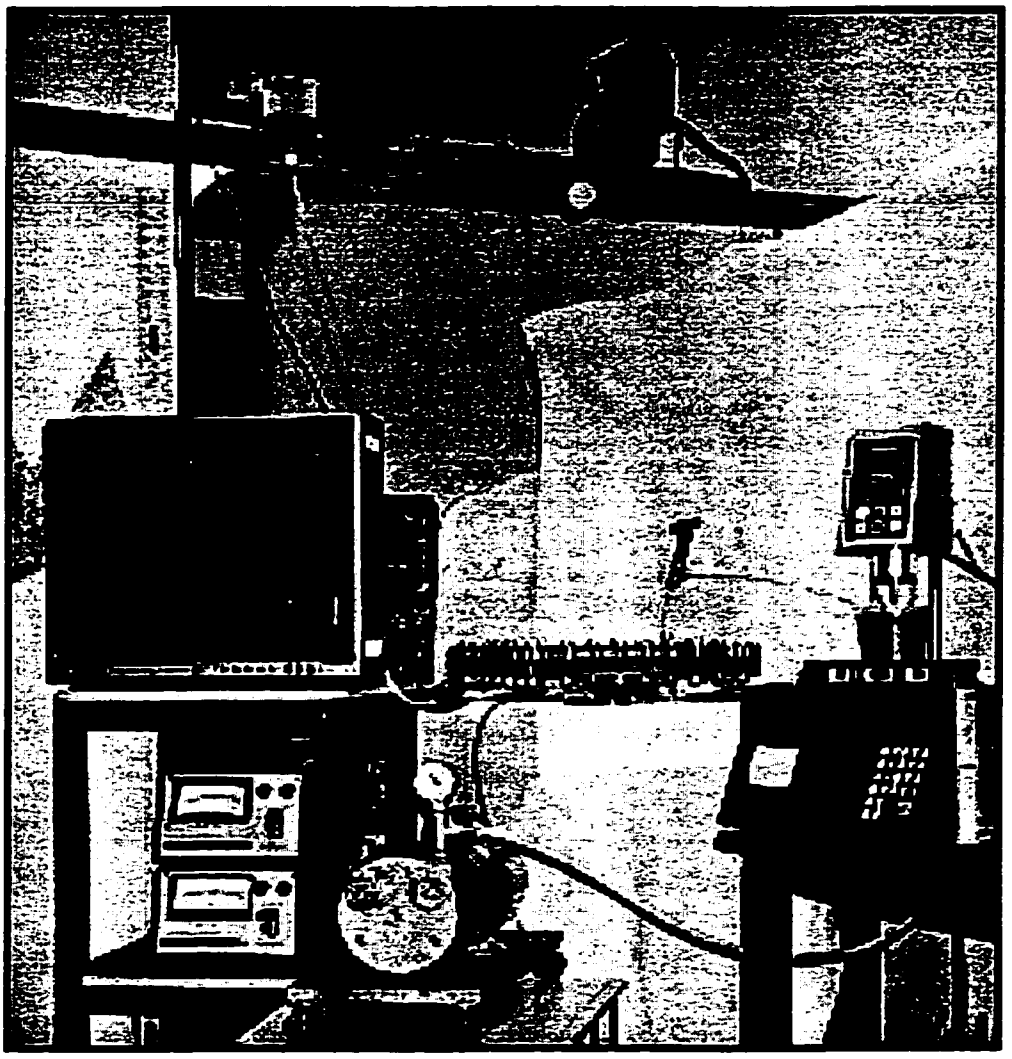

Figure 3.9 - Photo of the experimental set-up.

3.7 Experimentation

Plies of a particular cloth, i.e. chopped strand mat or woven roving fabric, were cut with 9in×5in dimensions. Preforms for experiments were prepared from a specific number of cloth layers; i.e. 8 layers for chopped strand mat experiments, and 9 layers for woven roving fabric. The number of layers were chosen such that the clamping force compresses the preform properly to avoid any flow over and under the perform assembly as well as between loose layers. Each preform was weighed using a digital balance before being stacked inside the mold cavity. The preform layers were then neatly stacked inside the mold cavity leaving a preform free area at the inlet port side. This preform free area was introduced to turn the flow mode from radial to unidirectional. Lead pieces, with a particular thickness, were placed between molds' top and bottom plates so that the cavity thickness could be measured after the experiment. Next, a melamine gasket was placed around the perimeter of the mold cavity, and a thin layer of silicone sealant was applied on the gasket to get the cavity properly sealed against leakage. The mold was closed and bolted together, then it was connected to the vacuum pump. The pressure transducers were installed and their signals were connected to the data logging system used. A level was used to make sure that the mold cavity was horizontal. The Hi8 video camera was mounted above the mold so that the filling process could be videotaped. The FLUKE data logging system was prepared and programmed to sample the data once every second, and a floppy disk was inserted into the FLUKE system drive. The video camera timer was synchronized with the FLUKE system clock so that the relationship between the flow front location and the pressure readings could be observed. The fluid container was filled

with the required fluid, the fluid was allowed to fill the container tube and evacuate the air entrapped inside, then the valve at the end of the tube was closed and connected to the mold. The vacuum pump was then started and the release valve was adjusted to get the appropriate vacuum level. The data logging system scanning process was started, and the scanned data was saved on the floppy disk. The video camera recording process was then started. The inlet valve was opened to allow the fluid to flow through the preform. Once the cavity was filled completely, the vacuum pump was shut down, the recording and scanning processes were stopped, and the inlet valve was closed. The viscosity of the fluid and the room temperature were taken right after the experiment using a Brookfield Model DV-II+ viscometer. The mold was then opened and cleaned to be prepared for the next experiment. Finally, the thickness of the lead pieces was measured to get the thickness of the preform used. Flow front profiles were obtained later from filling process recordings with the aid of a video projector.

CHAPTER 4

RESULTS AND DISCUSSION

4.1 Experimental Records:

Four groups of experiments, with different combinations of fluid and preform types, were conducted. Each group of experiments consists of three experiments with different vacuum levels. Each experiment was repeated twice to make sure that the results obtained are repeatable. Table 4.1 below shows the experimental records of the experiments conducted. Table 4.1(a) shows the experimental record of motor oil 10W30 with an average viscosity of 150 mPa.s, and OCF M8610 fiberglass mat with an average fiber volume fraction of 20%. Table 4.1 (b) shows the experimental record of motor oil 20W50 with an average viscosity of 440 mPa.s, and OCF M8610 fiberglass mat, with an average fiber volume fraction of 20%. Table 4.1 (c) shows the experimental record of Vinyl Ester resin with an average viscosity of 640 mPa.s, and woven roving fiberglass, with an average fiber volume fraction of 41%. Table 4.1 (d) shows the experimental record of Vinyl Ester resin, with an average viscosity of 640mPa.s, and OCF M8610 fiberglass mat, with an average fiber volume fraction of 20%.

In motor oil experimental groups (MOI and MOII), "MO" stands for motor oil, the letters "I/II" indicates the motor oil type ("I" indicates 10W30 motor oil, and "II" indicates 20W50 motor oil), the "X" letter indicates the second trial of the same

experiment. Finally, the numeric value at the end of the experiment name indicates the vacuum level used ("1" indicates the highest vacuum level, and "3"indicates the lowest one). The same applies for the rest of experimental groups, except that "RWR" in RWR group stands for resin-woven roving combination, and "RM" in RM group stands for resin-mat combination.

Filling time results given in Table 4.1 shows that the higher vacuum level filling process requires less filling time. This was the case in all experiment groups except in RM, in which the highest vacuum level experiment had the highest filling time. This peculiar behavior will be discussed later in this thesis.

Table 4.1(a) - Experimental record of motor oil 10W30 / glass fiber chopped strand mat (OCF M8610) experiment group (MOI).

Experiment name	MOI1	MOI2	MOI3	MOIX1	MOIX2	MOIX3
Vacuum level (inch Hg)	25	18	9	25	18	9
Room temperature (°C)	20	20.3	20.1	19.3	22.5	22.4
Number of layers	8	8	8	8	8	8
Preform mass (m_f) (g)	105.8	108.6	107.4	105.7	105.3	105.6
Original lead thickness (mm)	7.01	7.195	7.1	7.11	7.095	7.1
Final lead thickness (mm)	6.855	6.89	6.89	6.845	6.845	6.855
Fluid viscosity (μ) (mPa.s)	150.9	148.7	150.5	154.3	145.1	145.3
Fiber volume fraction (V_f) (%)	20.77	21.21	20.97	20.78	20.7	20.73
Filling time ($T_{filling}$) (s)	65	88	168	67	78	154
Inlet pressure (P_o) (kPa)	8.461	8.461	8.461	8.461	8.461	8.461
Fluid density (ρ) (kg/m^3)	750	750	750	750	750	750

Table 4.1(b) - Experiment record of motor oil 20W50 / glass fiber chopped strand mat (OCF M8610) experiment group (MOII).

Experiment name	MOII1	MOII2	MOII3	MOIIX1	MOIIX2	MOIIX3
Vacuum level (in Hg)	25	18	9	25	18	9
Room temperature (°C)	20.6	20.1	19.7	19.4	21.7	22.3
Number of layers	8	8	8	8	8	8
Preform mass (m_f) (g)	104.4	105	104.2	105.6	105.3	105.6
Original lead thickness (mm)	7.045	7.1	7.095	7.115	7.085	7.065
Final lead thickness (mm)	6.875	6.87	6.895	6.845	6.885	6.885
Fluid viscosity (μ) (mPa.s)	438.5	441.9	444.7	446.3	431.6	427.8
Fiber volume fraction (V_f) (%)	20.43	20.56	20.33	20.76	20.58	20.64
Filling time ($T_{filling}$) (s)	154	245	421	170	211	359
Inlet pressure (P_o) (kPa)	9.251	9.251	9.251	9.251	9.251	9.251
Fluid density (ρ) (kg/m^3)	820	820	820	820	820	820

Table 4.1(c) - Experiment record of Vinyl Ester resin / woven roving fiberglass experiment group (RWR).

Experiment name	RWR1	RWR2	RWR3	RWRX1	RWRX2	RWRX3
Vacuum level (in Hg)	25	18	9	25	18	9
Room temperature (°C)	20.2	20.5	20	21.8	21.9	21.7
Number of layers	9	9	9	9	9	9
Preform mass (m_f) (g)	211.65	210.55	210.25	210.85	211.35	210.40
Original lead thickness (mm)	6.995	7.02	7.08	7.02	7.04	7.05
Final lead thickness (mm)	6.845	6.825	6.82	6.845	6.83	6.87
Fluid viscosity (μ) (mPa.s)	647.7	642.9	651.2	630.7	630.1	632.6
Fiber volume fraction (V_f) (%)	41.60	41.51	41.48	41.45	41.64	41.21
Filling time ($T_{filling}$) (s)	217	289	647	171	242	579
Inlet pressure (P_o) (kPa)	9.976	9.976	9.976	9.976	9.976	9.976
Fluid density (ρ) (kg/m^3)	1015	1015	1015	1015	1015	1015

Table 4.1(d) - Experiment record of Vinyl Ester resin / glass fiber chopped strand mat (OCF M8610) experiment group (RM).

Experiment name	RM1	RM2	RM3	RMX1	RMX2	RMX3
Vacuum level (in Hg)	25	18	9	25	18	9
Room temperature (°C)	20.9	21.2	20.9	20.7	19.8	19.7
Number of layers	8	8	8	8	8	8
Preform mass (m_f) (g)	105.3	105.3	105.5	105.0	105.5	105.7
Original lead thickness (mm)	7.08	7.055	6.965	7.065	7.08	7.075
Final lead thickness (mm)	6.865	6.865	6.835	6.835	6.87	6.87
Fluid viscosity (μ) (mPa.s)	638.1	633.4	639.3	643.7	653.8	654.8
Fiber volume fraction (V_f) (%)	20.64	20.64	20.77	20.67	20.66	20.7
Filling time ($T_{filling}$) (s)	1256	772	820	1302	831	985
Inlet pressure (P_o) (kPa)	9.976	9.976	9.976	9.976	9.976	9.976
Fluid density (ρ) (kg/m^3)	1015	1015	1015	1015	1015	1015

4.2 Sample of Calculation:

Experiment MOI2 from the first experimental group was considered as a typical example to show the calculations and the results in details. The same analysis and procedure were followed for the rest of experiments.

4.2.1 Experimental Data:

Pressure, at two locations along the center line of the mold cavity (Figure 3.1), was measured using pressure transducers. The data was collected every second by the data logger system used. Figure (4.1) shows the pressure readings as a function of time at the two different locations in the mold cavity. As could be seen from Figure (4.1), the pressure build-up grows fast at the beginning, after which growth rate decreases gradually. The pressure difference (P1-P2) curve also rises fast at the beginning, after

which its increase rate decreases until reaching a maximum value, after that it starts decreasing.

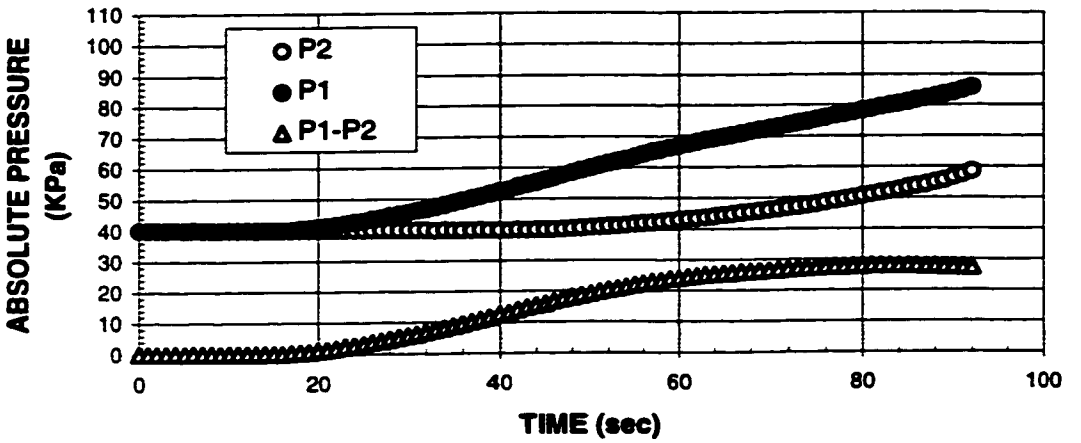

Figure 4.1 - Pressure changes as a function of time at the two pressure transducers locations for experiment MOI2.

The overall flow front propagation profiles were obtained by recording the filling process using a video camera, and tracing the flow front at different time steps from the recording using a video projector. Figure 4.2 shows the experimental flow front profiles for the example experiment. The flow profiles are almost straight lines with a little discrepancy observed in few profiles. Edge flow were not observed in this particular experiment, which was probably because of the precisely-cut preform.

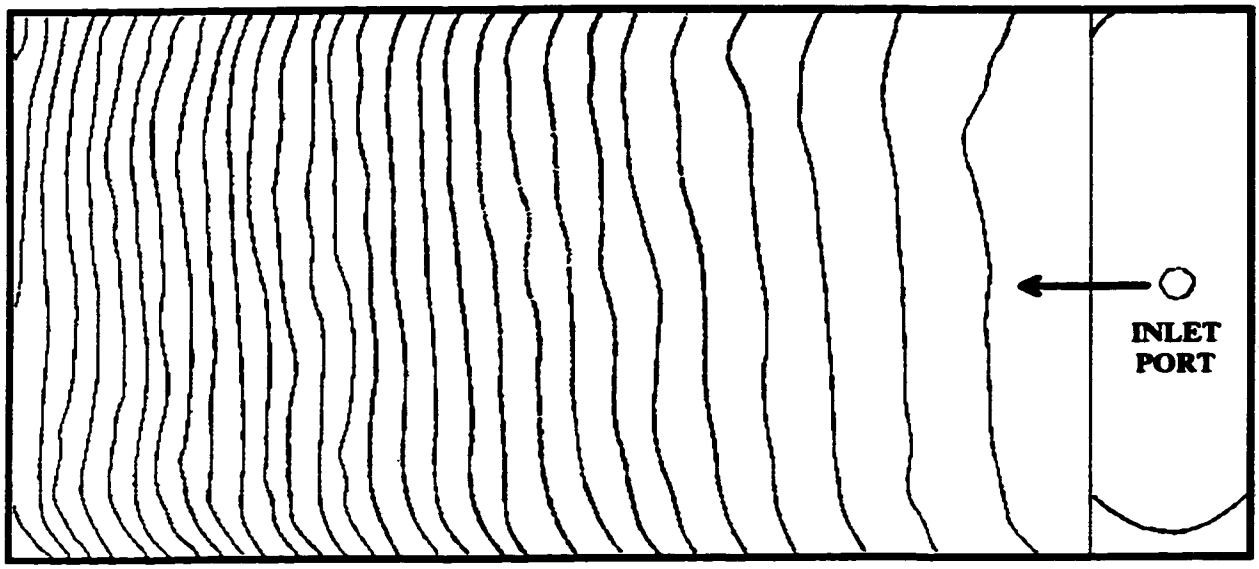

Figure 4.2 - Fluid flow patterns for experiment (MOI2).
(Time interval (Δt) = 3s, Filling time ($T_{filling}$) = 88s)

4.2.2 Determination of Fiber Volume Fraction (V_f):

The fiber volume fraction (V_f) is given by the following equation

$$V_f = \frac{\text{preform volume}}{\text{cavity total volume}} = \frac{m_f}{\rho_f V_T} \tag{4.1}$$

where

m_f = Preform mass (g)
ρ_f = Preform density = 2.56 (g / cm^3)
V_T = Cavity total volume (m^3) = $L\,W\,t_f$
L = The preform length (m)
W = The preform width (m)
t_f = The lead final thickness (m)

By substituting the known values into equation (4.1) we obtain the following general equation which is valid for all experiments.

$$V_f = 1.3455 \times 10^{-3} \frac{m_f}{t_f} \tag{4.2}$$

Substituting the values of m_f and t_f for experiment MOI2 from Table 4.1(a), we obtain

$$V_f = 21.21\% \tag{4.3}$$

4.2.3 Flow front propagation:

The distance between each two adjacent flow profiles was measured along the center line and multiplied by the scale factor to get the actual distance traveled. The distances were added up to get the total distance traveled from the preform edge. The scale factor was obtained using the following equation

$$S_F = \frac{L}{L_d} \tag{4.4}$$

where

L = preform actual length = 22.86cm (for all experiments)
L_d = preform length obtained from the flow front profiles drawing (Figure 4.2)

Figure (4.3) shows the flow front propagation curve of our example. The reference starting time (t=0s) was chosen to be at the moment the fluid started to fill the preform. It is clear that the flow was fast at the beginning of the filling process, after which it decreases gradually. This is obvious from the decreasing slope of the propagation curve.

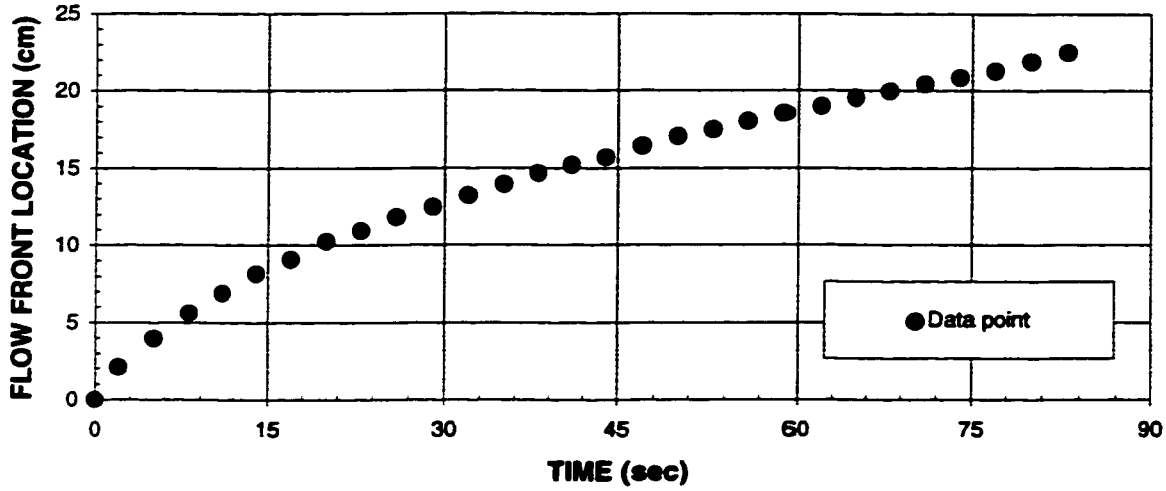

Figure 4.3 - Flow front propagation for experiment MOI2.

4.2.4 Flow front velocity:

The average velocity for each time interval, i.e. between each two adjacent flow profiles, was calculated by the following equation and assigned to the mean value of each time interval

$$\bar{q}_i = \frac{(L_i - L_{i-1})}{(T_i - T_{i-1})} \tag{4.5}$$

where

$\bar{q}_i$ = The average velocity in the time interval (i)
L_i = The location of the flow front at the end of the time interval (i)
L_{i-1} = The location of the flow front at the beginning of the time interval (i)
T_i = The time at end of the time interval (i)
T_{i-1} = The time at the beginning of the time interval (i)

The velocity of the flow front as a function of time for experiment MOI2 is shown in Figure (4.4) below. The negative decreasing slope of the velocity curve indicates decelerating flow. A discrepancy from the trend line is clear in this experiment, and this could be interpreted as the direct result of mat surface-density variation.

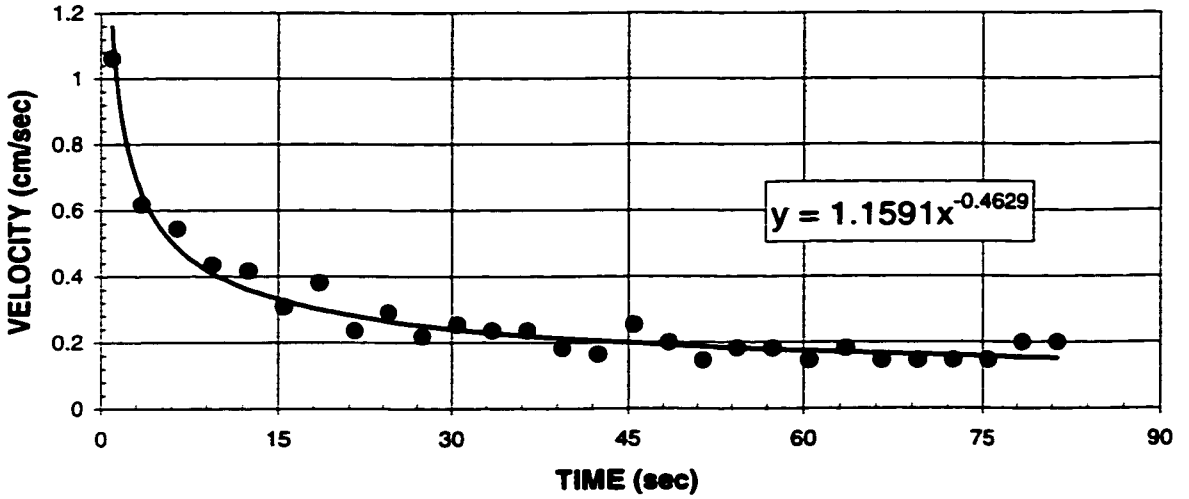

Figure 4.4 - Flow front velocity as a function of time for experiment MOI2.

4.2.5 Average Permeability measurement:

The average permeability was measured by considering the constant inlet and outlet (vacuum) pressures, the filling time and the total preform length. The following equation was used to calculate the average permeability:

$$K_{avg.} = -\mu \frac{L^2}{T_{filling}(P_{VAC.} - P_O)} \tag{4.6}$$

where:

$K_{avg.}$ = preform average permeability
μ = viscosity of the fluid used
L = preform length
$T_{filling}$ = the filling time to completion
$P_{VAC.}$ = vacuum pressure used
P_O = inlet pressure

The fluid inlet pressure (P_O) for each experiment can be calculated using the following equation

$$P_O = \rho g H \tag{4.7}$$

where

ρ = density of the fluid used in the experiment
g = gravity acceleration = 9.81 (m/s^2)
H = fluid height

For the case of experiment MOI2, in which motor oil 10W30 was used, the density and the height of the motor oil container is given below

$$\begin{aligned} \rho &= 750 \text{ kg} / \text{m}^3 \\ H &= 1.15 \text{ m} \end{aligned} \tag{4.8}$$

Substituting these values into equation (4.7) gives

$$P_O = 8.461 \text{ kPa (gauge pressure)} \tag{4.9}$$

and since

$$P \text{ (absolute pressure)} = P \text{ (gauge pressure)} + \text{Atmospheric Pressure} \tag{4.10}$$

and the atmospheric pressure is (101) kPa, the 10W30 motor oil inlet pressure for MOI2 experiment is given as

$$P_O = 109.461 \text{ kPa (absolute pressure)} \tag{4.11}$$

Vacuum pressure may be transferred to absolute pressure by the following equation

$$\left(P_{VAC.}\right)_{ABS.}\text{ (kPa)} = -3.3864\,P_{VAC.}\text{(inch Hg)} + 101 \tag{4.12}$$

Substituting the values of different variables, given in Table (4.1), into equation (4.6) above gives:

$$K_{avg.} = 1.272 \times 10^{-9}\,\text{m}^2 \tag{4.13}$$

4.2.6 Transient permeability measurement

The permeability was measured from the moment the fluid reached the first pressure transducer, at which the pressure readings were available from the two pressure transducers used in the experiment. The permeability was calculated using one of the following equations depending on the flow front location

$$\left(K_t\right)_i = \begin{cases} -\mu \dfrac{\left(L_i - L_{T1}\right)}{\left(t_i - t_{T1}\right)} \dfrac{\left(L_i - L_{T1}\right)}{\left(P_2 - P_1\right)_i} & t_{T1} \le t_i \le t_{T2} \\ -\mu \dfrac{\left(L_i - L_{T1}\right)}{\left(t_i - t_{T1}\right)} \dfrac{\left(L_i - L_{T1}\right)}{\left(P_{VAC.} - P_1\right)_i} & t_{T2} \le t_i \le t_f \end{cases} \tag{4.14}$$

where:

$(K_t)_i$ = transient permeability at time (t_i)

μ = fluid viscosity

L_i = flow front location at time (t_i)

L_{T1} = location of pressure transducer # 1

t_i = the time at which permeability is to be calculated

t_{T1} = the time at which flow front reached pressure transducer # 1

t_{T2} = the time at which flow front reached pressure transducer # 2

t_f = the time at which the fluid completely filled the preform

P_1 = pressure trancducer # 1 reading at time (t_i)

P_2 = pressure trancducer # 2 reading at time (t_i)

$P_{VAC.}$ = vacuum pressure used in the experiment

Figure (4.5) below shows the transient permeability values as function of time measured experimentally for experiment MOI2. Transient permeability seems to be decreasing with time and approaching the average permeability value, which is reached at the end of filling process.

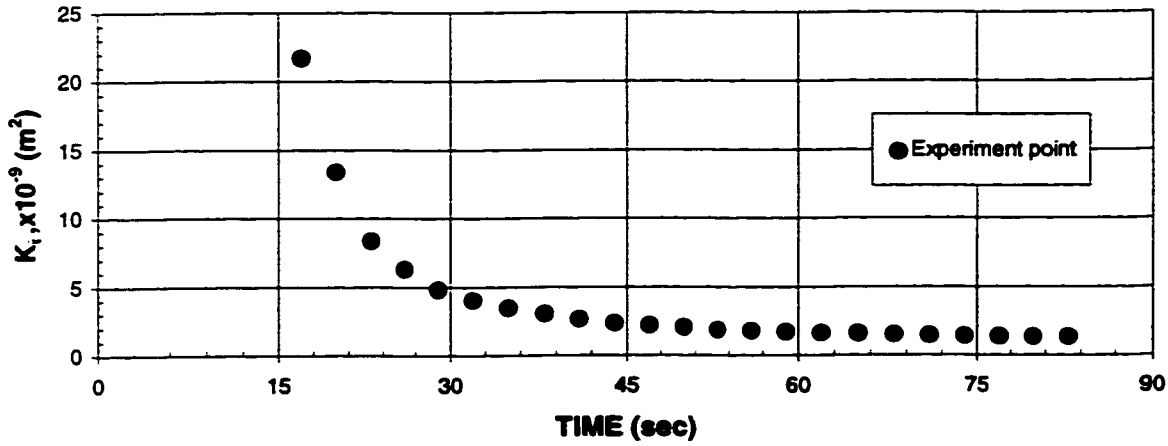

Figure 4.5 - Transient permeability vs. time for experiment MOI2.

4.2.7 Constant inlet-pressure scale relation curve:

Scale relations for a constant inlet-pressure boundary condition were derived by Xiao, et al. [32] and are given by the following functional equation:

$$\frac{P_O K}{\mu q(t) \ell} = F_1\left(\frac{t P_O}{\mu}\right) \tag{4.15}$$

where

P_O = inlet pressure
K = permeability
μ = viscosity of the fluid used
$q(t)$ = flow front velocity at time (t)
ℓ = characteristic length of the mold
t = time

The left side of equation (4.15) can be interpreted as the ratio of the pressure force to the friction force, whereas the right side is a normalized dimensionless time. For the purpose of our work, equation (4.15) should be rearranged and the new conditions should be taken into consideration. Taking the vacuum pressure used in our work into account, equation (4.15) becomes:

$$\frac{K_{avg.}(P_O - P_{VAC.})}{\mu q(t) L} = F_1\left(\frac{t(P_O - P_{VAC.})}{\mu}\right) \tag{4.16}$$

where:

$K_{avg.}$ = average permeability
$P_{VAC.}$ = vacuum pressure
L = preform length
P_O = fluid inlet pressure

Due to variation of mat surface density, there was scatter in the velocity values obtained experimentally as shown in Figure (4.4). As a result, the trend line equation was

used to calculate the velocity values to be used in equation (4.16) above. Figure (4.6) shows the dimensionless curve for experiment MOI2. The dimensionless curves for all experiments will be compared to verify the scale relation given in equation (4.16). According to the functional relation given by equation (4.16), the data obtained from geometrically similar mold cavities should follow the same curve.

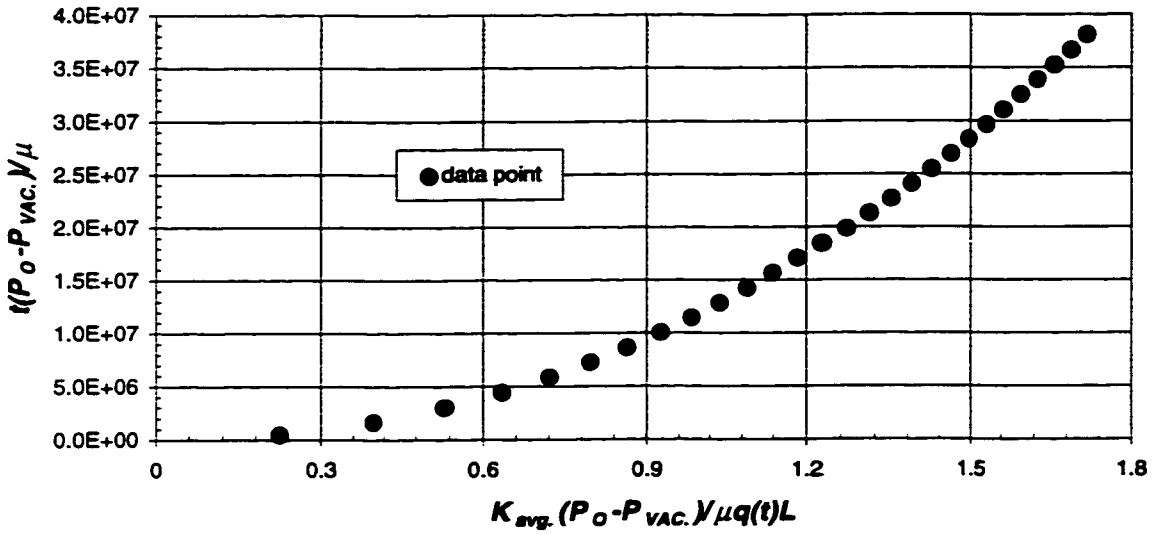

Figure 4.6 - Dimensionless curve for experiment MOI2.

4.3 Results and Discussion:

4.3.1 Pressure curves:

Pressure was measured at two locations through the mold cavity using pressure transducers, and the data was collected every second by the data acquisition system used. The pressure profiles for all experiments conducted are shown in appendix A. Each figure includes the two trials for each experiment. Both pressure transducers read the vacuum pressure applied until the fluid reaches the pressure transducer location. At this moment the pressure starts building up at this particular location. As seen from the pressure plots, the pressure build-up grows fast at the beginning, after which the growth rate decreases gradually. A saturated value at the end of the filling process was only achieved in RM1 and RM2 experiments. This saturated value is about the same as the fluid inlet pressure. As expected, the pressure at the first pressure transducer location (the one closer to the inlet port) starts building up first, and was approaching a saturated value at the end of the filling process. On the other hand, the pressure at the second pressure transducer location starts building up later. By examining the pressure difference (P1-P2) plots, it is noticed that the pressure difference grows fast at the beginning of the filling process, after which the increase rate decreases gradually until reaching a maximum value, in most cases, after which it starts decreasing.

4.3.1.1 Effect of the vacuum level:

The absolute pressure values (P1 and P2) followed a general trend, in which the low vacuum level experiment had the highest maximum absolute pressure values, followed by the medium vacuum level, then the high vacuum level experiment (Figure 4.7). It should be noted however that the low vacuum level experiments have longer filling time. On the other hand, the maximum pressure difference was increasing with vacuum level (Figure 4.8).

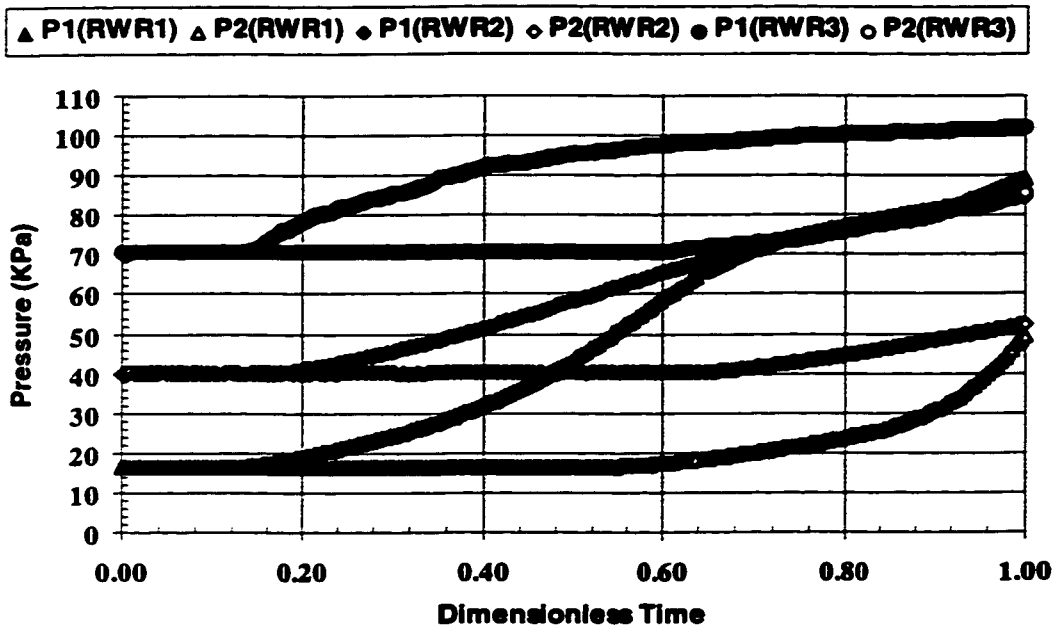

Figure 4.7 - Absolute pressure changes as a function of dimensionless time , i.e. the time divided by the total filling time, at the two pressure transducers locations for RWR experiments.

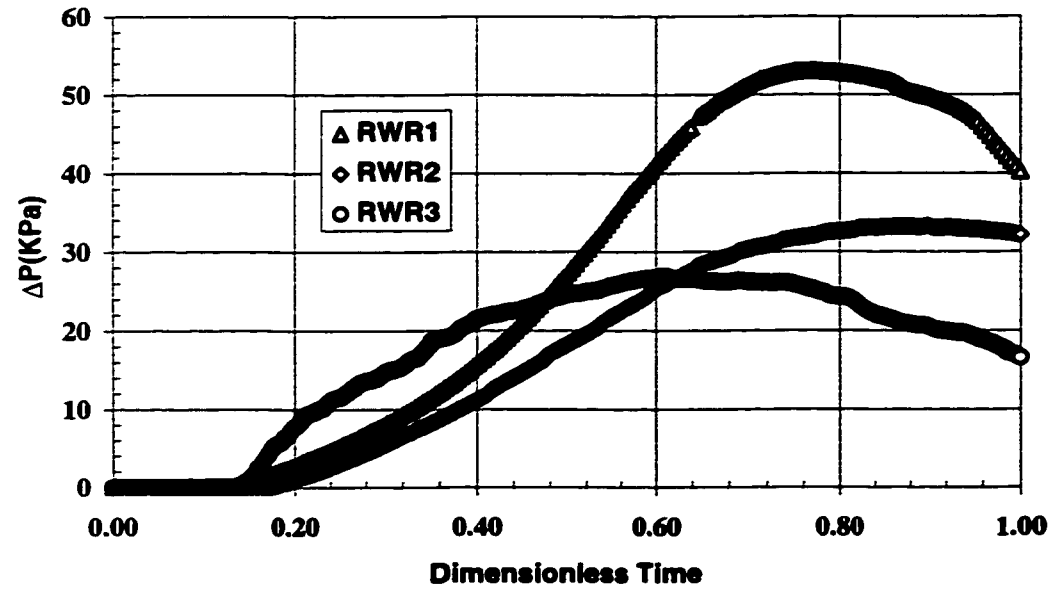

Figure 4.8 - Pressure difference (P1-P2) changes as a function of dimensionless time for RWR experiments.

4.3.1.2 Effect of fluid:

Consider motor oil experiments and resin-mat experiments, where the same preform was used in all experiments with three different fluids. Resin experiments had the highest maximum absolute pressure values (Figure 4.9) and the highest maximum pressure difference values (Figure 4.10), whereas the motor oils 20W50 and 10W30 had the medium and the lowest values, respectively. This resin-mat group behavior is expected to be related to the wetting-out (micro-flow) process.

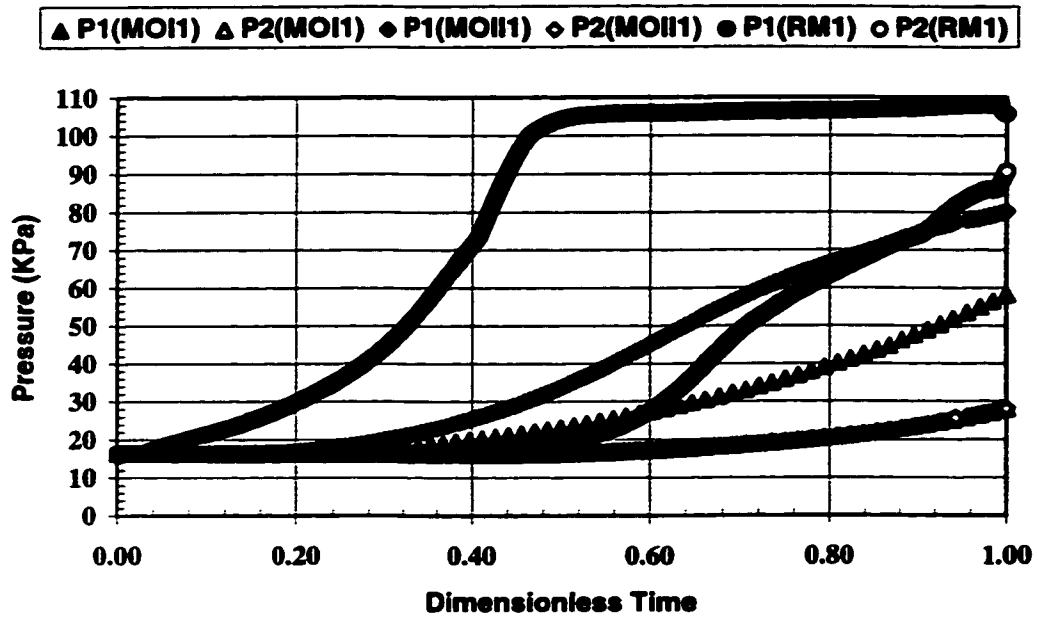

Figure 4.9 - Absolute pressure changes as a function of dimensionless time at the two pressure transducers locations for mat preform-different fluids experiments at the high vacuum level.

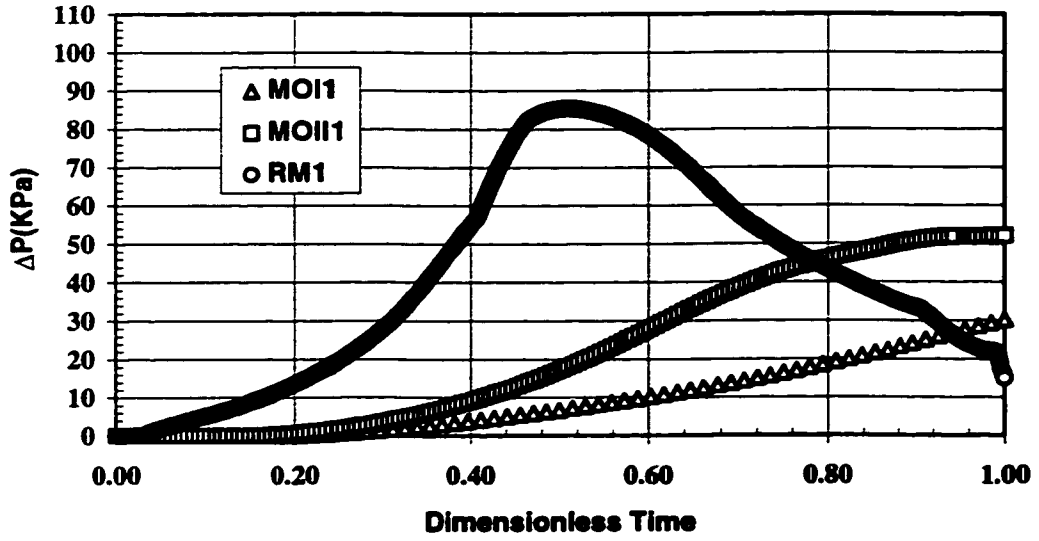

Figure 4.10 - Pressure difference (P1-P2) changes as a function of dimensionless time for mat preform-different fluids experiments at the high vacuum level.

4.3.1.3 Effect of preform type:

Consider resin-woven roving (RWR) and resin-mat (RM) experiments, where the same fluid was used with two different preforms. Mat experiments showed higher maximum absolute pressure values (Figure 4.11) and maximum pressure difference values (Figure 4.12). Wetting-out (micro-flow) process is believed to be responsible for this resin behavior. Besides, the macro-structure of woven-roving preform, where many large macro-channels are formed between fiber bundles, helped the resin to follow mainly through the large channels. This made the pressure inside the cavity less than that in the case of fiberglass mat.

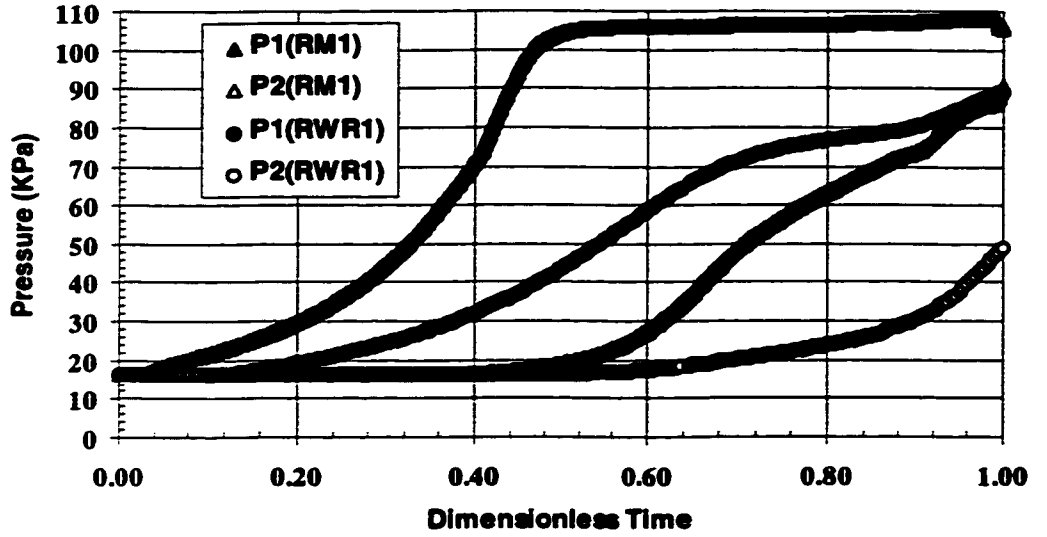

Figure 4.11 - Absolute pressure changes as a function of dimensionless time at the two pressure transducers locations for resin-different preforms experiments at the high vacuum level.

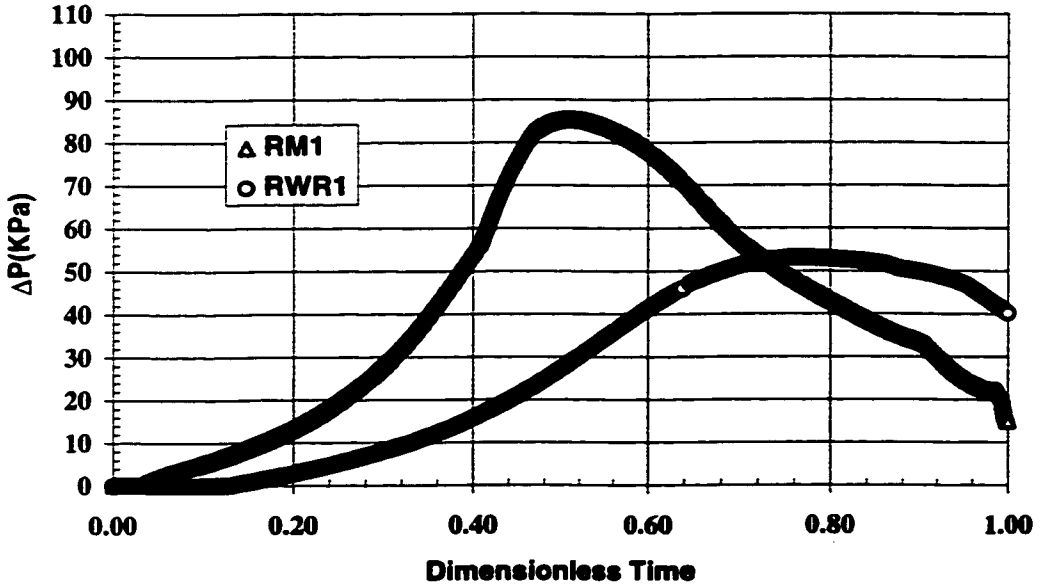

Figure 4.12 - Pressure difference (P1-P2) changes as a function of dimensionless time for resin-different preforms experiments at the high vacuum level.

4.3.2 Filling process:

4.3.2.1 Flow front profiles:

In liquid transfer molding processes, a dry fiber preform must be impregnated by the incoming resin during mold filling. The area in the preform without resin or partially filled with the resin is called a dry spot. Inappropriately placed inlets and outlets, and the variation of the permeability in the preform are the primary reasons for dry spot formation during mold filling. The presence of dry spots in a composite part has been regarded as the most serious problem in liquid transfer molding processes, since dry spots degrade the part performance and quality and as a result the part must be discarded.

To study the edge injection strategy, a small area at the inlet port was kept free from preform so as to turn the flow from radial to unidirectional. Preforms used in our experimental work (i.e. fiberglass mat and woven roving fiberglass) were considered to have a uniform surface density (i.e. the preform mass per unit area) and in-plane permeabilities. However in real life, preforms were found to have variation in the surface density which of course affects their porosities, when stacked into a mold, and their in-plane permeabilities accordingly. Gauvin, et al. [37] reported that the nominal mat surface density published by the material suppliers is an average value, and the actual value at various positions in the mat can significantly differ from that average value. They added that the surface density variation could of course influence the local flow behavior and affect the flow parameters predicted by Darcy's law. Finally, they concluded that surface density variation may explain why sometimes there are defects from one part to another in apparently the same molding conditions. This explains the nonuniformities and rough profiles observed in our experiments conducted and shown in Appendix B. Figure (4.13)

shows the photographs of the fabrics used in our experimental work. The surface density variation could be easily seen in M8610 mat (Figure 4.13a). Its right half seems to have lower surface density as the background could be seen through the fabric. On the other hand, the left half is dense enough to hide the background colour. The nonuniformity of the flow front and the deviation from a straight line were the worst at the outlet port side, obviously observed in experiments MOIX2, MOIIX2, RWR1, RWR2, RWRX2 and RWR3. This nonuniformity caused dry spots at the corners near the outlet port area in a few experiments. Although the fluid may leave the mold cavity through the vacuum line, this is not enough to assure good filling. Fluid was noticed to leave the mold cavity in a few experiments while the mold cavity had not been properly filled yet. This leaves the preform with a dry spots which are significant problems in composites. One way to assure an appropriate filling is to allow the resin to come out from the mold cavity for a specific period of time (flushing time).

In the resin transfer molding process, a fiber preform is cut into a desired shape and preplaced in the mold, then the resin is injected to fill the mold. Usually, the fiber preform is not cut precisely enough to fit the mold, and a small clearance is left between the fiber preform and the mold edges. This small clearance usually creates a preferential flow path, called edge flow, during the mold filling stage. This edge flow may disrupt the flow pattern and result in incomplete wetting of the fiber preform. Moreover, it was not possible to get a nice cut in the case of woven roving fiberglass due to fiber bundles slippage in front of the cutter. This rough cut could be seen in the photo of woven roving fiberglass fabric shown in Figure (4.13b). The edge flow phenomenon was clearly noticed in RWRX1, RWR2, RWR3, RWRX3 and RMX3 experiments. Flow front profiles

figures were labeled to show the interesting points. Figures (4.14) and (4.15) are good examples for the nonuniformity and edge flow phenomenon mentioned earlier.

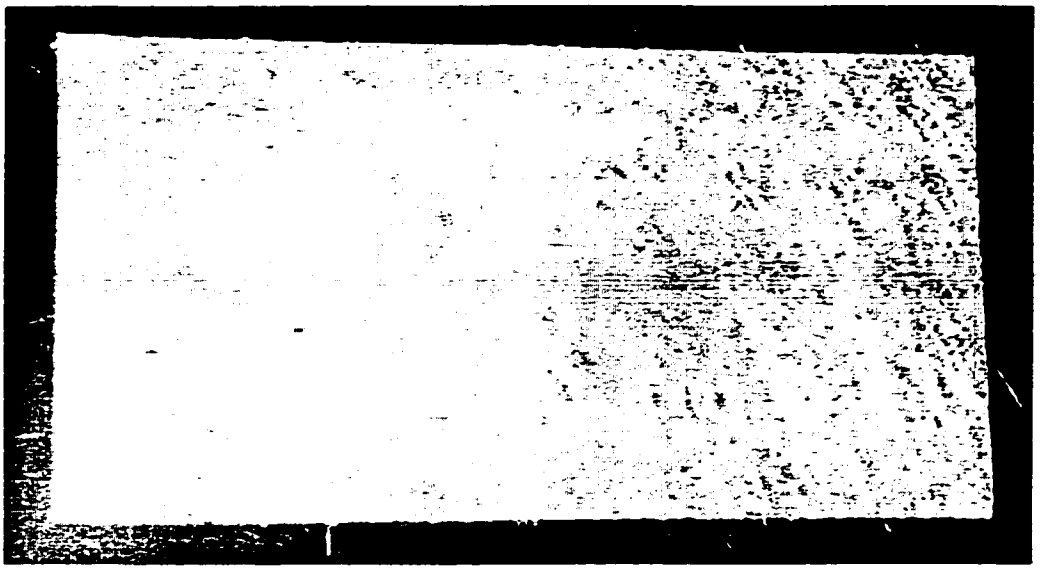

(a)

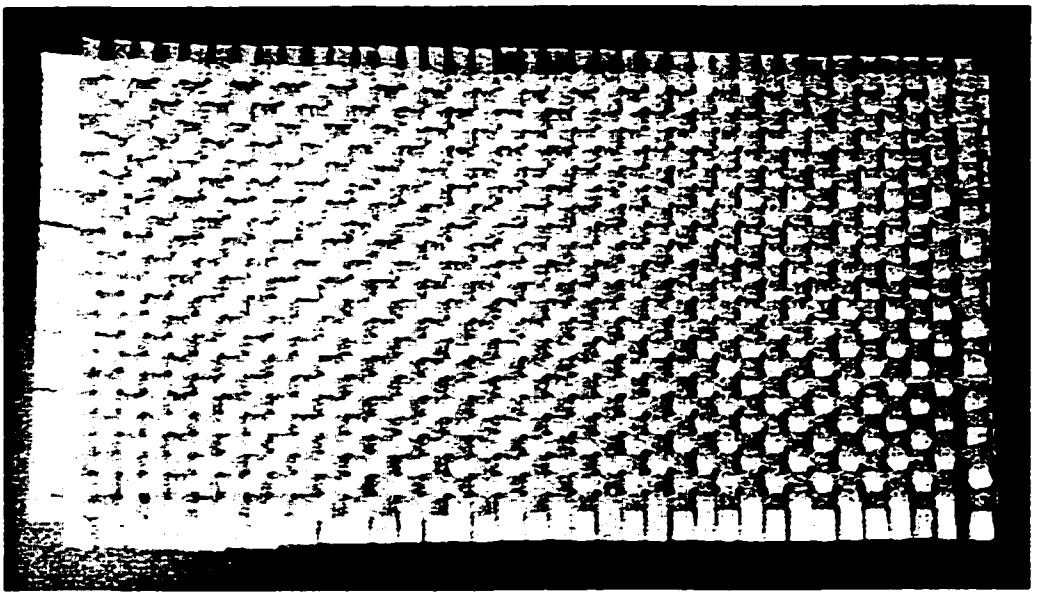

(b)

Figure (4.13) - Photographs of the fabrics used: (a) OCF M8610 chopped strand fiberglass mat (b) Bay Mills style 302 plain weave woven roving fiberglass.

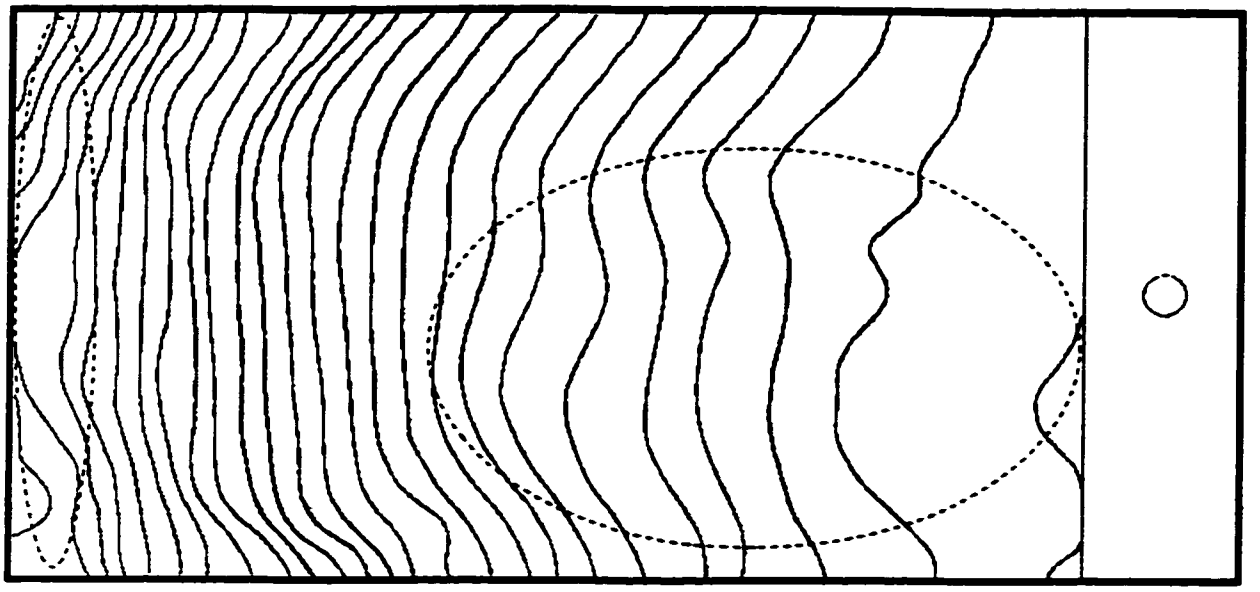

Figure 4.14 - Fluid flow patterns for experiment (RWR1).
($\Delta t = 8s$, $T_{filling} = 217s$)

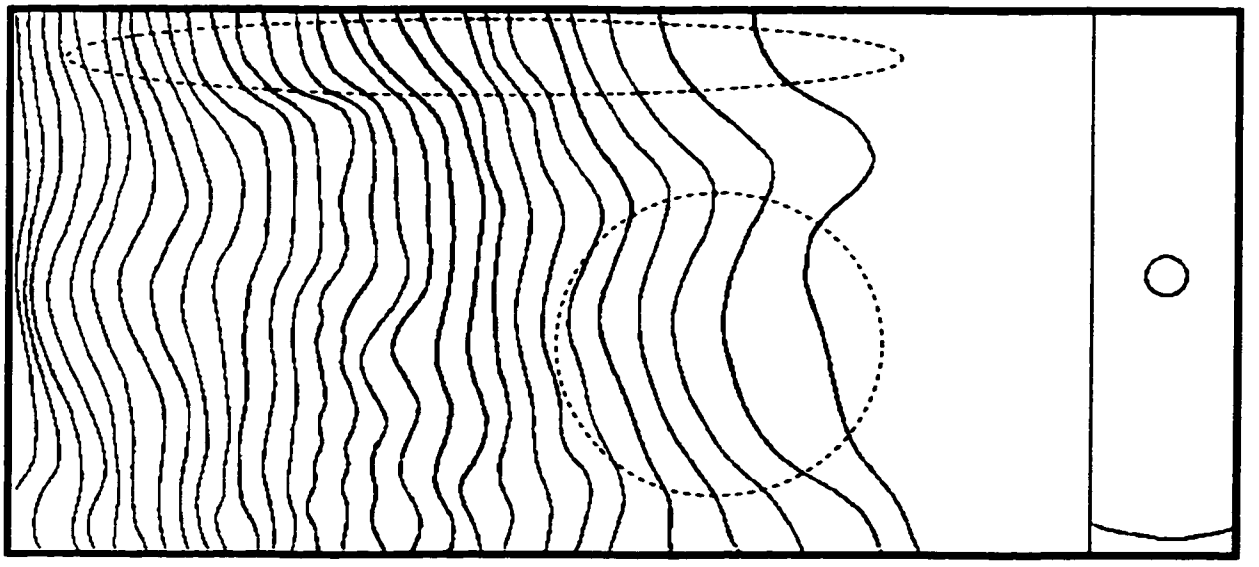

Figure 4.15 - Fluid flow patterns for experiment (RWRX3).
($\Delta t = 20s$, $T_{filling} = 579s$)

4.3.2.2 Flow front position and velocity:

Flow front position and velocity plots of all experiments conducted are shown in Appendix C. The (a) part of each figure shows the flow front position as a function of time, while the (b) part shows the flow front velocity changes with time.

Studying the progression plots reveals that the filling process starts with a high flow front velocity, after which it decreases gradually approaching a saturated value at the end of the filling process. This is clear from the slope of the progression curve, in which the slope has a large value at the beginning and decreases gradually approaching the zero value. This behavior could be observed in the velocity charts as well. The velocity decreases with time due to pressure gradient decrease, as a result the flow profiles become more dense as approaching the vent location. It is noticed that the fluid initial velocity increases as the vacuum level increases. On the other hand, the fluid front velocity is approaching a saturated value at the end of the filling process, and this saturated value decreases as the vacuum decreases. A typical example of flow front progression and velocity curves is shown in Figure (4.16).

The preform effect can be studied by considering the RWR and RM experimental groups (Appendix C). As expected, the velocity charts shows that the initial and the saturated velocities have greater values in RWR case, since the woven roving fiberglass has a higher permeability. On the other hand, the fluid effect may be studied by considering MOI, MOII and RM groups (Appendix C). It is clearly noticed that the initial and the saturated velocities values have the largest values in the MOI case, while the RM group has the lowest values. This also agrees with our expectations, in which higher viscosity fluids have lower velocities.

Most experiments showed a good agreement between the velocity experimental data points and the trend line, while a few others showed discrepancies especially at the vent location side (Figure 4.16). This discrepancy is mainly attributed to the variation in the preform surface density. The discrepancy at the vent side is also attributed to the fact that the fluid is being attracted to the vent port. As a result, the fluid starts leaving the mold cavity rather than filling the rest of the cavity.

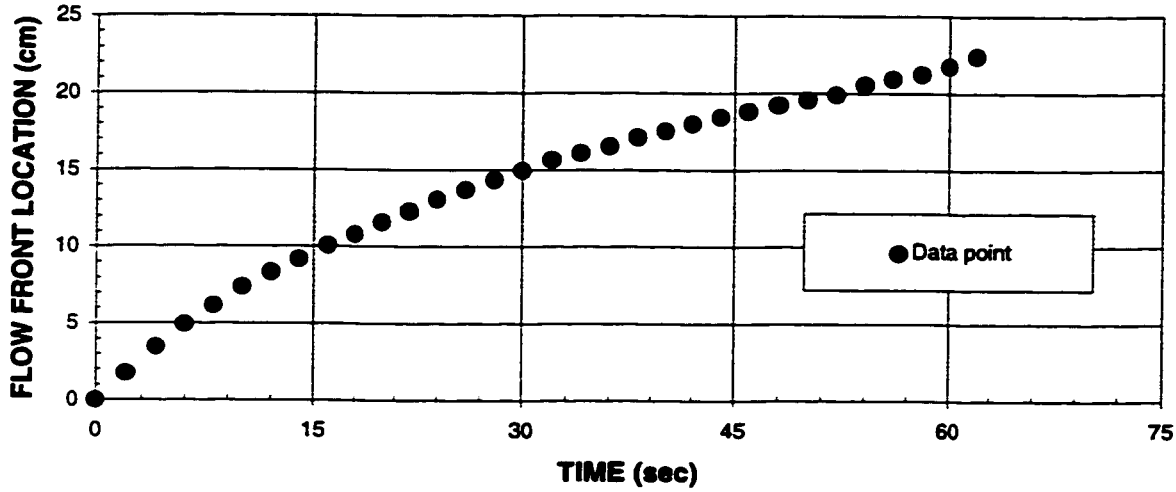

Figure 4.16(a) - Flow front propagation for experiment MOIX1.

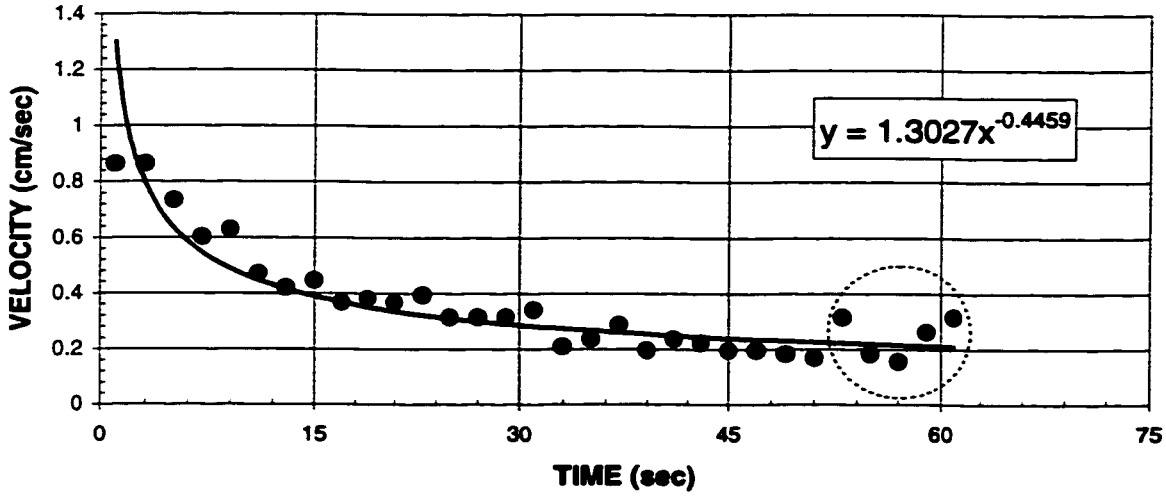

Figure 4.16(b) - Flow front velocity as a function of time for experiment MOIX1.

4.3.2.3 Filling time:

The filling time is the time required for the fluid to fill the mold cavity that contains the preform. Figures (4.17- 4.20) below show the filling time plotted against the vacuum level for MOI, MOII, RWR and RM experiment sets, respectively.

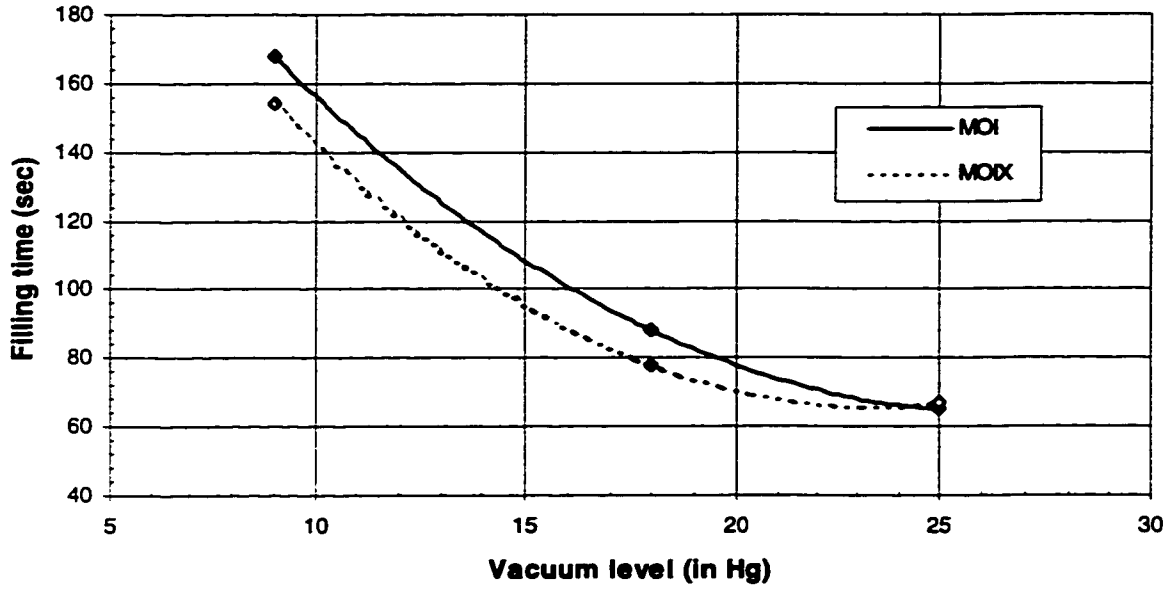

Figure 4.17 - Filling time vs. vacuum level (MOI set).

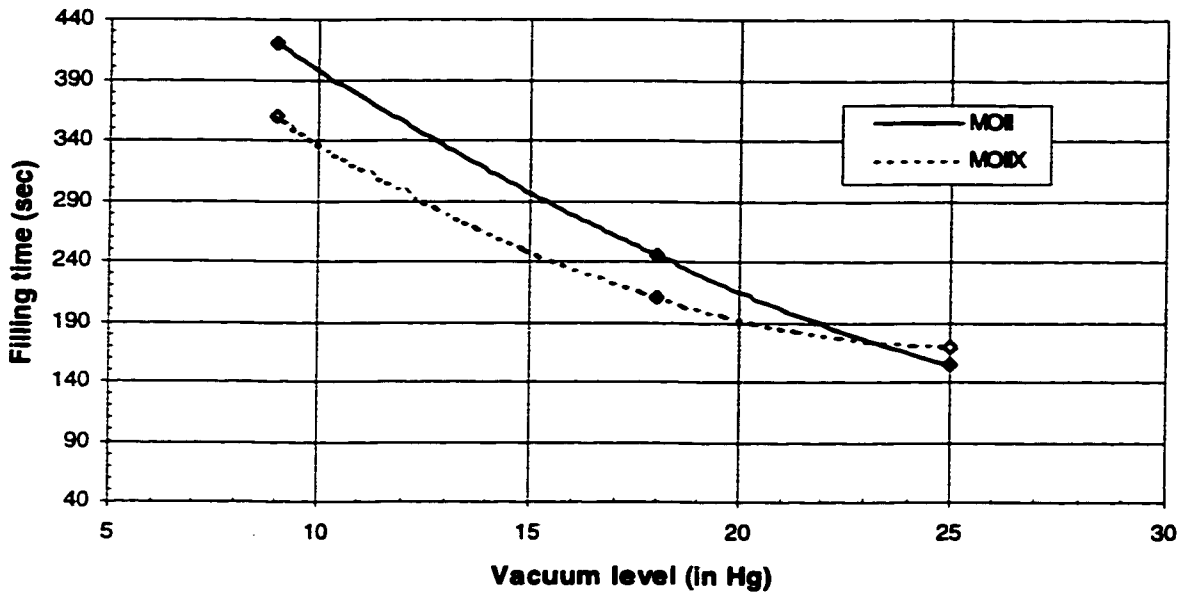

Figure 4.18- Filling time vs. vacuum level (MOII set).

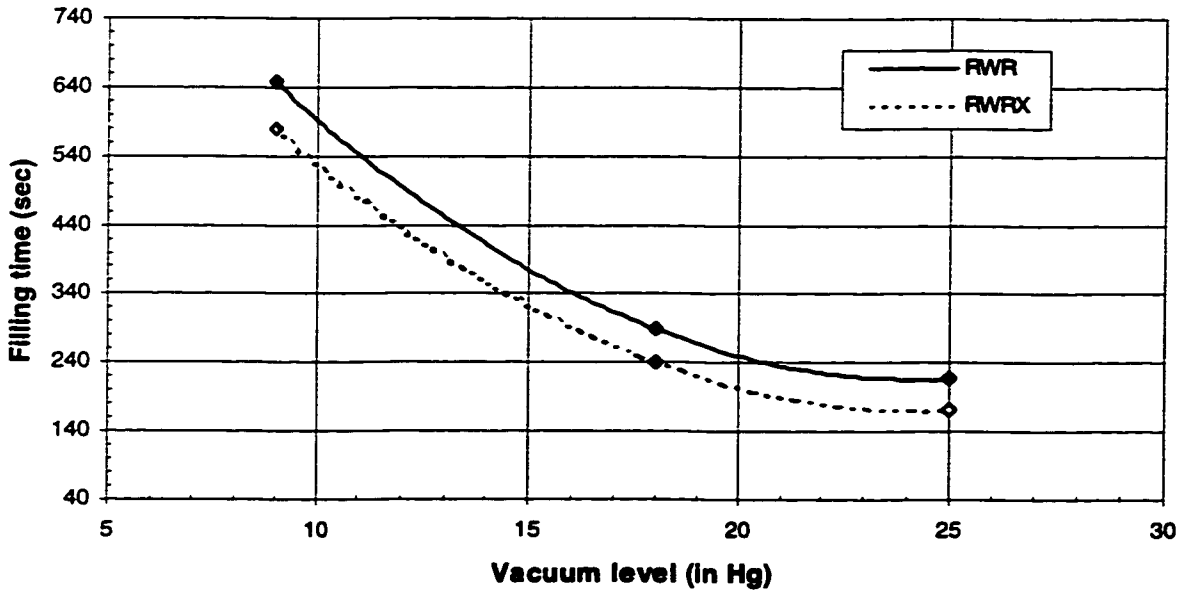

Figure 4.19 - Filling time vs. vacuum level (RWR set).

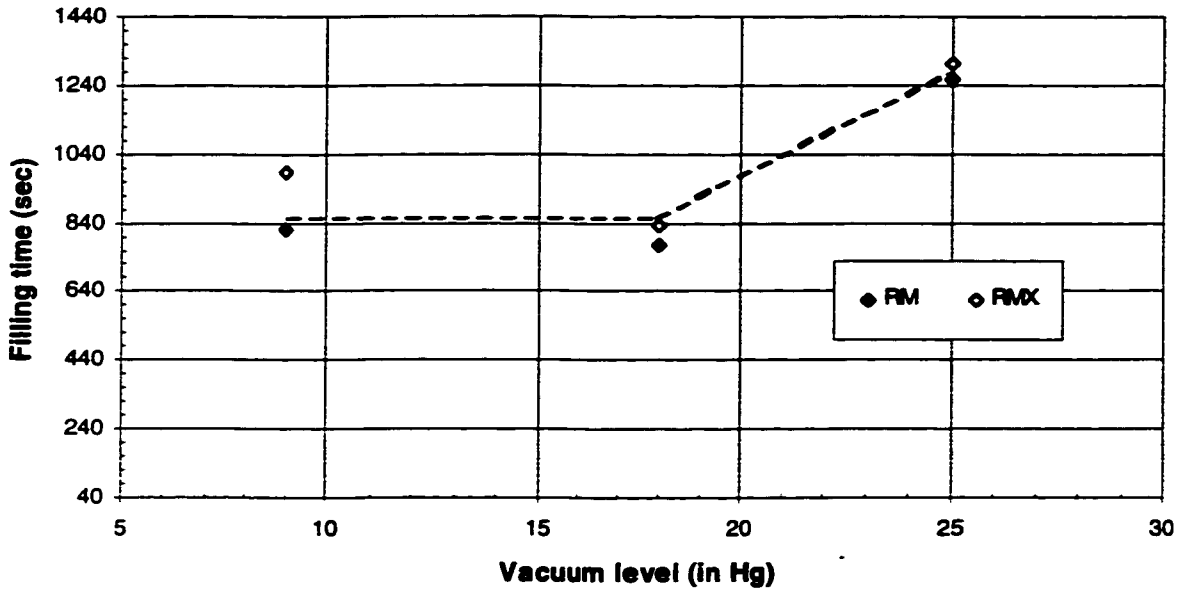

Figure 4.20 - Filling time vs. vacuum level (RM set).

4.3.2.3.1 Effect of vacuum level:

Consider MOI, MOII and RWR experimental sets shown in Figures (4.17, 4.18 and 4.19), respectively. The two experimental trials show good agreement. It is obvious that the filling time decreases as the vacuum level increases for all the considered sets. On the other hand, RM experimental set, shown in Figure (4.20), does not follow the previous trend, i.e. the filling time in this set has its maximum value at the maximum vacuum level, and the medium vacuum level has the minimum filling time. This peculiar trend will be discussed later in this thesis (section 4.3.4).

4.3.2.3.2 Effect of fluid :

Consider Figures (4.17, 4.18 and 4.20) where the same preform type (mat) was used with different fluid types; 10W30 motor oil, 20W50 motor oil and resin,

respectively. The resin (650 mPa.sec) shows the highest filling time at all vacuum levels used, and the10W30 (150 mPa.sec) motor oil has the lowest, while the 20W50 (450 mPa.sec) motor oil was intermediate. It is clear that as the fluid viscosity increases the required filling time increases, too.

4.3.2.3.3 Effect of the preform type:

Consider Figures (4.19) and (4.20) where the resin was used with different preform types; woven roving and mat, respectively. The filling time in case of mat is greater than that of woven roving preform at all vacuum levels used.

4.3.3 Permeability measurement:

All the permeability studies done by other researchers utilized the positive pressure filling technique. Vacuum driven filling technique will be utilized in this work to measure the permeability of two different preform types. In the chopped strand mat, the fibers are randomly oriented, but are all in one plane. Thus the in-plane permeability is isotropic (K_x=K_y), and the out-of-plane principal permeability is perpendicular to the plane of fibers. Since the filling process in RTM process is usually modeled as 2-D flow process, only the in-plane permeability will be measured in this work. On the other hand, only the permeability in the long (warp) direction of the woven roving preform was measured.

4.3.3.1 Average permeability:

The average permeability is the permeability of the preform considering the inlet and the outlet constant pressures, and the filling time for each experiment as shown in equation (4.6). The average permeability values obtained are tabulated in Table (4.2) below, and shown in Figure (4.21) as a function of vacuum level for all experiment sets.

Table 4.2 - Average permeability values.

Experiment	$K_{avg.} \times 10^{-9}$ (m^2)
MOI1	1.303
MOI2	1.272
MOI3	1.202
MOIX1	1.292
MOIX2	1.400
MOIX3	1.266
MOII1	1.584
MOII2	1.342
MOII3	1.389
MOIIX1	1.461
MOIIX2	1.522
MOIIX3	1.567
RWR1	1.648
RWR2	1.639
RWR3	1.300
RWRX1	2.037
RWRX2	1.918
RWRX3	1.411
RM1	0.281
RM2	0.604
RM3	1.007
RMX1	0.273
RMX2	0.580
RMX3	0.859

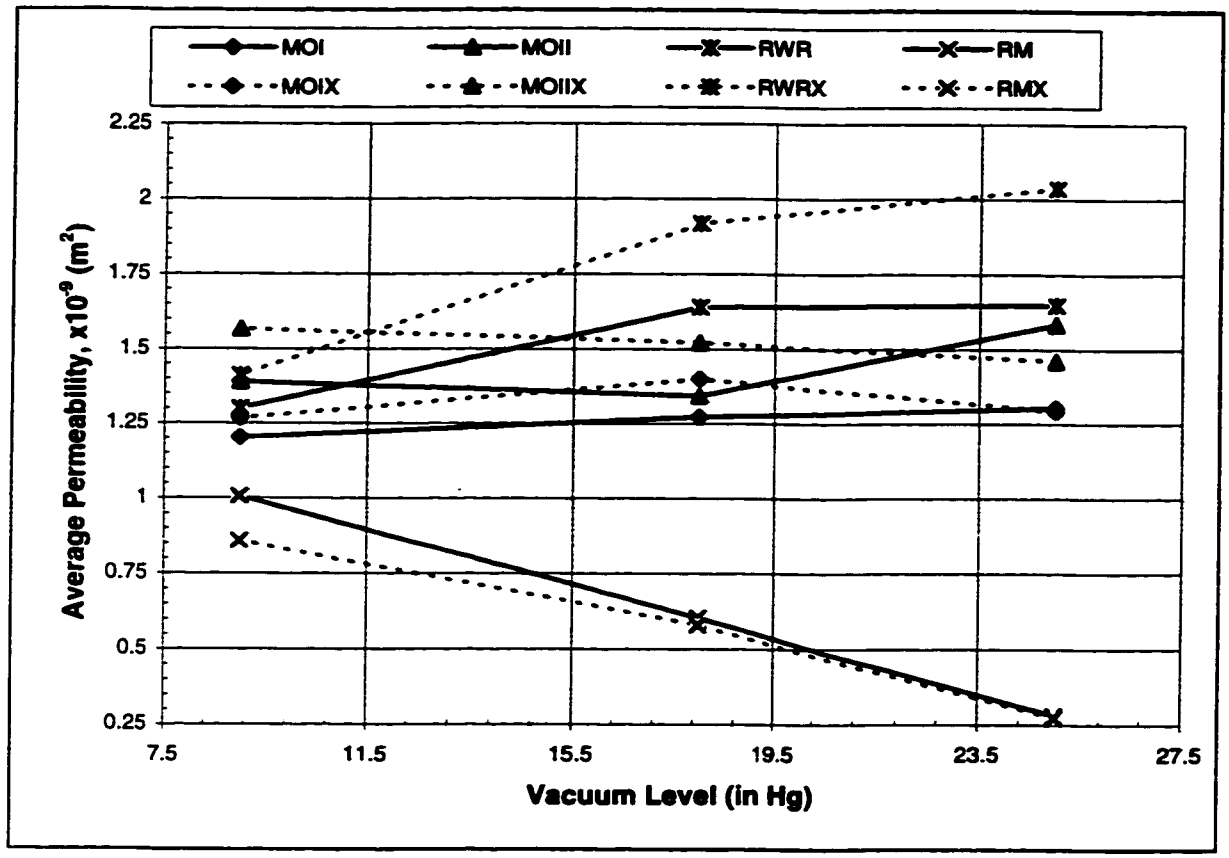

Figure 4.21 - Average permeability vs. vacuum level for all experiment sets.

4.3.3.1.1 Effect of vacuum level:

The average permeability is almost constant in the MOI and MOII experimental sets, and therefore, there is no vacuum level effect on the measured average permeability. RWR set shows an increase in the measured average permeability as the vacuum level is increased from the low level to the medium one, whereas the average permeability stays constant between the medium and the high vacuum level. On the other hand, the measured average permeability of the RM set decreases as the vacuum level increases. This different behavior of RM group will be discussed in section (4.3.4) later in this thesis.

4.3.3.1.2 Effect of fluid :

Consider MOI, MOII and RM experimental sets shown in Figure (4.21) above. MOI and MOII sets show almost the same average permeability values at all vacuum levels, whereas the RM set has lower values. Moreover, the permeability value measured with resin decreases as the vacuum level increases. This resin-mat (RM) behavior is believed to be the result of the interactions between fiber and fluid at the microscopic level.

4.3.3.1.3 Effect of the preform type:

Consider RWR and RM sets shown in Figure (4.21) above. It can be noticed that RM has a lower average permeability at all vacuum level used, and this average permeability increases with the vacuum level.

4.3.3.2 Transient permeability:

Transient Permeability is the permeability of the preform as a function of time considering the local pressure at two different locations through the preform as given by equation (4.14).

4.3.3.2.1 Effect of vacuum level:

Transient permeability plotted against normalized time is shown for each experiment set in Figures (4.22 - 4.25). Consider MOI, MOII and RWR sets shown in Figures (4.22 - 4.24) below. The highest transient permeability values are obtained using the high vacuum level, while the medium and the low vacuum levels give intermediate and lowest transient permeability values, respectively. There is, however, overlapping between the

permeability values in RWR set for the high and medium vacuum levels at the beginning of the filling process. The RM set (Figure 4.25), however, shows an opposite trend throughout the filling process; the highest permeability values are obtained at the lowest vacuum level, and the medium and high levels show intermediate and lowest values. This behavior will be also discussed in section (4.3.4) of this thesis. The same overlapping noticed in RWR can be noticed here with the overlapping occurs at all vacuum levels.

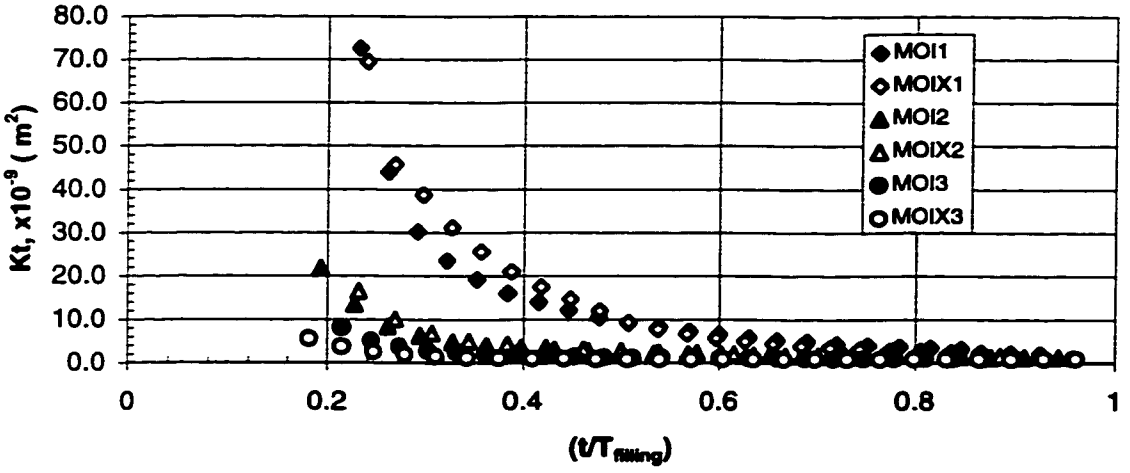

Figure 4.22 - Transient permeability vs. normalized time (MOI set).

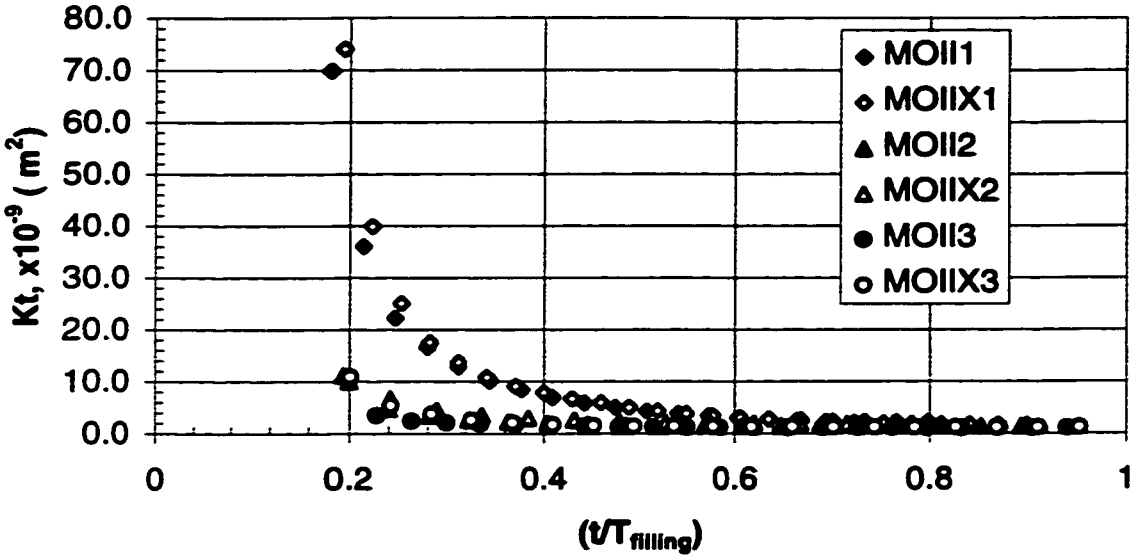

Figure 4.23 - Transient permeability vs. normalized time (MOII set).

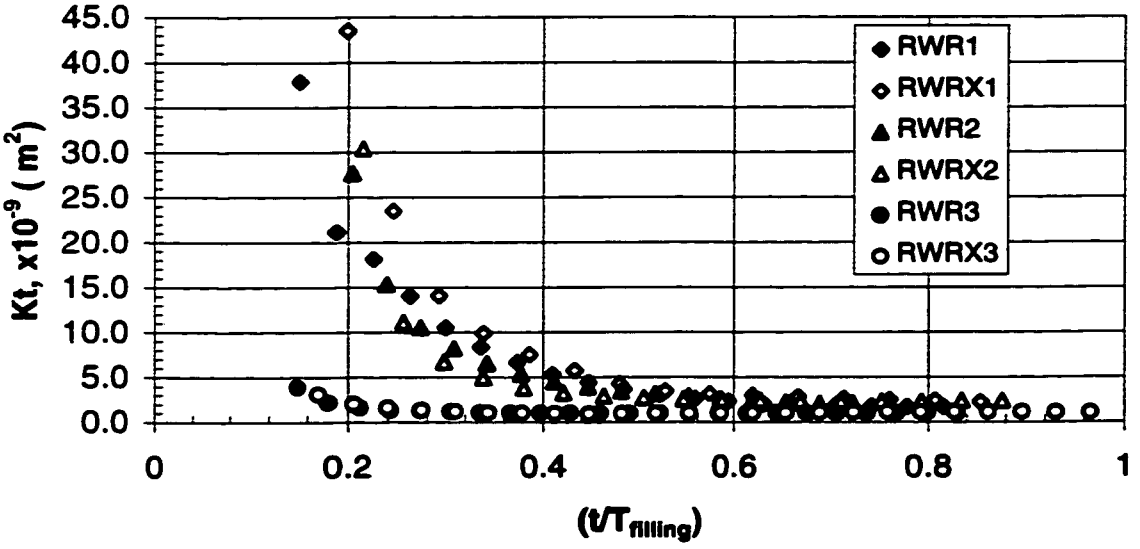

Figure 4.24 - Transient permeability vs. normalized time (RWR set).

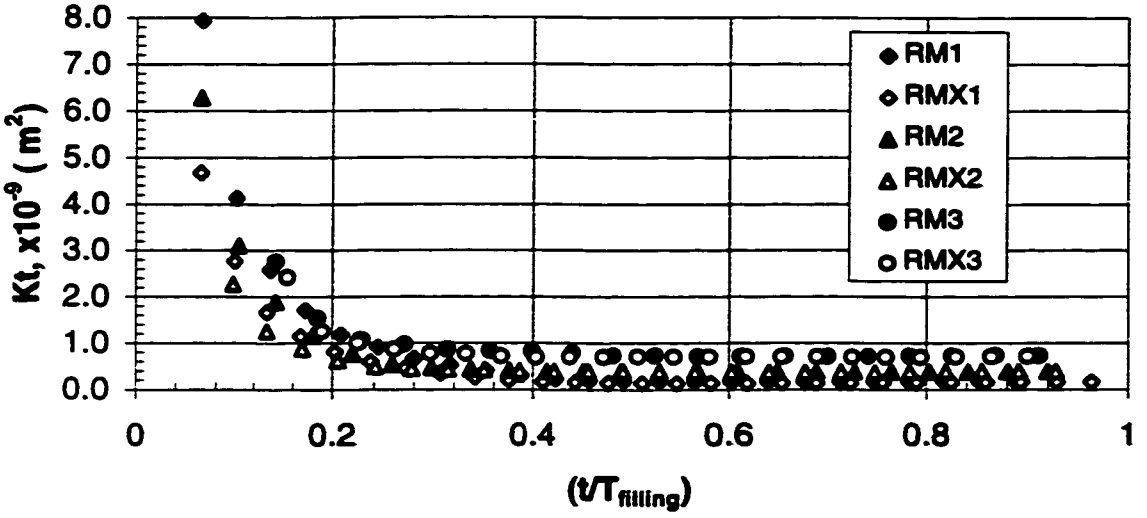

Figure 4.25 - Transient permeability vs. normalized time (RM set).

4.3.3.2.2 Effect of fluid:

Figures (4.26-4.28) present the transient permeability plotted as a function of normalized time for MOI, MOII, and RM experiment sets at the same vacuum level. Figure (4.26) shows the plots at the high vacuum level (25 in Hg), Figure (4.27) at the medium level (18 in Hg) and Figure (4.28) at the low one (9 in Hg). MOI set has the highest transient permeability at all the vacuum levels, MOII set has the intermediate values and RM set has the minimum ones. This is clearly a function of the fluid viscosity; where the higher viscosity gives a lower transient permeability values. An overlapping is noticed in MOI and MOII sets at the medium and low vacuum levels at the beginning of the filling process.

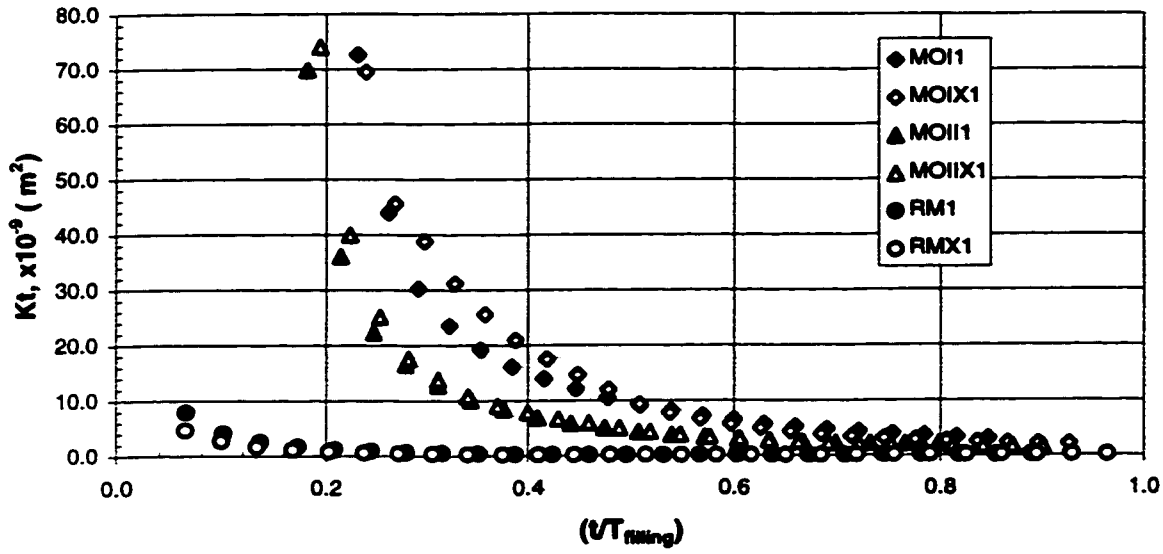

Figure 4.26 - Transient permeability vs. normalized time (High vacuum level).

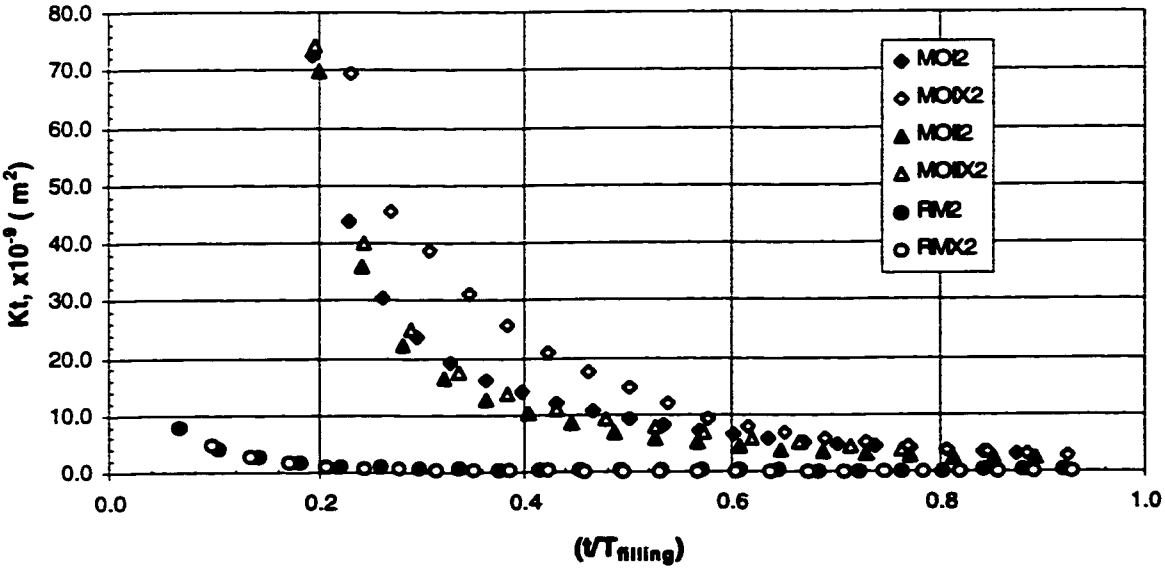

Figure 4.27 - Transient permeability vs. normalized time (Medium vacuum level).

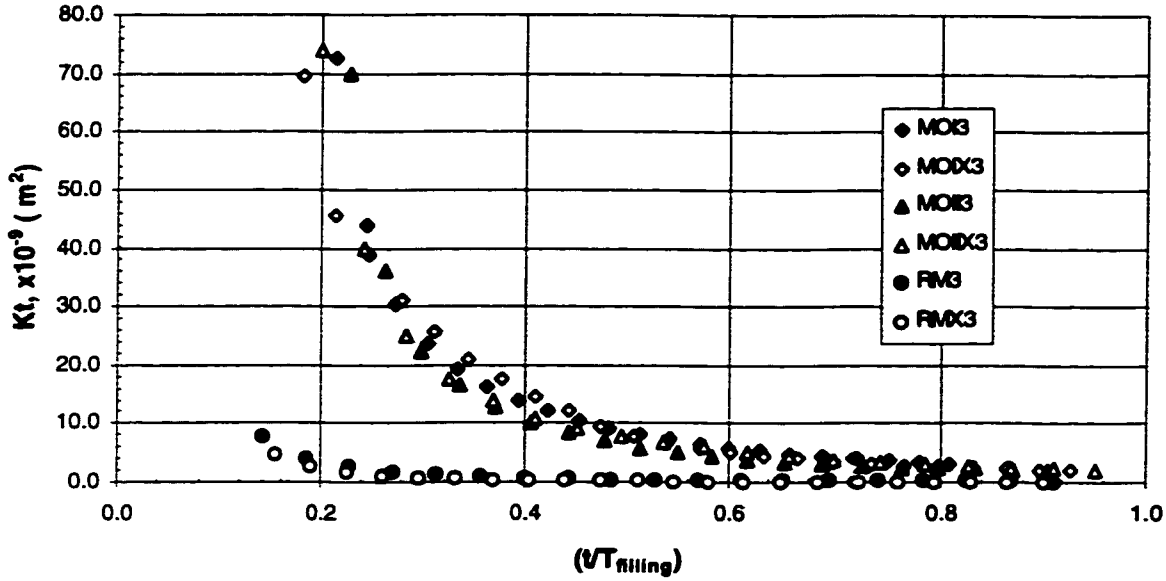

Figure 4.28 - Transient permeability vs. normalized time (Low vacuum level).

4.3.3.2.3 Effect of the preform type:

RWR and RM experiment sets were considered to study the effect of the preform on the transient permeability. Figures (4.29-4.31) show the transient permeability plotted as a function of the normalized time at the high , medium and low vacuum levels, respectively. Obviously, the transient permeability of the woven roving preform (RWR set) is greater than that of mat preform (RM set).

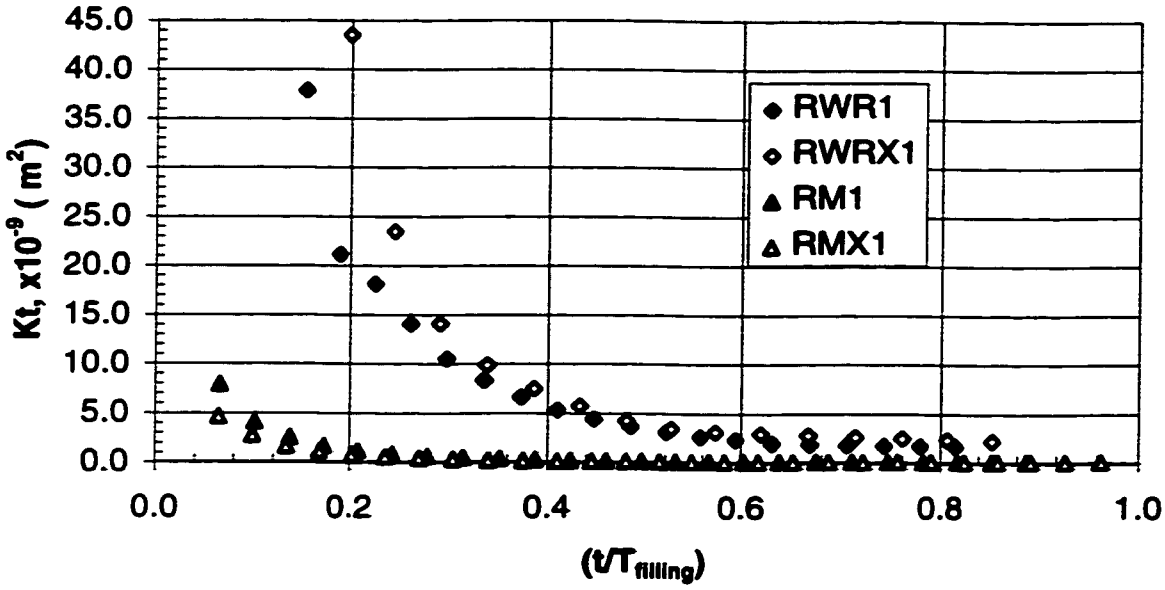

Figure 4.29 - Transient permeability vs. normalized time (High vacuum level).

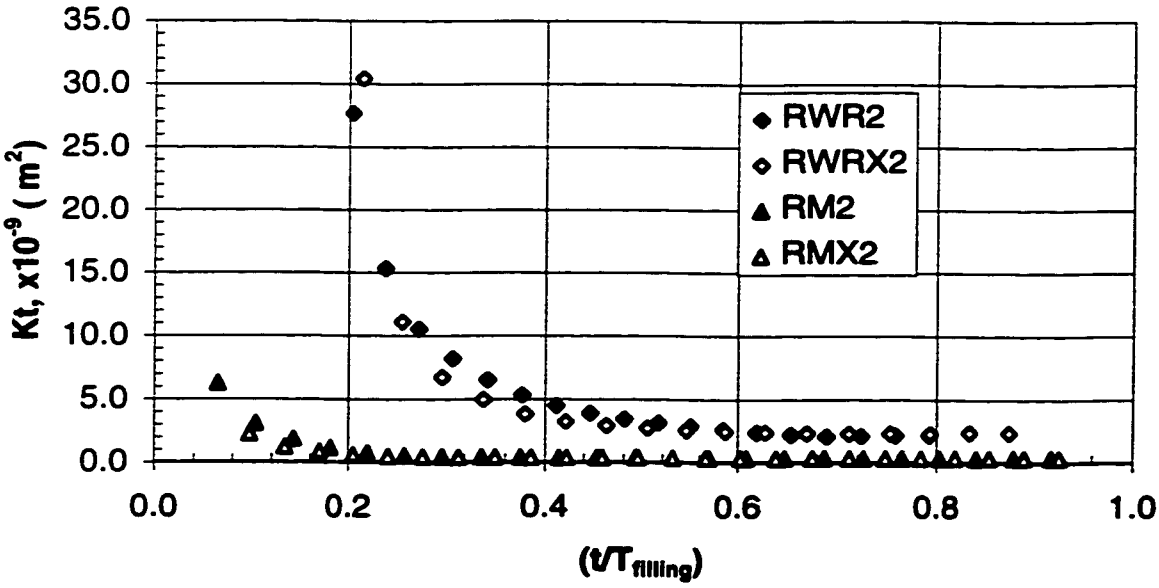

Figure 4.30 - Transient permeability vs. normalized time (Medium vacuum level).

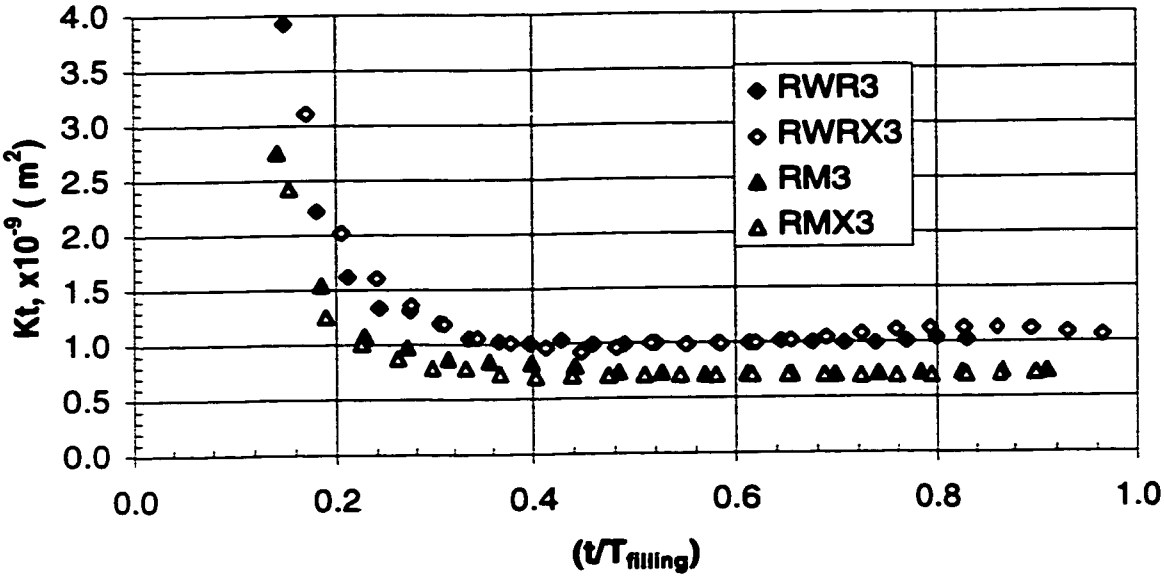

Figure 4.31 - Transient permeability vs. normalized time (Low vacuum level).

4.3.4 Wetting-out Process:

In the resin transfer molding (RTM) manufacturing process, two types of flow occur simultaneously, i.e., the micro-flow and the macro-flow. The macro-flow involves distribution of the fluid through the mold cavity by filling the gaps between the fiber bundles. On the other hand, the micro-flow involves penetration of the resin into fiber bundles.(i.e. filling the gaps among the fibers in the bundles). At low flow velocity, the micro-flow is ahead of the macro-flow due to capillary effect. On the other hand, the macro-flow is ahead of the micro-flow at high flow velocity, since the filling process is dominated by the applied pressure. This flow nature complicates the mold filling process, and may lead to potential problems such as dry spots and voids. Due to the fact that the physical and mechanical properties, as well as the finish of the final product, are strongly affected by voids and dry spots, the mold filling stage is one of the key issues in the RTM process.

Figures (4.32-4.39) below show photos of the mold cavity at the end of the filling process for different experiments. Dry spot phenomenon was clearly noticed in some of the experiments conducted (Figures 4.34b,4.35a,4.37a,4.39b) at the vent location side. This phenomenon is attributed to the disturbance that occurs to the flow profiles due to variations in the preform surface density. As a result, the flow profile takes a pattern ,different from a straight line, that depends on the preform surface density distribution. Consequently, the fluid reaches the vent port before properly filling the whole mold cavity leaving the dry area isolated from the vacuum line (Figures B.7b, B.8a, B.10a, B.12b). Since the pressure difference between the vacuum line and the mold cavity is

greater than that between the fluid in the mold cavity and the isolated dry area, this area is left mainly dry forming what is called a dry spot area.

The wetting-out process was not noticed in the motor oil experiments, even with the highest vacuum level, due to high flow rates. As could be seen in (Figures 4.32,4.33), the preform right edge and even the surface fibers could be recognized easily which indicates poor wetting-out. On the other hand, the wetting-out process was clearly noticed in the resin experiments (Figures 4.34-4.39). Although transparent appearance, which is a good indicator of better wetting, was noticed in the RWR experiments (note the pressure transducers locations (black circles) in Figures 4.34-4.36), the preform was not properly wetted-out even with the highest vacuum level (Figure 4.34). Surface fiber bundles and the preform right edge could be recognized which indicates that the preform was not properly wetted out. This transparent appearance was not noticed in the motor oil experiments which leads to the fact that the wetting out was better achieved in RWR experiments. The high vacuum level gave the best wetting out. This fact could be drawn by considering the high vacuum level (Figure 4.34) and the low vacuum level (Figure 4.36) experiments. As could be seen, the preform of the high vacuum level is more transparent than that in case of low vacuum level. All pressure transducers ports are visible through the transparent preform in the high vacuum level experiment (Figure 4.34), whereas the transducers ports are not clear in the low vacuum level experiment (Figure 4.36) except the first one. Besides, the surface preform bundles in the low vacuum experiment are much clearer than those in the case of high vacuum level. The preform was nicely wetted-out in RM experiment group (Figures 4.37-4.39). The preform was so transparent in all vacuum levels, as a result, it was not possible to recognize the

preform right edge. Moreover, the transducers ports appeared clearly as dark black circles. However, the high vacuum level experiment (Figure 4.37) gave the best wet-out with the transducers ports nicely revealed. Medium and low vacuum experiments (Figures 4.38,4.39) ended up with just part of the preform properly wetted-out.

As mentioned earlier in this thesis (chapter 1), the natural wet-out of an arbitrary surface by any liquid occurs only if the contact angle between the surface and the contacting liquid is less than 90°. At the point of first contact, the contact is tangential between fibers. As the liquid wets the fibers a concave meniscus is formed and the wetting front starts to move inward to minimize the surface energy. The liquid continues to move inward until the equilibrium is achieved and no pressure differential exists across the liquid surface, at which the flow ceases. The only way natural wetting can continue is if the liquid front touches another fiber prior to reaching the equilibrium position. It is to be expected that in organized reinforcements there will be regions that are naturally wet-out by the radial flow in the absence of any external pressure. On the other hand, other areas in the tow require additional driving pressures to permit full wet-out.

The pressure profiles of RM experiments, i.e. the pressure change with location through preform, are shown in Figure (4.40) at different time steps during the filling process. Note that each pressure profile starts at the inlet pressure and ends at the vacuum level used, which is the pressure at the flow front during the filling process. Getting the approximate length of the good wetted area of the preform, i.e. the area with the transparent appearance, from (Figures 4.37-4.39), one could find the pressure difference required to achieve a properly wetted preform from the pressure profiles plots. The pressure difference required to get an appropriate preform wetting out is tabulated in

Table (4.3) below. This data was collected twice during the filling process. The first time was at the moment the flow reached the second pressure transducer port location (Figures 3.1,3.5), and the second one was at the end of the filling process. These pressure difference values may be nondimensionalized, so that they can be more useful and meaningful, using the following relations:

$$\text{Dimensionless Pressure Difference} = \frac{\Delta P_{avg.}}{\frac{1}{2}\rho \bar{V}^2} \qquad \bar{V} = \frac{L}{T_{filling}} \tag{4.17}$$

where:

$\Delta P_{avg.}$ = the average pressure difference required to get good wet-out
$\bar{V}$ = the average filling velocity
ρ = the fluid mass density
L = the preform length
$T_{filling}$ = the filling time

The Reynolds numbers (*Re*) for resin-mat experiments were obtained and tabulated in Table (4.3) using the following equation:

$$Re = \frac{\rho \bar{V} L}{\mu} \tag{4.18}$$

where μ is the fluid viscosity.

The RM group behaved in a peculiar way as discussed earlier. In the filling time study all the experiments (but RM group) showed the same trend, i.e. the cavity filling time decreases as the vacuum level increases. The RM group showed a different trend; the minimum filling time was achieved using the medium vacuum level (i.e. the filling time was about 1000s with the low level, about 840s with the medium, and about 1280s

with the high vacuum level). Moreover, the RM group showed the opposite trend in the case of permeability comparisons. This strange behavior is attributed to the fluid-preform compatibility. It was noticed that the wet-out was not properly achieved in the case of low and medium vacuum levels, whereas the high vacuum level gave the best wet-out. This was noticed from the transparent appearance of the preform at the end of the filling process in each experiment. The more transparent the preform, the best wet-out of the individual fibers is achieved. The good wet out of the preform indicates that there is more micro flow among the fibers in the fiber tows. This makes the high vacuum level experiment takes more time to fill the mold cavity. In other words, filling the mold cavity using the high vacuum level is the same as filling larger volume, thus it takes longer time to complete the filling process. Since the average permeability was calculated using equation (4.6), in which the filling time is involved, the same trend in filling time study is to be expected. Since equation (4.14) was used to calculate the transient permeability, in which the time is also involved, the same trend as in the average permeability is expected.

The wet-out of a preform is a measure of how well the liquid impregnates the fibers. The equilibrium contact angle (θ) that the liquid forms with the solid is a direct indication of the degree of wetting, i.e. the attraction of the liquid for the solid. When $\theta>0°$, the liquid is said to be non-spreading. However, the wetting is still possible under pressure application to spread the liquid over the solid surface. When $\theta=0°$, the liquid is called a spreading liquid. Steenkamer, et. al [38] measured the contact angles that motor oil and Vinyl ester make with the single glass fibers. They found that Vinyl ester had an average contact angle of 31.5°, whereas motor oil was spreading (i.e. $\theta=0°$). This explains

the motor oil behavior in MOI and MOII groups, in which motor oil easily followed the macro-channels, formed between fiber bundles, rather than penetrating the fiber bundles themselves. As a result, the macro-flow was so fast, and the mold cavity was apparently filled in a short time, whereas the micro-flow was just started. On the other hand, resin with a 31.5° contact angle hardly followed the macro-channels under pressure. This made the resin takes longer time to impregnate the fiber bundles, giving the micro-flow (wetting) a chance to occur under the required pressure difference.

Table 4.3 - Approximate dimensionless pressure difference required for good wetting out.

	ΔP (kPa)				Reynolds #
Experiment	**At pressure transducer #2**	**At the end of the filling process**	$\Delta P_{avg.}$ **(kPa)**	$\frac{\Delta P_{avg.}}{\frac{1}{2}\rho \bar{V}^2} \times 10^9$	$\frac{\rho \bar{V} L}{\mu}$
RM1	19	24	21.5	1.279	0.07
RMX1	25	24	24.5	1.566	0.06
RM2	25	25	25	0.562	0.11
RMX2	25	34	29.5	0.768	0.10
RM3	30	36	33	0.837	0.10
RMX3	29	33	31	1.134	0.08
			$\left(\frac{\Delta P_{avg.}}{\frac{1}{2}\rho \bar{V}^2}\right)_{avg.}$	**1.024**	

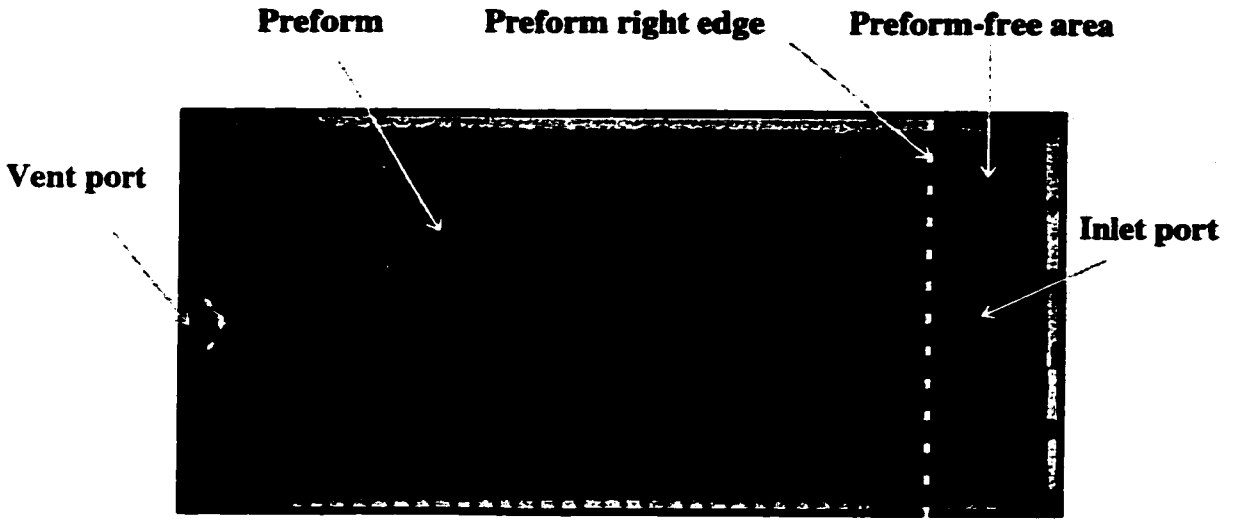

Figure 4.32(a) - Photo of MOI1 mold cavity at the end of the filling process.

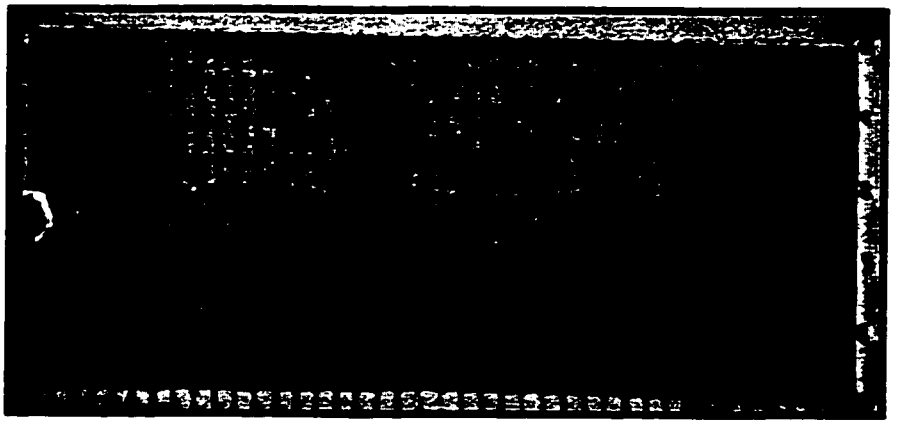

Figure 4.32(b) - Photo of MOIX1 mold cavity at the end of the filling process.

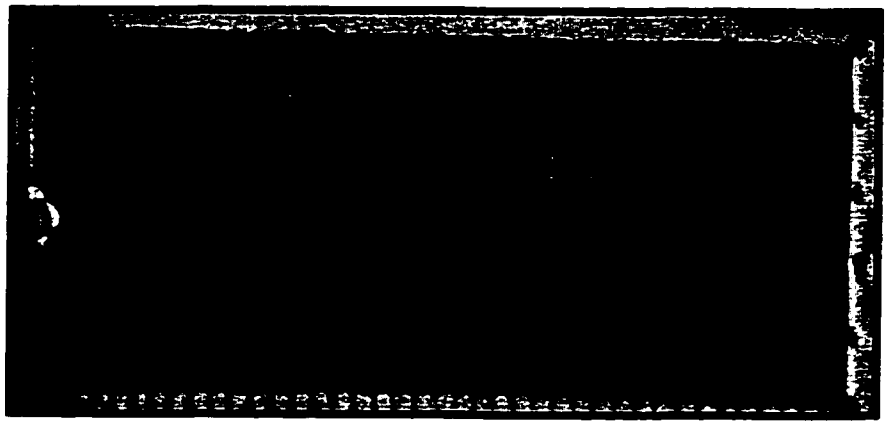

Figure 4.33(a) - Photo of MOII1 mold cavity at the end of the filling process.

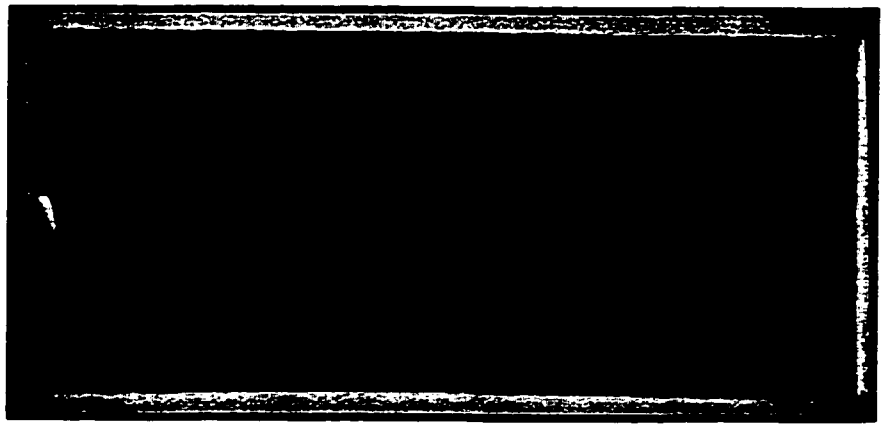

Figure 4.33(b) - Photo of MOIIX1 mold cavity at the end of the filling process.

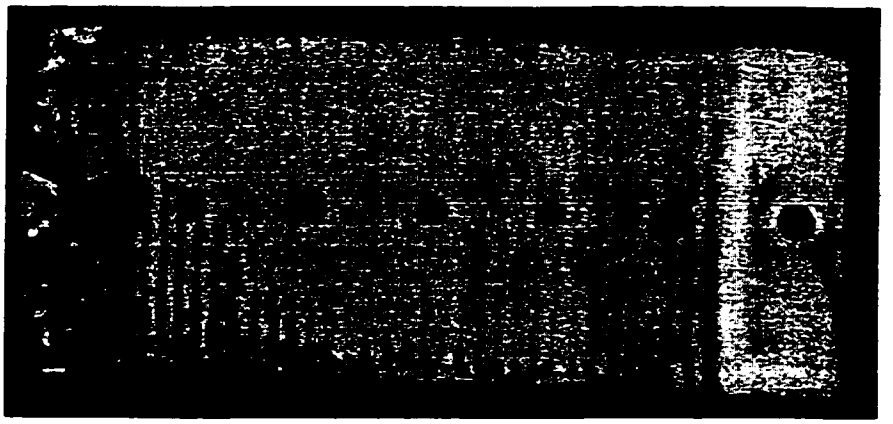

Figure 4.34(a) - Photo of RWR1 mold cavity at the end of the filling process.

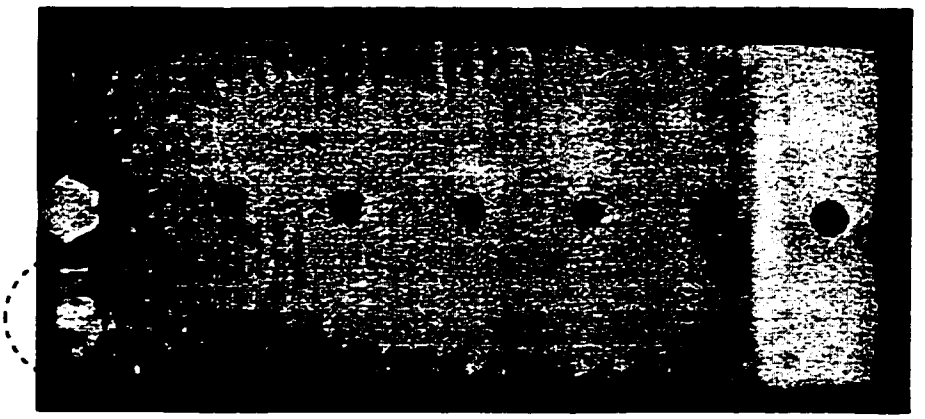

Figure 4.34(b) - Photo of RWRX1 mold cavity at the end of the filling process.

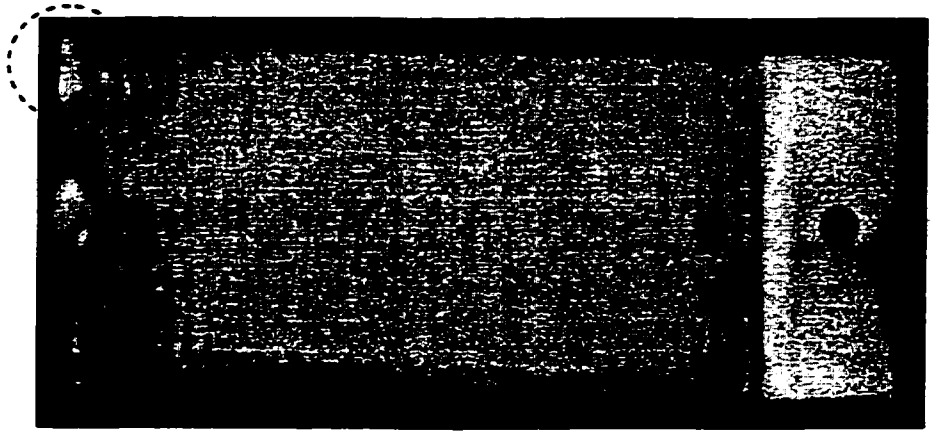

Figure 4.35(a) - Photo of RWR2 mold cavity at the end of the filling process.

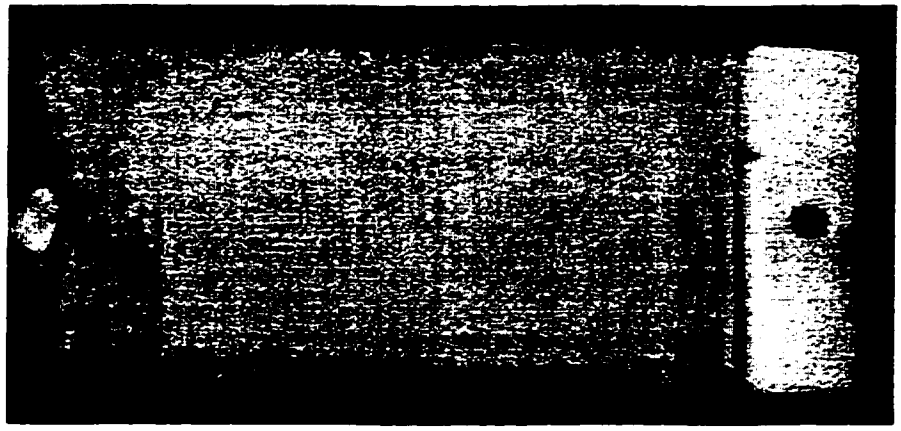

Figure 4.35(b) - Photo of RWRX2 mold cavity at the end of the filling process.

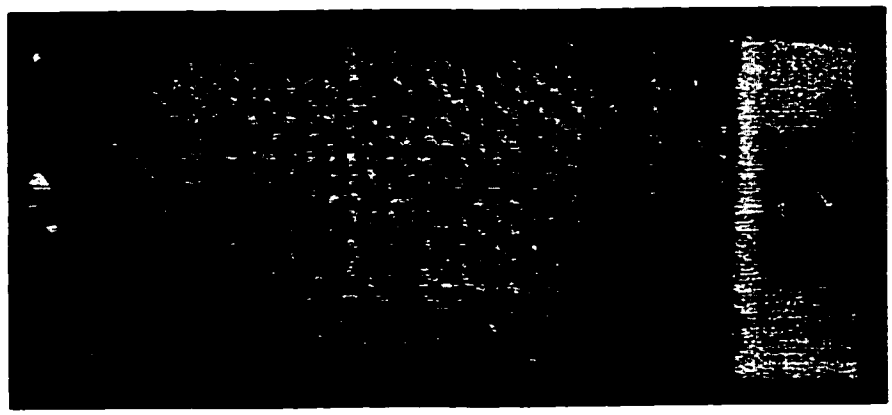

Figure 4.36(a) - Photo of RWR3 mold cavity at the end of the filling process.

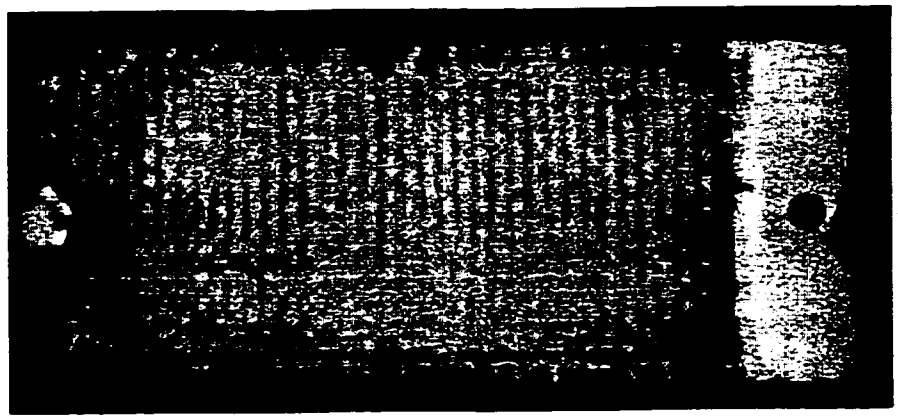

Figure 4.36(b) - Photo of RWRX3 mold cavity at the end of the filling process.

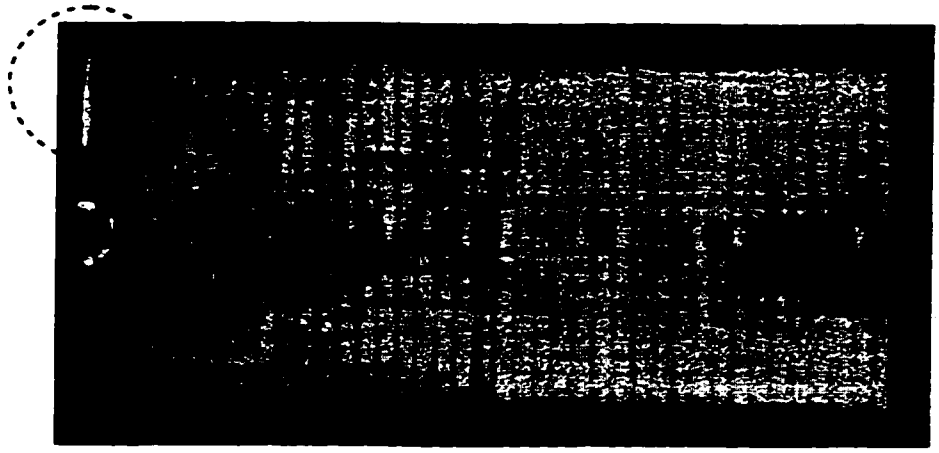

Figure 4.37(a) - Photo of RM1 mold cavity at the end of the filling process.

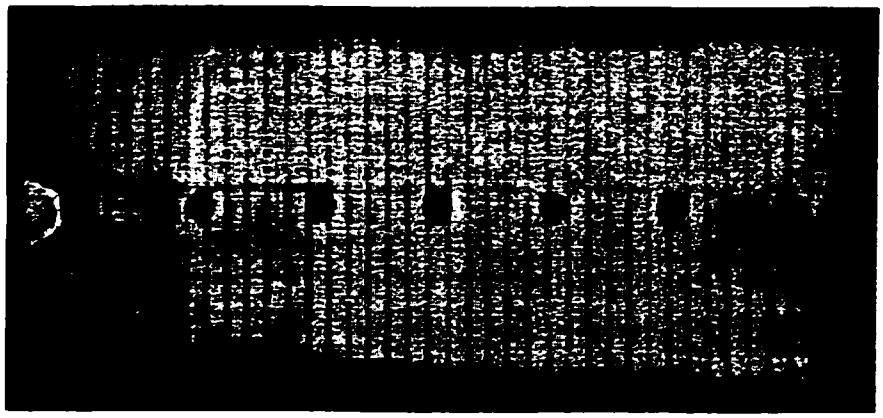

Figure 4.37(b) - Photo of RMX1 mold cavity at the end of the filling process.

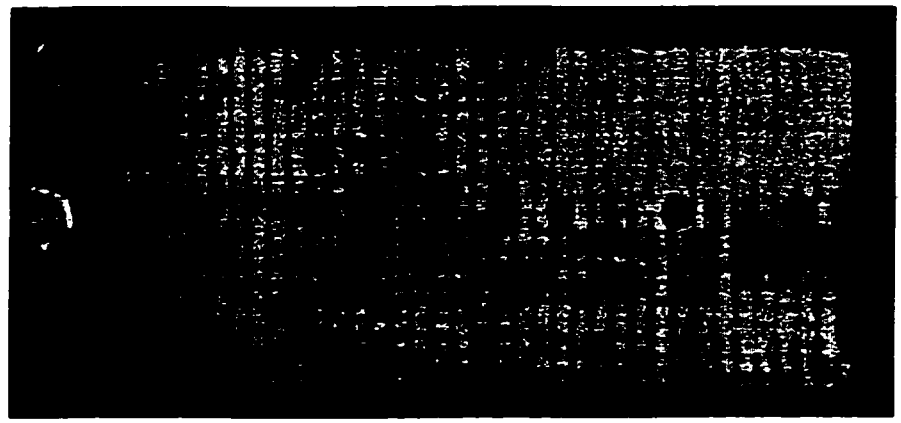

Figure 4.38(a) - Photo of RM2 mold cavity at the end of the filling process.

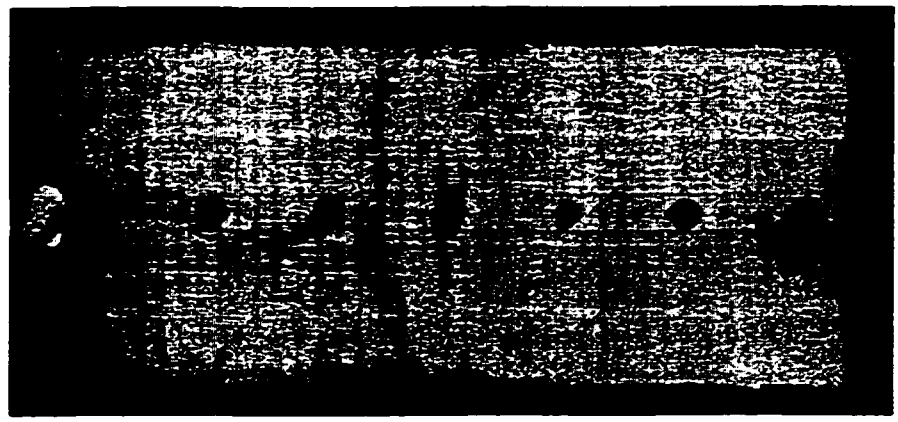

Figure 4.38(b) - Photo of RMX2 mold cavity at the end of the filling process.

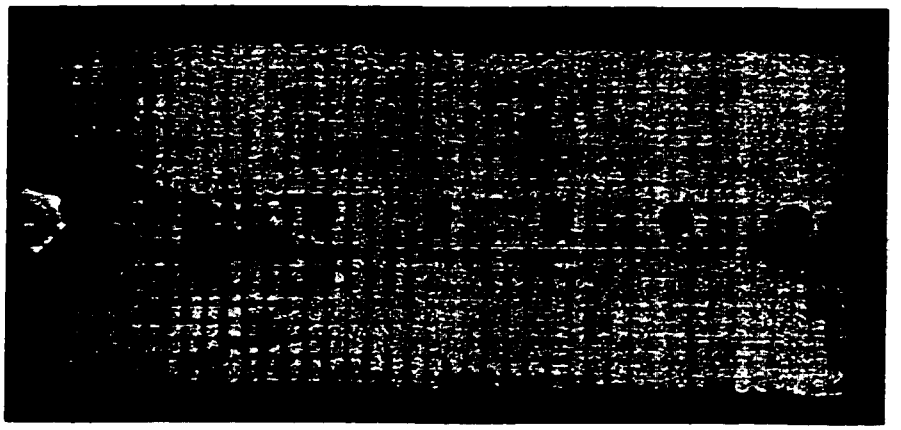

Figure 4.39(a) - Photo of RM3 mold cavity at the end of the filling process.

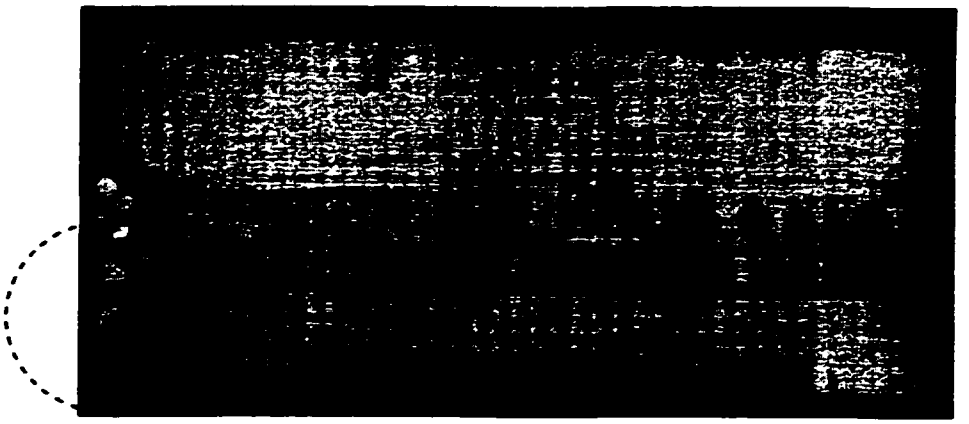

Figure 4.39(b) - Photo of RMX3 mold cavity at the end of the filling process.

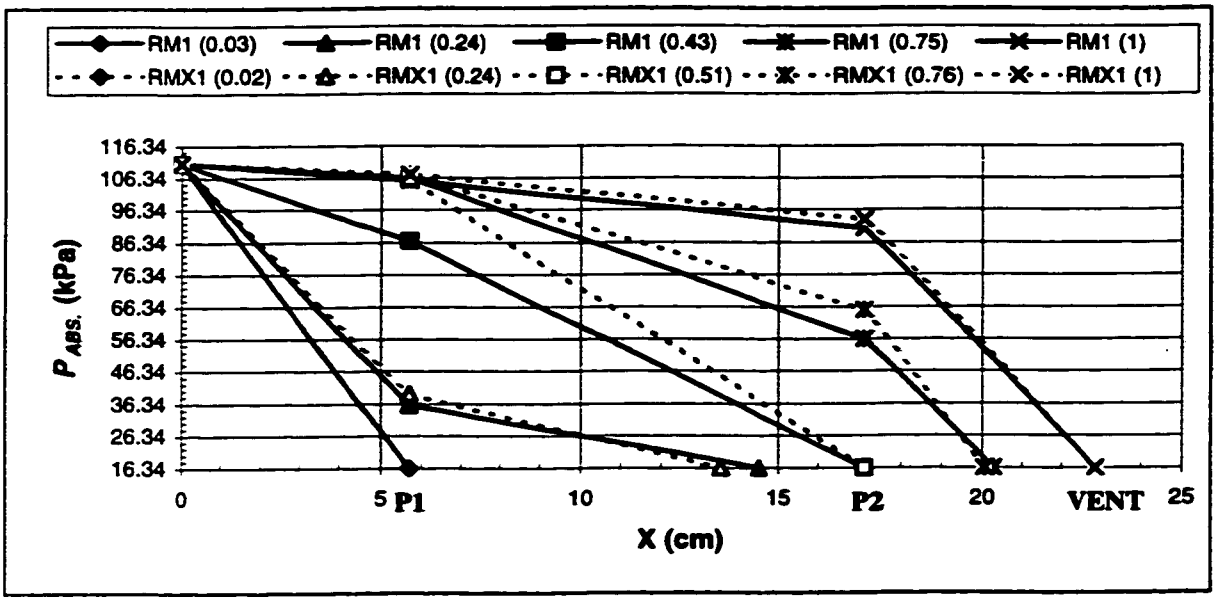
RM1 (0.03)
RM1 (0.24)
RM1 (0.43)
RM1 (0.75)
RM1 (1)
RMX1 (0.02)
RMX1 (0.24)
RMX1 (0.51)
RMX1 (0.76)
RMX1 (1)
116.34
106.34
96.34
86.34
76.34
66.34
56.34
46.34
36.34
26.34
16.34
P ABS. (kPa)
0
5 P1
10
15 P2
20
VENT
25
X (cm)

(a)

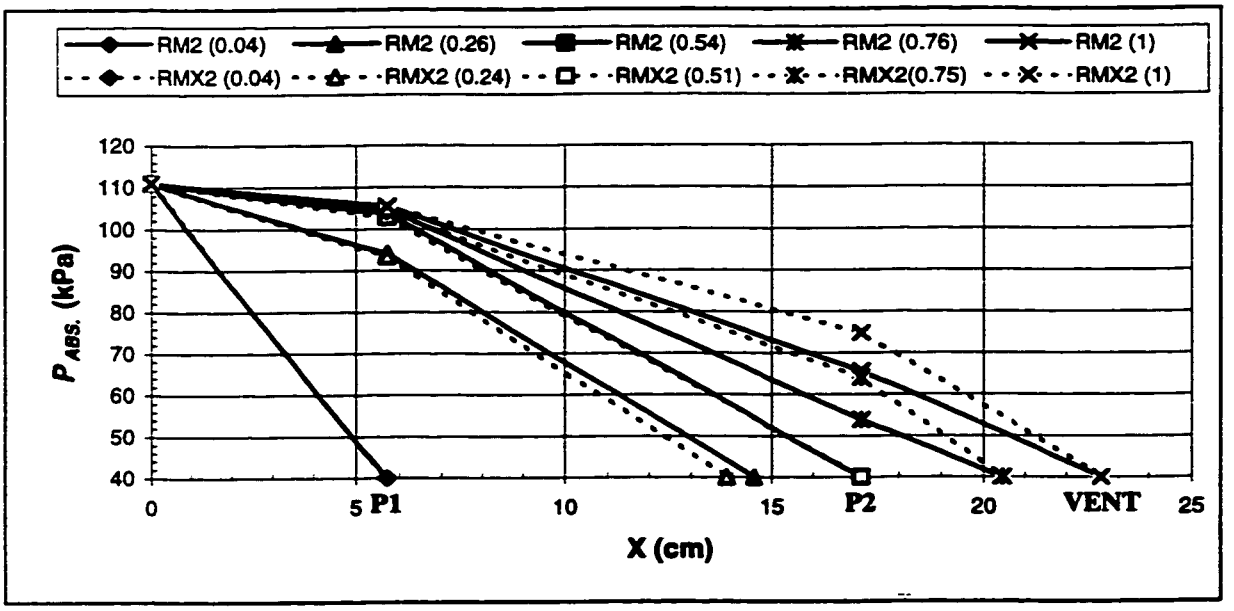
RM2 (0.04)
RM2 (0.26)
RM2 (0.54)
RM2 (0.76)
RM2 (1)
RMX2 (0.04)
RMX2 (0.24)
RMX2 (0.51)
RMX2(0.75)
RMX2 (1)
120
110
100
90
80
70
60
50
40
P ABS. (kPa)
0
5 P1
10
15 P2
20
VENT
25
X (cm)

(b)

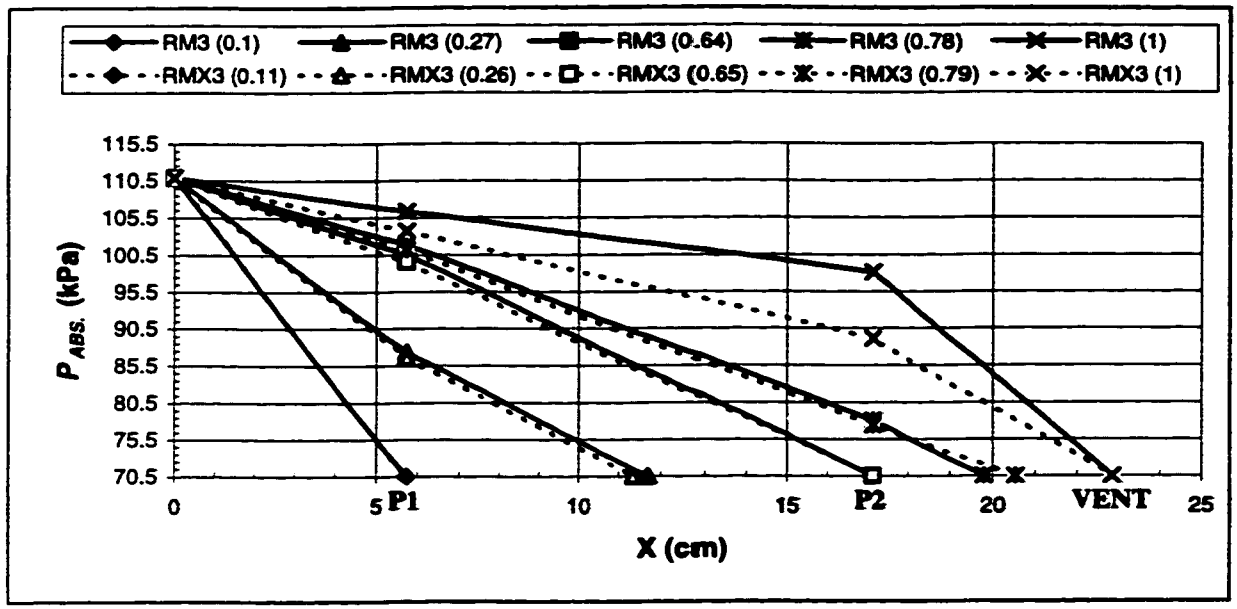

(c)

Figure 4.40 - Pressure profiles of RM experiment group at different time steps during the filling process. (The number next to the experiment name indicates the dimensionless time variable, i.e time divided by the total filling time.)

4.3.5 Constant inlet-pressure scale relation verification:

According to the functional relation given by equation (4.16), the data obtained from geometrically similar mold cavities should follow the same curve when plotted as $\frac{t(P_O - P_{VAC.})}{\mu}$ versus $\frac{K_S(P_O - P_{VAC.})}{\mu q(t) L}$. Figure (4.41) shows those dimensionless curves for the four experimental groups conducted. A good agreement was achieved with MOI, MOII and RWR groups, while RM group showed a significant discrepancy. This peculiar behavior is attributed to the fact that more micro-flow occurs in the RM experimental

group, i.e. longer filling time is required. In addition, same $\frac{K_S(P_O - P_{VAC.})}{\mu q(t) L}$ points were picked up to plot the curves, whereas time is involved in $\frac{t(P_O - P_{VAC.})}{\mu}$ calculation.

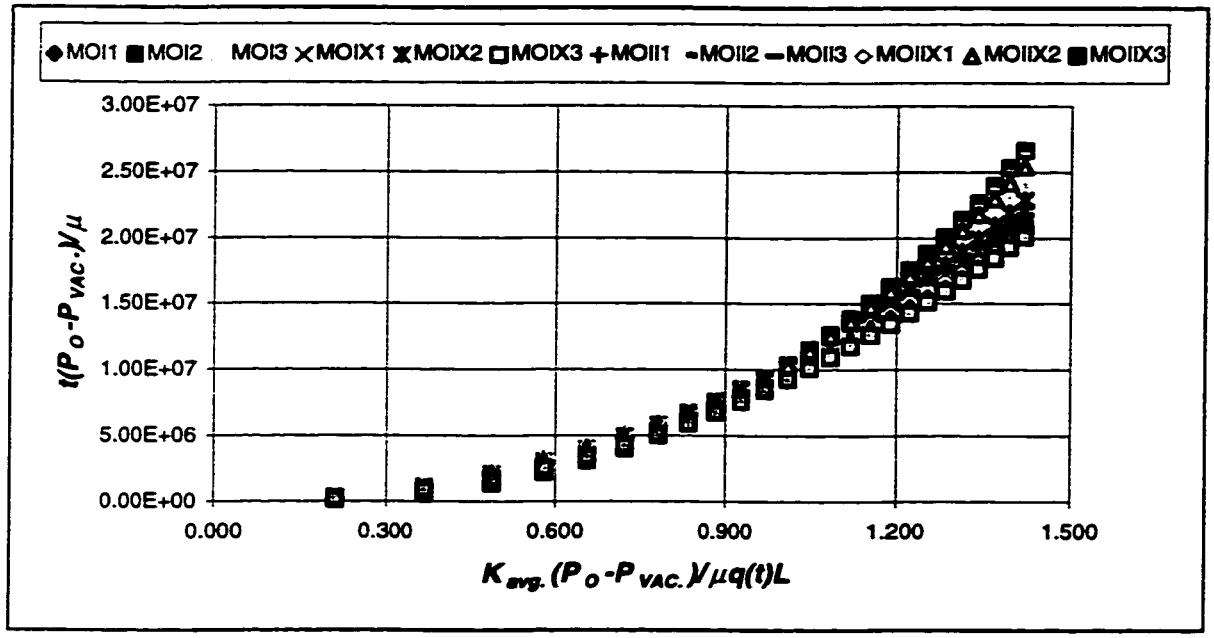

Figure 4.41(a) - Functional relation dimensionless curves of MOI and MOII experimental groups.

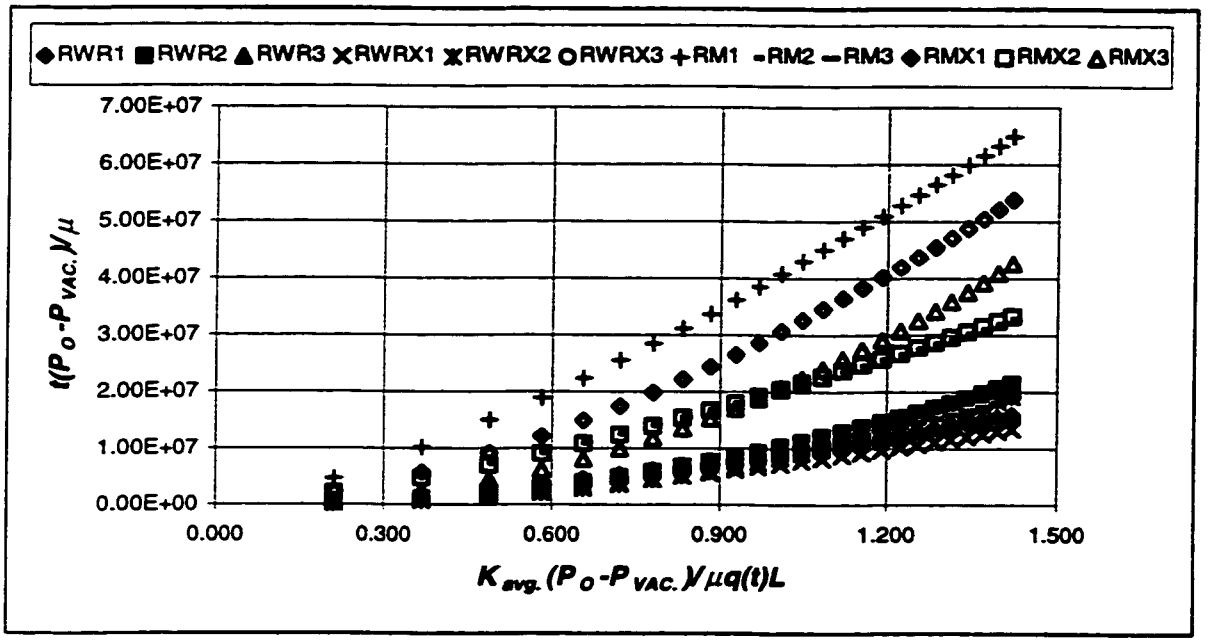

Figure 4.41(b) - Functional relation dimensionless curves of RWR and RM experimental groups.

CHAPTER 5

CONCLUSIONS AND RECOMMENDATION FOR FUTURE WORK

5.1 Summary:

The influence of vacuum level, fluid type and preform on the mold filling phase of the resin transfer molding process was experimentally investigated for a flat mold with unidirectional flow. Permeabilities of M8610 mat and woven roving fiberglass preforms were measured using different liquids and vacuum levels. Effect of vacuum level and liquid type on the measured permeabilities was studied. The wetting-out process of the different preforms was experimentally investigated. Finally, experimental verification of the constant inlet-pressure boundary condition scale relation derived by Xiao, et al. [32] was conducted.

General observations noticed during our experimental work are summarized in the following points:

- Wetting-out (micro-flow) process:
    - Due to the fact that motor oil is spreading on the glass fiber surface, i.e. its contact angle is zero, the motor oil easily followed the macro-channels rather than penetrating fiber bundles themselves. As a result, the apparent filling process was fast. Consequently, wetting was not observed in the motor oil experimental groups (MOI and MOII) even with the highest vacuum level.

- Since resin has a contact angle of about 31.5°, it was hard for the resin to follow even the macro-channels. As a result, the filling process happened slowly, which enabled the micro-flow (wetting) to be nicely achieved in the RM group, in which the wetting was the best with the highest vacuum level. However, the wetting was not properly achieved in the RWR group.
- An experimental study revealed that an average dimensionless pressure difference $\left(\frac{\Delta P_{avg.}}{\frac{1}{2}\rho \bar{V}^2} \right)$ of about (1×10^9) was required to get good wet-out in the resin-mat system in the Reynolds number range of ($0.06 \leq Re \leq 0.11$).

- Constant inlet-pressure scale relation:
  - The constant inlet-pressure scale relation was experimentally verified. While a good agreement was achieved in MOI, MOII and RWR experiment groups, RM showed a large deviation. The wetting-out mechanism is expected to be responsible for this deviation.
- Permeability:
  - Motor oil experiments showed constant average permeability values with no vacuum level effect. Whereas, RWR group had lower permeability value at the low vacuum level, while the medium and high vacuum levels gave a constant value. On the other hand, average permeability values in RM group were decreasing as vacuum level was increasing. The wetting-out (micro-flow) process mechanism is expected to be the reason for that RM behavior.

- Transient permeability values were increasing as vacuum level was increasing for all experimental groups except RM group, in which the opposite trend was noticed. This trend was also attributed to the micro-flow mechanism.
- Motor oil 10W30 had the highest transient permeability values, whereas, motor oil 20W50 and resin had intermediate and low permeability values, respectively.
- Preform effect study revealed that the RWR group had greater transient permeability values compared to the RM group.

- Mold-filling process:
  - The pressure build-up inside the mold cavity was growing fast at the beginning of the filling process, after that the growth rate was decreasing gradually. A saturated pressure value, equal to the inlet pressure, was only achieved in RM1 and RM2 experiments at the end of the filling process.
  - The pressure difference (*P1-P2*) was also growing fast at the beginning, then its increase rate was decreasing gradually. A maximum value was achieved, in most cases, after which the pressure difference started decreasing.
  - The maximum pressure difference value achieved was noticed to be increasing with vacuum level in all experimental groups except 10W30 motor oil experimental group (MOI), in which the the maximum pressure difference value was nearly the same for all vacuum levels.
  - Rein-mat (RM) group showed the highest maximum pressure values compared to MOI and MOII groups. This behavior is expected to be the result of micro-flow (wetting) process noticed in RM group.

- Resin-mat group also showed higher maximum pressure values compared to resin-woven roving (RWR) group. This is also expected to be due to more micro-flow occurred in RM group.
- Rough flow profiles, which are attributed to preform surface density variation, were noticed in all experiments conducted. The worst roughness in the profiles was noticed close to the vent side.
- Edge flow, which is a result of non precisely-cut preforms, was noticed in a few experiments.
- Fluid was noticed to leave the mold cavity before thoroughly wetting out the preform, leaving it with a poor wet-out and sometimes with dry spots. Edge flow and roughness in the flow profiles are believed to be the main reasons for this phenomenon.
- Flow front velocity was decreasing with time, reaching a saturated value at the end of the filling process.
- Initial and saturated velocity values were noticed to be increasing with vacuum level.
- Woven roving fiberglass showed higher initial and saturated velocity values compared to the M8610 mat.
- Motor oil 10W30 showed higher initial and saturated velocity values compared to 20W50 motor oil and resin (RM group) experiments, in which resin had the lower velocity values.
- Discrepancy in velocity values, due to preform surface density variation, was noticed in most experiments, specially at the vent side.

- Less filling time was required to fill the preform using higher vacuum level in all experiments except RM experiments. This peculiar behavior is expected to be related to the wetting-out (micro-flow) process.
- As expected, resin (650 mPa.s) experiments had the longest filling times, followed by 20W50 motor oil (440 mPa.s), then 10W30 motor oil (150 mPa.s).
- M8610 mat had longer filling time than woven roving fiberglass preform due to more micro-flow in M8610 case.

5.2 Conclusions:

The following conclusions could be drawn from the work conducted:

- High vacuum level is recommended to get good wet-out in resin experiments.
- An average dimensionless pressure difference $\left(\frac{\Delta P_{avg.}}{\frac{1}{2}\rho \overline{V}^2} \right)$ of about (1×10^9) was required to get good wet-out in the resin-mat system in the Reynolds number range of ($0.06 \leq Re \leq 0.11$).
- The peculiar behavior of resin-mat experiments is attributed to the wetting-out mechanism.
- The constant inlet-pressure scale relations were experimentally verified.
- The permeability is a function of fluid used.
- Due to micro-flow lag behind macro-flow, the mold cavity may be apparently filled by the resin leaving the preform poorly wetted-out.

5.3 Recommendation for Future Work:

A real composite part, made using resin and catalyst, should be manufactured using the same experimental set-up used in our work to study the manufactured part experimentally. The manufactured part should be sectioned at different locations along the flow direction and viewed under the microscope to confirm whether the preform wetting-out was properly achieved or not.

The filling process, which occurs at two different scales, i.e. the macro-flow and the micro-flow, should be studied thoroughly using fluid dynamics approach. Moreover, the surface energy of the fluid and preform should be taken into account to understand the interaction between the fluid and the preform used.

Hayward, et al. [30] mentioned that the effect of vacuum assistance was found not to be equivalent to an increase in resin injection pressure. This statement was not verified experimentally, as a result, an experimental study should be conducted to verify their statement.

REFERENCES

1. Potter, K., *Resin Transfer Molding,* Chapman and Hall, 1st ed., UK, 1997.
2. Lambe, T., and Whitman, R., *Soil Mechanics,* J. Wiley & Sons, New York, 1969.
3. Scheidegger, A., *Physics of Flow Through Porous Media,* U. Toronto Press, 3rd ed., Toronto, 1974.
4. Ozisik, M., *Basic Heat Transfer,* New York, McGraw-Hill, 1977.
5. Johnson, C., *Engineered Materials Handbook,* Vol. 1, Composites, ASM International, 1987, pp. 564-568.
6. Diallo, M., Gauvin, R., and Trochu, F., 1995, "Experimental Analysis of Flow through Multi-layer Fiber Reinforcements in Liquid Composite Molding," *Pre-prints of the 4th International Conference on Automated Composites (ICAC/4),* The Albert Hall, Nottingham, UK, 6-7 Sep., 1995, Vol. 1, pp. 201-210.
7. Kikuchi, A., Higuerey, E., and Coulter, J., 1995, "An Experimental Investigation of Resin Flow Sensing During Molding Process," *Journal of Engineering Materials and Technology,* Vol. 117, pp. 86-93.
8. Kranbuehl, D., Delos,S., Yi, E., Mayer, J., and Jarvie, T., 1986a, "Dynamic Dielectric Analysis: Nondestructive Material Evaluation and Cure Cycle Monitoring," *Journal of Polymer Engineering and Science,* Vol. 26, No. 1, pp. 338-345.
9. Kranbuehl, D., Delos,S., and Jue, P., 1986b, "Dielectric Properties of the Polymerization of an Aromatic Polyimide," *Polymer,* Vol. 27, No. 1, pp. 11-18.

10. Weitzenbock, J., Shenoi, R., and Wilson, P., 1995, "Flow Front Measurement in RTM," *Pre-prints of the 4th International Conference on Automated Composites (ICAC/4)*, The Albert Hall, Nottingham, UK, 6-7 Sep., 1995, Vol. 2, pp. 307-314.

11. Trochu, F.. Hoareau, C., Gauvin, R., and Vincent, M., 1993, " Experimental Analysis and Computer Simulation of Resin Transfer Molding Through Multilayer Fiber Reinforcement," *Proceedings of the 9th International Conference on Composite Materials (ICCM/9)*, Madrid, 12-16 July,1993,Vol. III, pp. 481-488.

12. Ahn, S., Lee, W., and Springer, S.,1995, "Measurement of the Three-dimensional Permeability of Fiber Preforms Using Embedded Fiber Optic Sensors," *Journal of Composite Materials*, Vol. 29, No. 6, pp. 714-733.

13. Kranbuehl, D., Delos, S., Hoff, M., and Haverty, P., 1989a, "Use of the Frequency Dependence of the Impedance to Monitor Viscosity During Cure," *Journal of Polymer Engineering and Science*, Vol. 29, No. 5, pp. 285-289.

14. Kranbuehl, D., Haverty, P., and Hoff, M., 1989b, "Monitoring the Cure Processing Properties of Unsaturated Polysters in situ During Fabrication," *Journal of Polymer Engineering and Science*, Vol. 29, No. 15, pp. 988-992.

15. Hart, S., Kranbuehl, D., Loos, A., Hinds, B., and Koury, J., 1992, "Intelegent Sensor-model Automated Control of PMR-15 Autoclave Processing," *37th International Society for the Advancement of Materials and Process Engineering Symposium*, G. C. Girimes, R. Turpin, C. Forberg, B. Rasmussen, and J. Whitney, eds., Society for the Advancement of Materials and Process Engineering, Covina, Ca., pp. 224-230.

16. Loos, A., Macrae, J., Kranbuehl, D., Hood, D., and Hasko, G., "Verification of a Multidimensional Resin Transfer Molding Flow Model," *Proceedings of the 10th International Conference on Composite Materials (ICCM/10)*, Vol. III, Whistler, B.C., Canada, August 1995.

17. Bruschke, M., and Advani, S., 1991, "RTM: Filling Simulation of Complex Three Dimensional Shell-like Structures," *SAMPE Quarterly*, October, 1991, pp. 2-11.

18. Pollard, M., 1992, "Permeability of Fiber Mats Used in Resin Transfer Molding," *24th International SAMPE Technical conference*, October 20-22, 1992, pp. 408-420.

19. Trouchu, F., Gauvin, R., and Gao,D.,1993, "Numerical Analysis of the Resin Transfer Molding Process," *Advances in Polymer Technology* ,vol. 12,pp. 329-342.

20. Gauvin, R., and Trochu, F., 1993, "Comparison between Numerical and Experimental Results for Mold Filling in Resin Transfer Molding," *Plastic, Rubber and Composites Processing and Applications*, Vol. 19, pp.151-157.

21. Li, S., and Gauvin, R., 1991, "Numerical Analysis of the Resin Flow in Resin Transfer Molding," *Journal of Reinforced Plastics and Composites*, Vol. 10, No. 3, pp. 314-327.

22. Chan, A., Larive, D., and Morgan, R.,1993, "Anisotropic Permeability of Fiber Preforms: constant Flow Rate Measurement," *Journal of Composite materials*, Vol. 27, No.10, pp. 996-1008.

23. Gauvin, R., Trouchu, F., Lemenn, Y., and Diallo, L.,1996, "Permeability Measurement and Flow Simulation Through Fiber Reinforcement," *Polymer Composites*, Vol. 17, No. 1, pp. 34-42.

24. Lekakou, C., Johri, M., Norman D., and Bader, M., 1996, "Measurement Techniques and Effects on In-Plane Permeability of Woven Clothes in Resin Transfer Molding" *Composites: Part A 27 A*, pp. 401-408.

25. Um, M., And Lee, W.,1991, "A Study on the Molding Filling Process in Resin Transfer Molding," *Polymer Engineering and Science,* Vol. 31, No. 11, pp. 765-771.

26. Wu, H., Wang, T., and Lee, L., 1994, "Trans-Plane Fluid Permeability Measurement and its Applications in Liquid Composite Molding," *Polymer Composites,* Vol. 15, No. 4, pp. 289-298.

27. Rudd, C., Owen, M., and Middleton, V., 1990, "Effect of Process Variables on Cycle Time During Resin Transfer Molding for High Volume Manufacture," *Materials Science and Technology,* Vol. 6, pp. 656-665.

28. Stabler, W., Tatterson, G., Sadler, R., and El-Shiakh, A.,1992, "Void Minimization in the Manufacture of Carbon Fiber Composites by Resin Transfer Molding," *SAMPE Quarterly,* Jan,1992, pp. 38-42.

29. Lundstrom, T., Gebart, B., and Lundemo, C., 1993, "Void Formation in RTM," *Journal of Reinforced Plastics and Composites,* Vol. 12,, pp. 1339-1349.

30. Hayward, J., and Harris, B., 1990, "Effect of Process Variables on the Quality of RTM Mouldings," *SAMPE Journal.*Vol. 26, No. 3, pp. 39-46.

31. Lundstrom, T., and Gebart, B., 1994, "Influence from Process Parameters on Void Formation in Resin Transfer Molding," *Polymer Composites,* Vol. 15, No. 1, pp. 25-33.

32. Xiao, X., Lin, S., and Hoa, S., 1995, "Scale Relations for Mold Filling Simulation in Resin Transfer Molding," *Science and Engineering of Composite Materials*, Vol. 4, No. 2, pp. 131-141.

33. Cai, Z., 1992, "Simplified Mold Filling Simulation in Resin Transfer Molding," *Journal of Composite Materials,* Vol. 26, No. 17, pp. 2606-2630.

34. Wu, S., *Polymer Interface and Adhesion,* Marcel Dekker Inc., New York, 1982.

35. Larson, R. and Higdon, J., 1986, "Microscopic flow near the surface of two-dimensional porous media. Part 1: Axial flow," *Journal of Fluid Mechanics,* Vol. 166, pp. 449-472.

36. Adams, K., Miller, B., and Rebenfeld, L., 1986, "Forced In-Plane Flow of an Epoxy Resin in Fibrous Networks," *Polymer Engineering and Science,* Vol. 26, No. 20, pp. 1434-1441.

37. Gauvin, R., Kerachni, A., and Fisa, B., 1993, "Variation of Mat Surface Density and Its Effect on Permeability Evaluation for RTM Modeling," *48th Annual Conference, Composite Institute, The Society of the Plastics Industry,* session 8-F, pp. 1-6.

38. Steenkamer, D., Mcknight, S., Wilkins, D., and Karbhari, V., 1995, "Experimental characterization of permeability and fibre wetting for liquid moulding," *Journal of Materials Science,* Vol. 30, pp. 3207-3215.

APPENDIX A
Pressure Curves

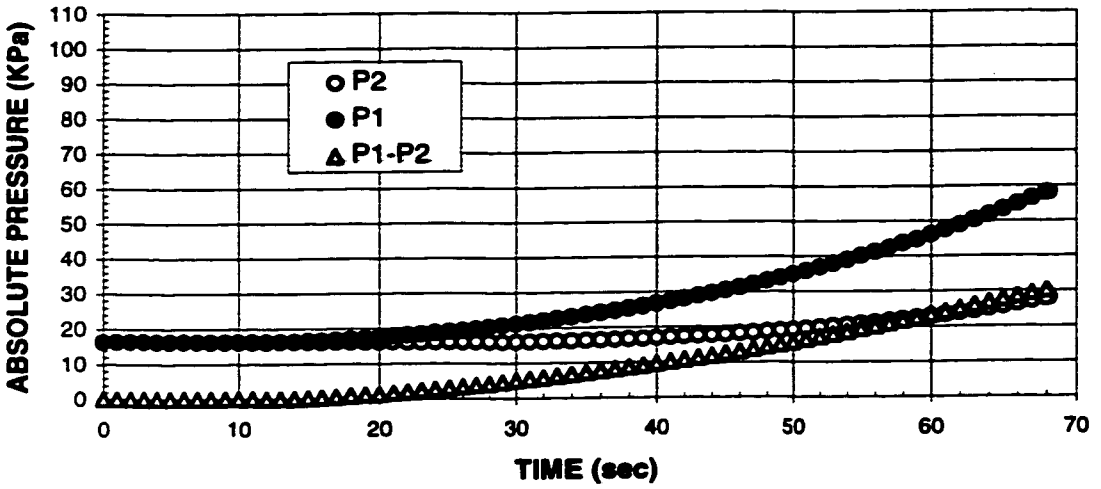

Figure A.1(a) - Pressure changes as a function of time at the two pressure transducers locations for experiment MOI1.

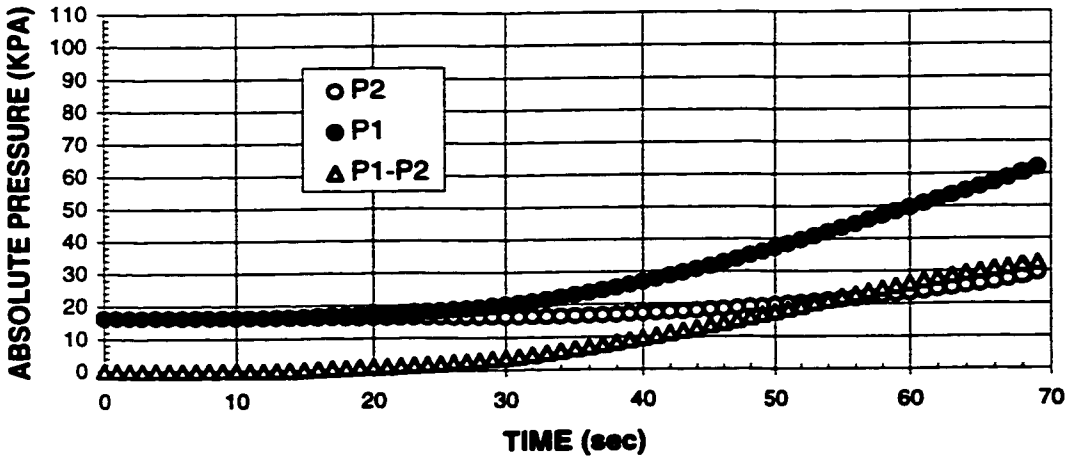

Figure A.1(b) - Pressure changes as a function of time at the two pressure transducers locations for experiment MOIX1.

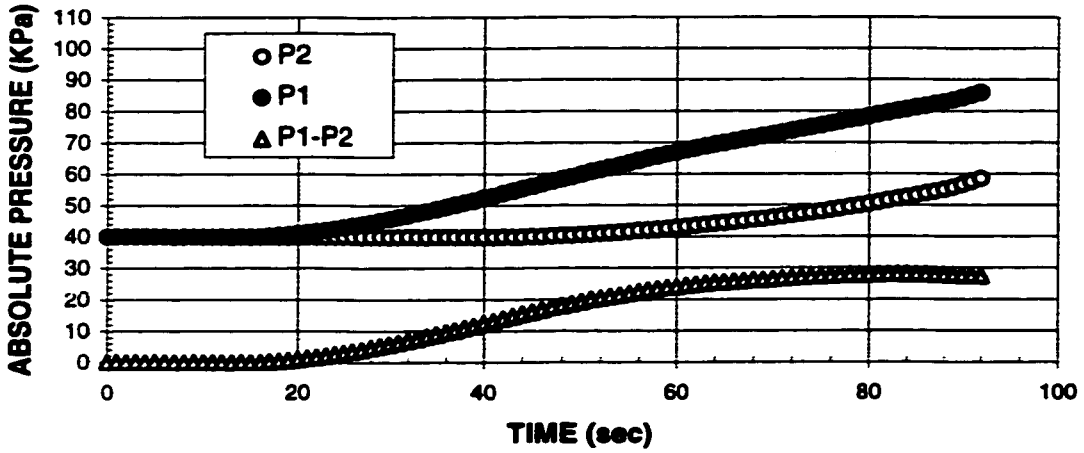

Figure A.2(a) - Pressure changes as a function of time at the two pressure transducers locations for experiment MOI2.

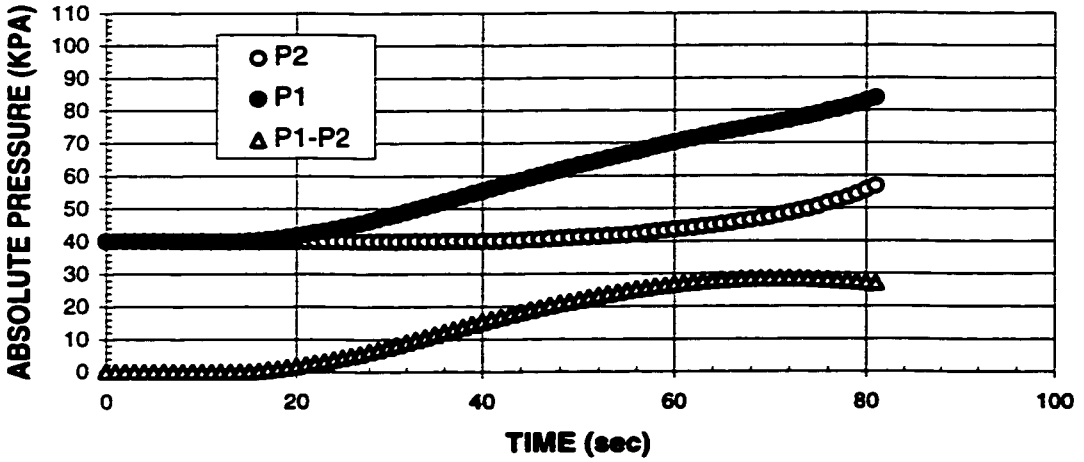

Figure A.2(b) - Pressure changes as a function of time at the two pressure transducers locations for experiment MOIX2.

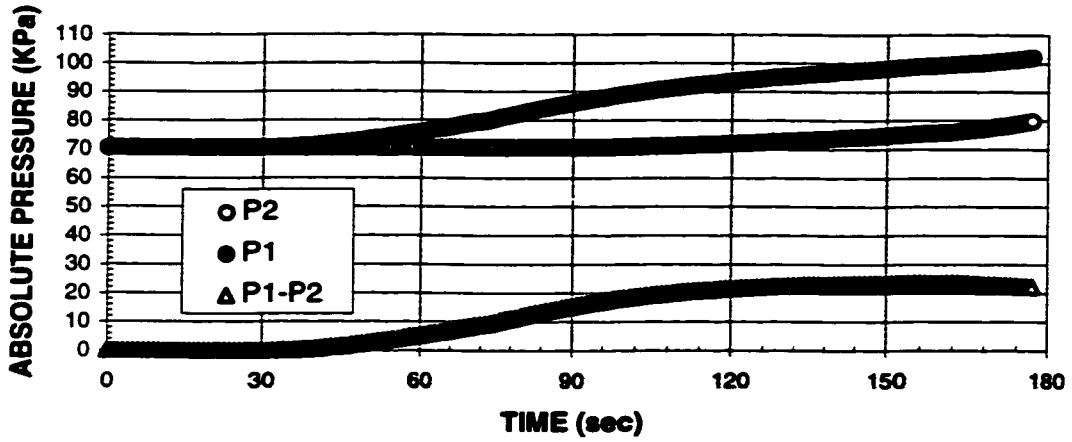

Figure A.3(a) - Pressure changes as a function of time at the two pressure transducers locations for experiment MOI3.

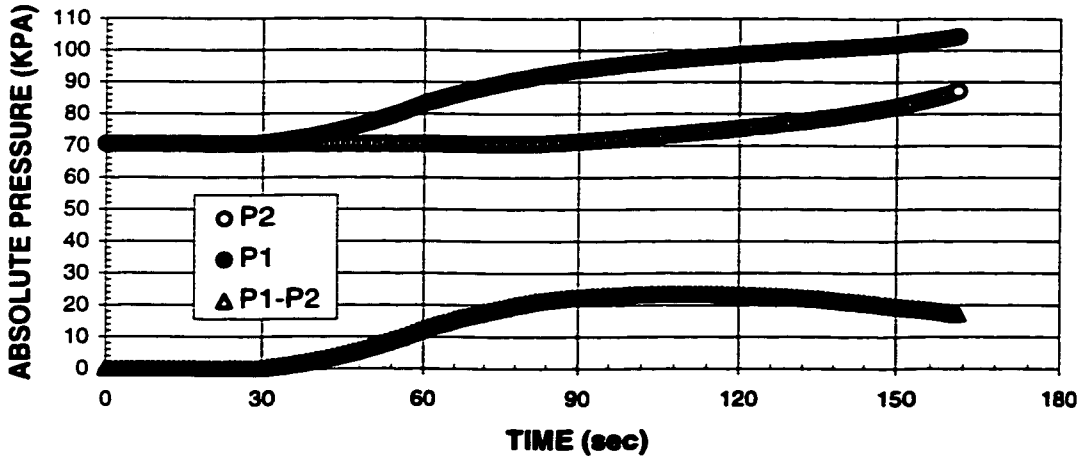

Figure A.3(b) - Pressure changes as a function of time at the two pressure transducers locations for experiment MOIX3.

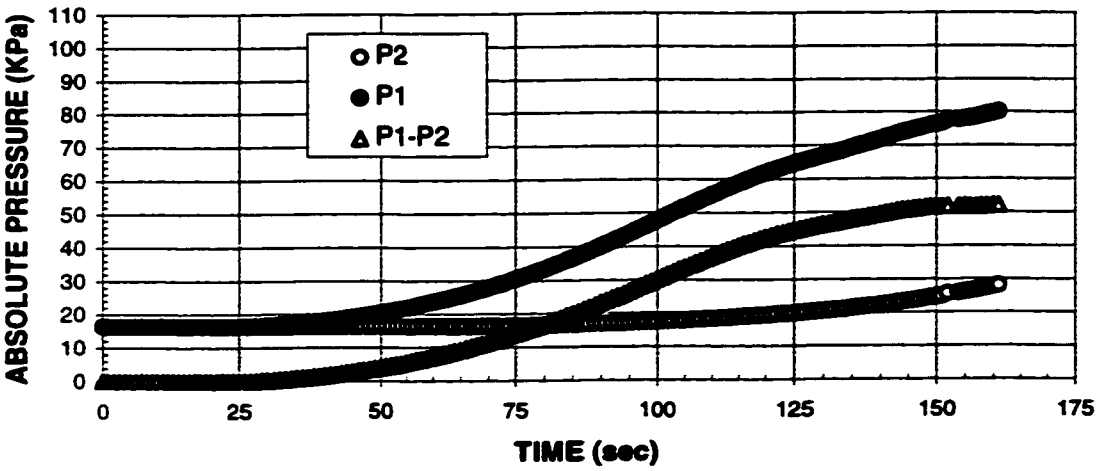

Figure A.4(a) - Pressure changes as a function of time at the two pressure transducers locations for experiment MOII1.

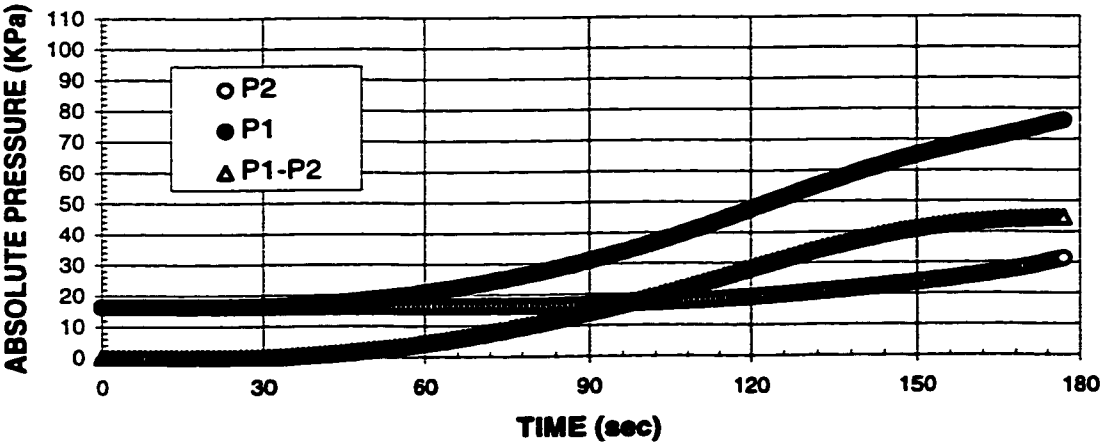

Figure A.4(b) - Pressure changes as a function of time at the two pressure transducers locations for experiment MOIIX1.

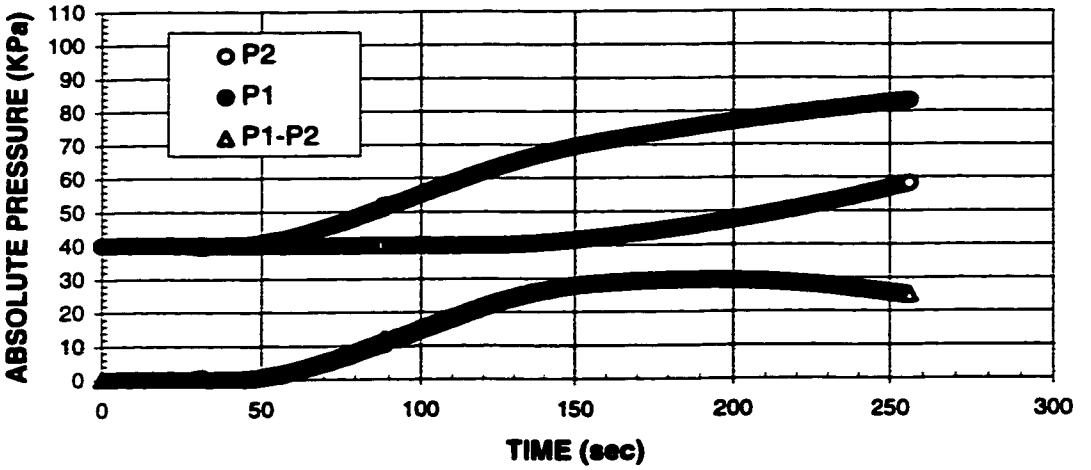

Figure A.5(a) - Pressure changes as a function of time at the two pressure transducers locations for experiment MOII2.

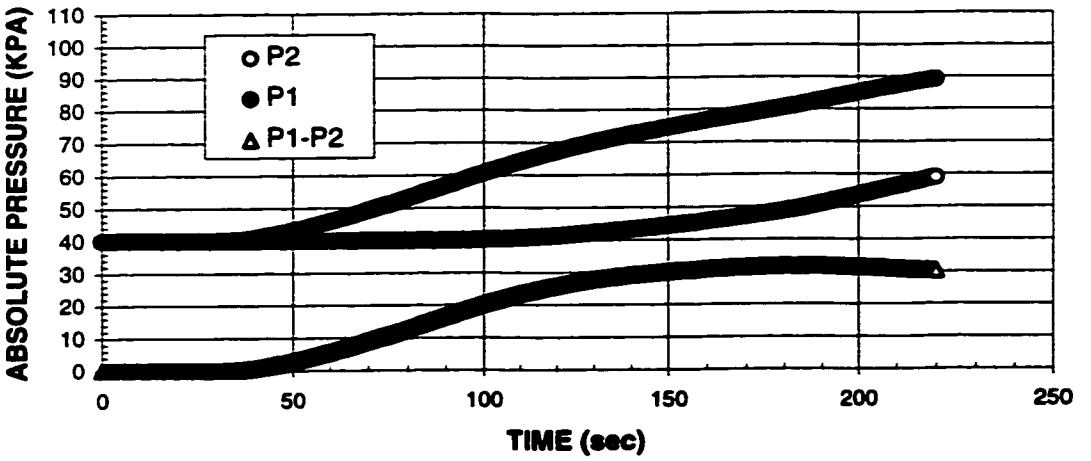

Figure A.5(b) - Pressure changes as a function of time at the two pressure transducers locations for experiment MOIIX2.

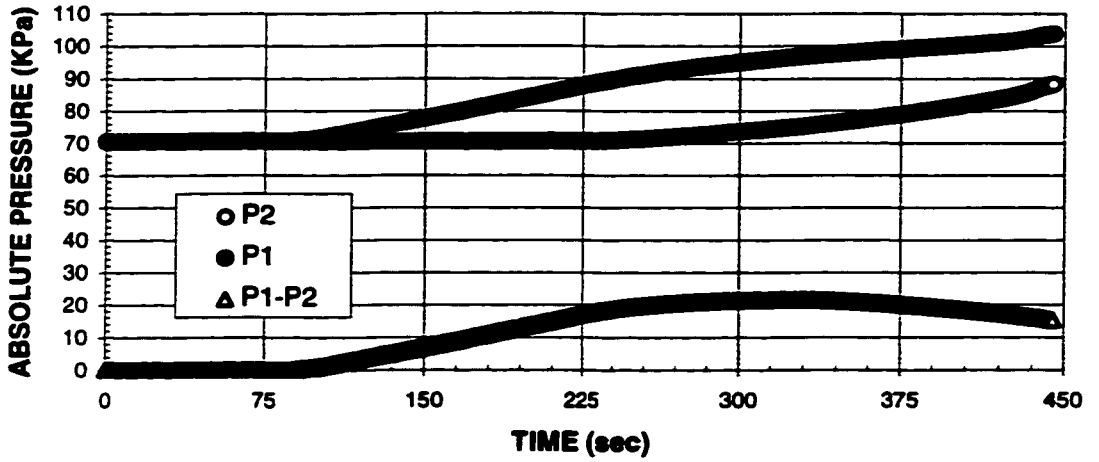

Figure A.6(a) - Pressure changes as a function of time at the two pressure transducers locations for experiment MOII3.

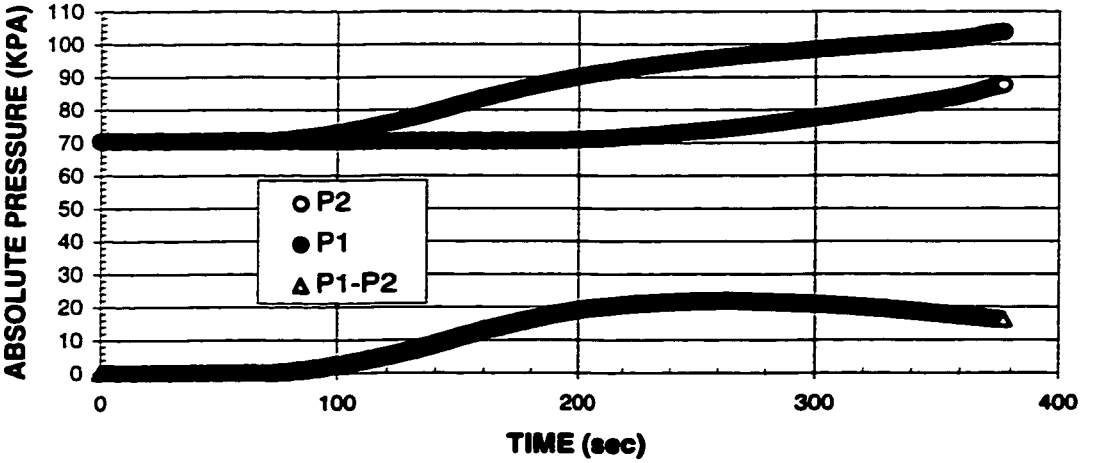

Figure A.6(b) - Pressure changes as a function of time at the two pressure transducers locations for experiment MOIIX3.

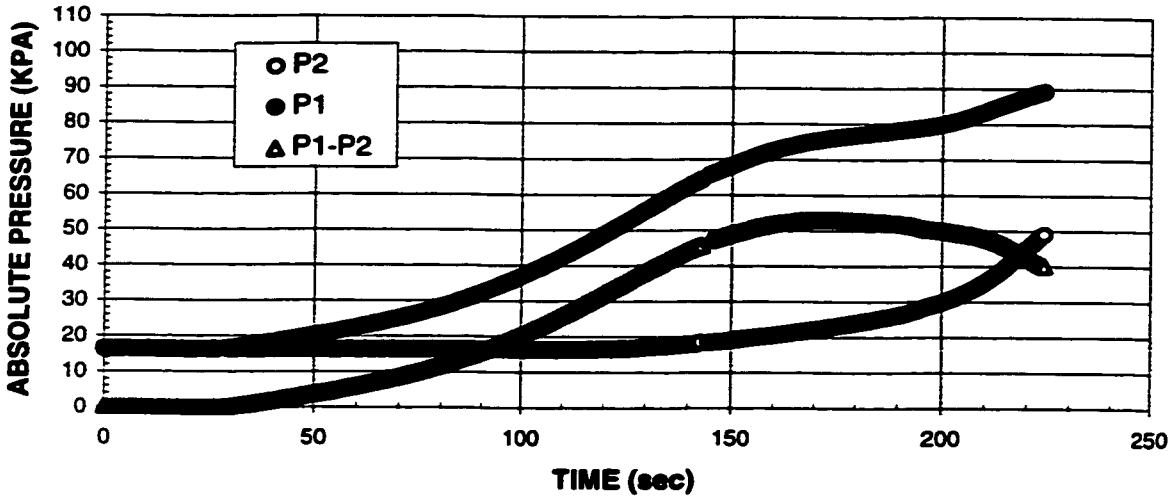

Figure A.7(a) - Pressure changes as a function of time at the two pressure transducers locations for experiment RWR1.

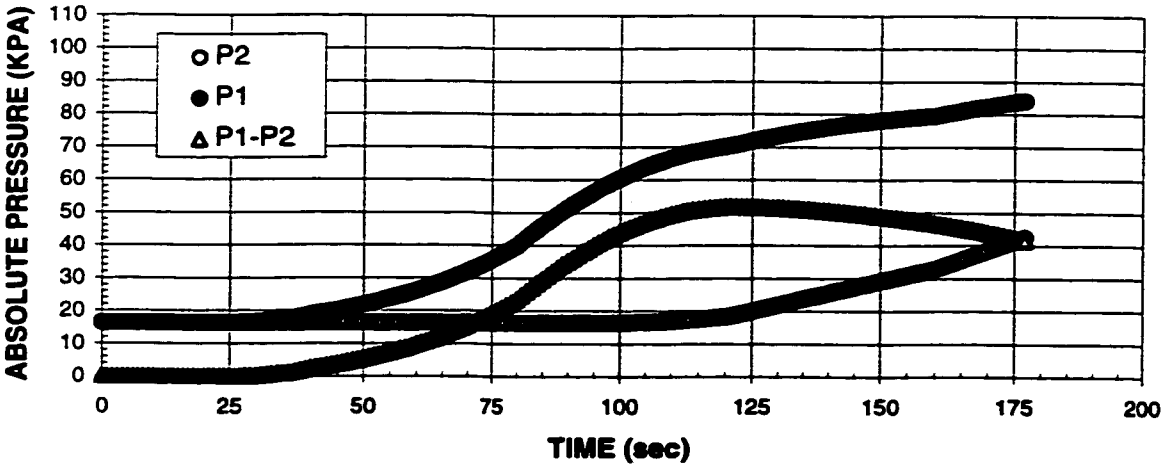

Figure A.7(b) - Pressure changes as a function of time at the two pressure transducers locations for experiment RWRX1.

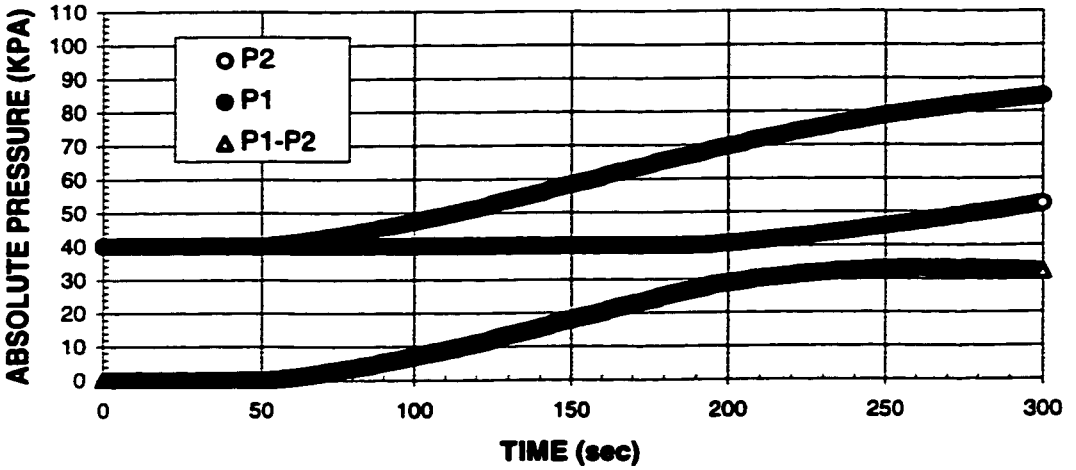

Figure A.8(a) - Pressure changes as a function of time at the two pressure transducers locations for experiment RWR2.

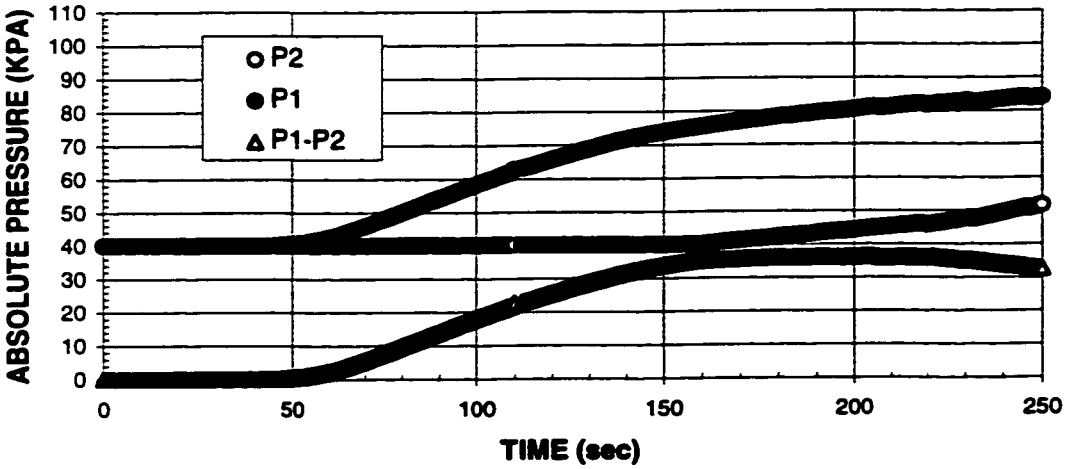

Figure A.8(b) - Pressure changes as a function of time at the two pressure transducers locations for experiment RWRX2.

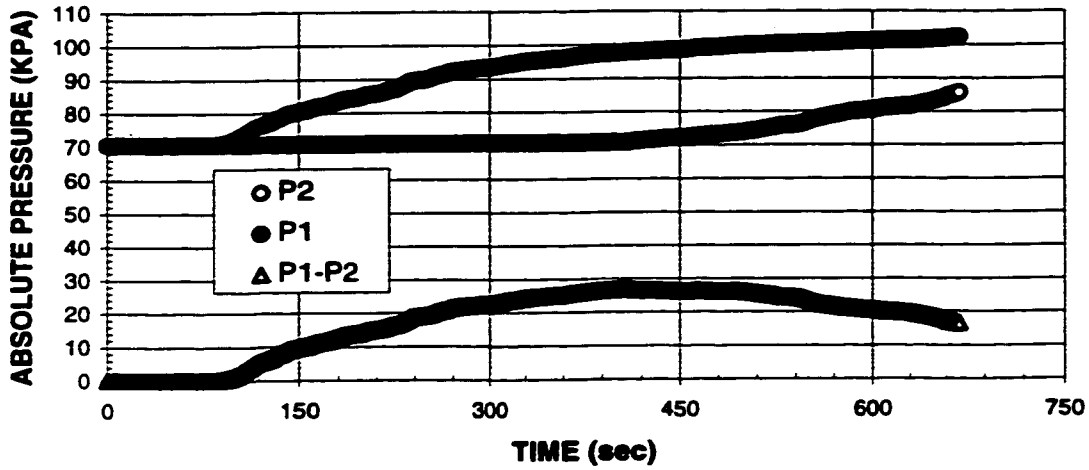

Figure A.9(a) - Pressure changes as a function of time at the two pressure transducers locations for experiment RWR3.

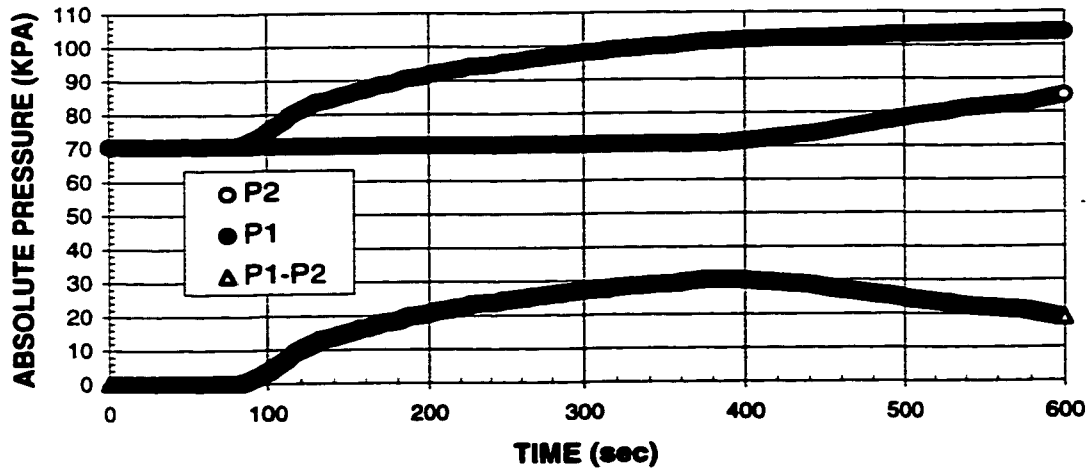

Figure A.9(b) - Pressure changes as a function of time at the two pressure transducers locations for experiment RWRX3.

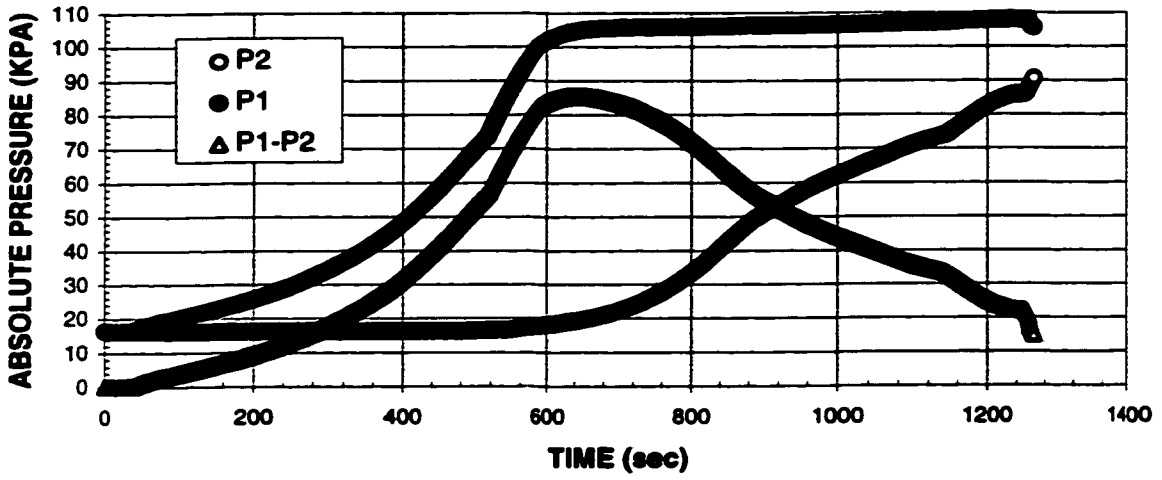

Figure A.10(a) - Pressure changes as a function of time at the two pressure transducers locations for experiment RM1.

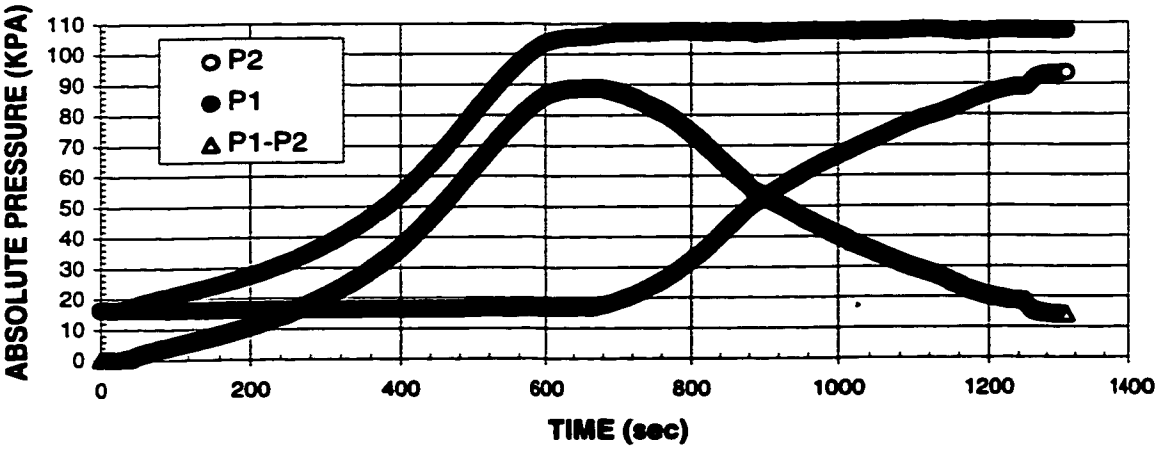

Figure A.10(b) - Pressure changes as a function of time at the two pressure transducers locations for experiment RMX1.

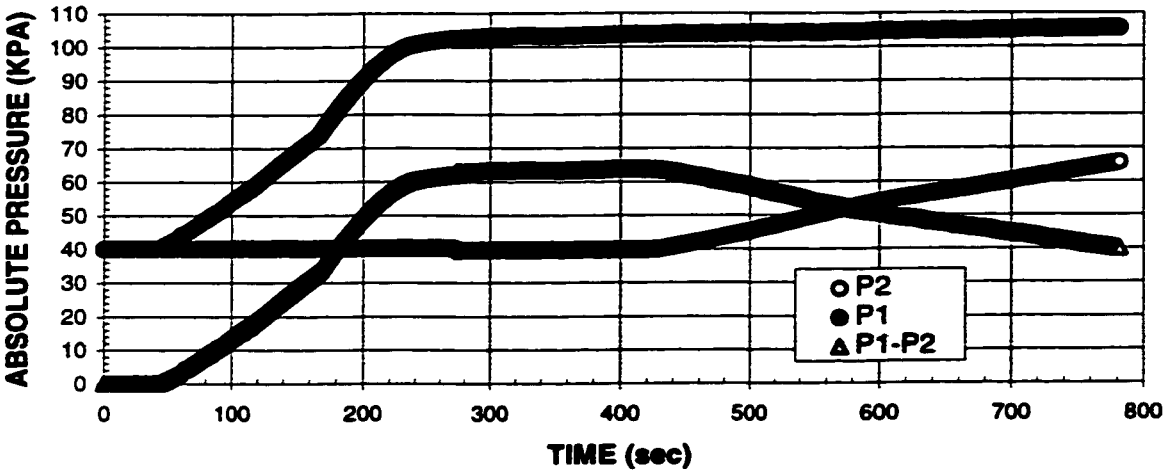

Figure A.11(a) - Pressure changes as a function of time at the two pressure transducers locations for experiment RM2.

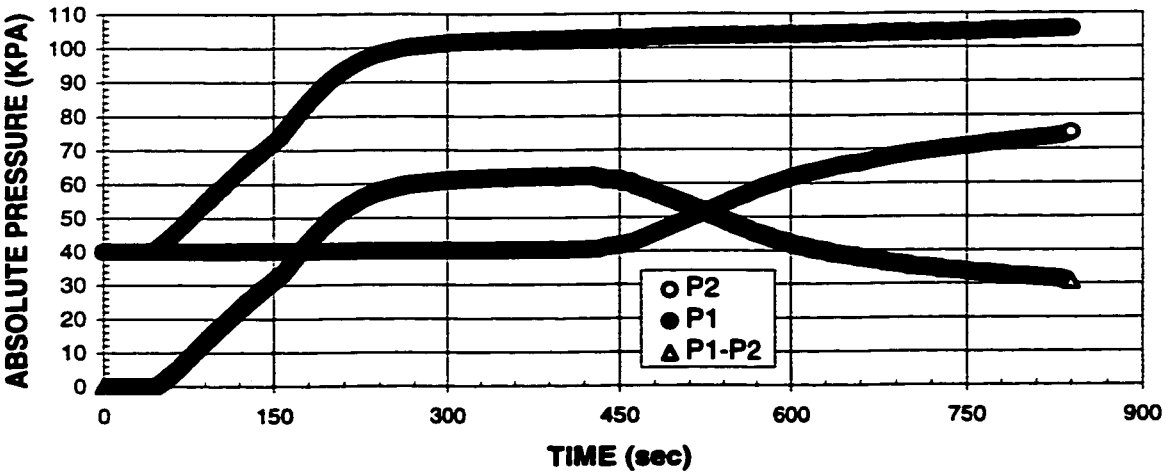

Figure A.11(b) - Pressure changes as a function of time at the two pressure transducers locations for experiment RMX2.

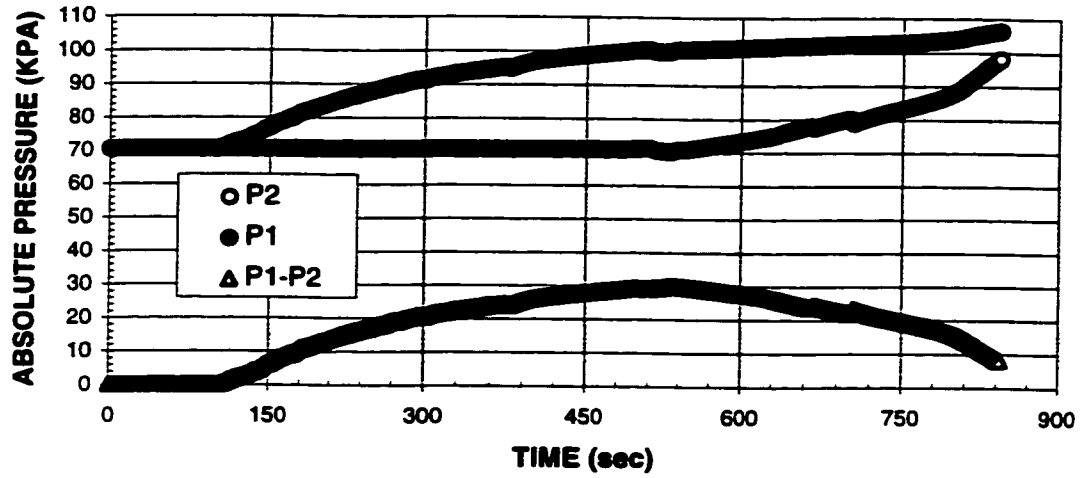

Figure A.12(a) - Pressure changes as a function of time at the two pressure transducers locations for experiment RM3.

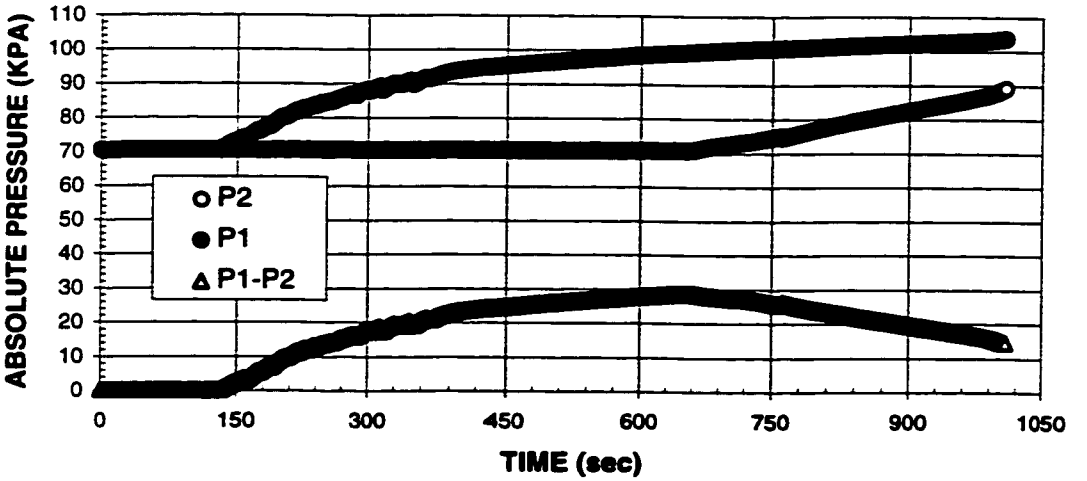

Figure A.12(b) - Pressure changes as a function of time at the two pressure transducers locations for experiment RMX3.

APPENDIX B
Fluid Flow Front Profiles

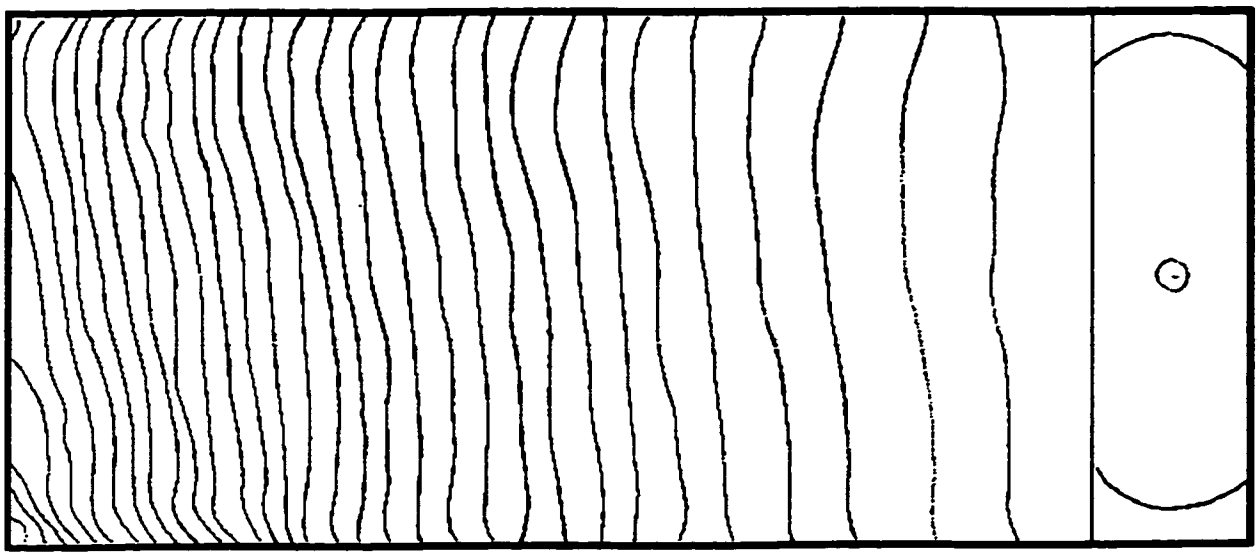

Figure B.1(a) - Fluid flow patterns for experiment (MOI1).
(time interval (Δt) = 2s and filling time ($T_{filling}$) = 65s)

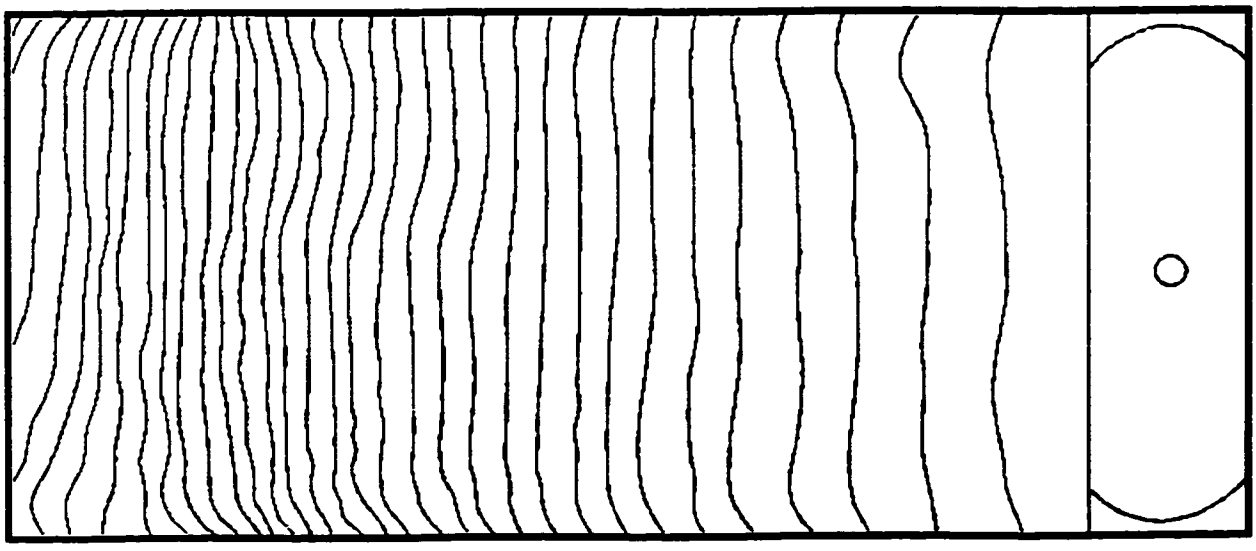

Figure B.1(b) - Fluid flow patterns for experiment (MOIX1).
(Δt = 2s, $T_{filling}$ = 67s)

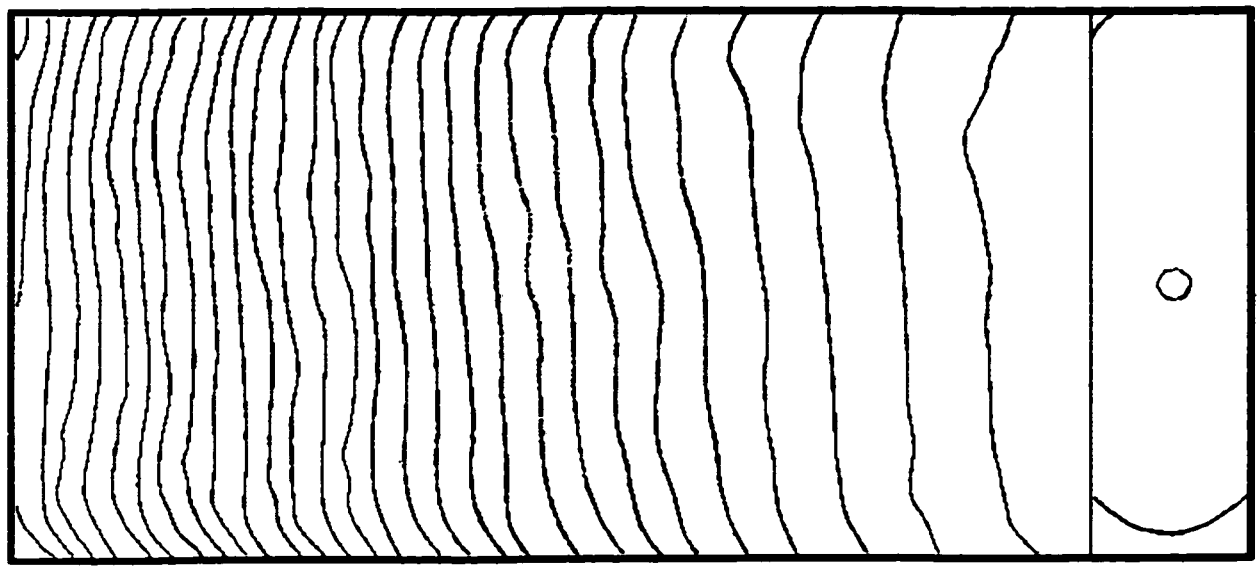

Figure B.2(a) - Fluid flow patterns for experiment (MOI2).
($\Delta t = 3s$, $T_{filling} = 88s$)

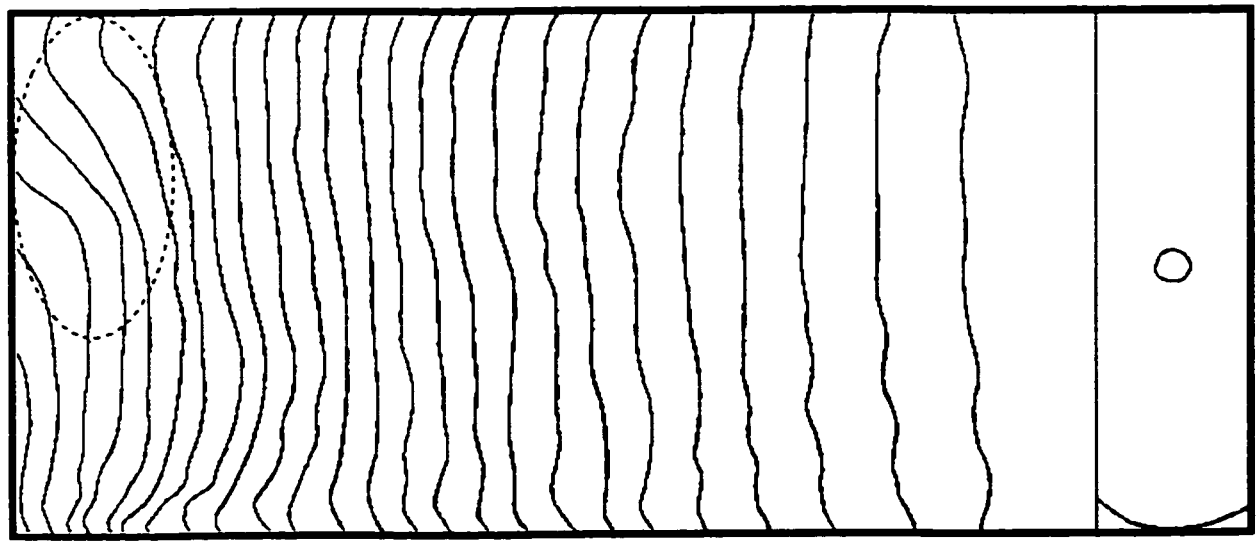

Figure B.2(b) - Fluid flow patterns for experiment (MOIX2).
($\Delta t = 3s$, $T_{filling} = 78s$)

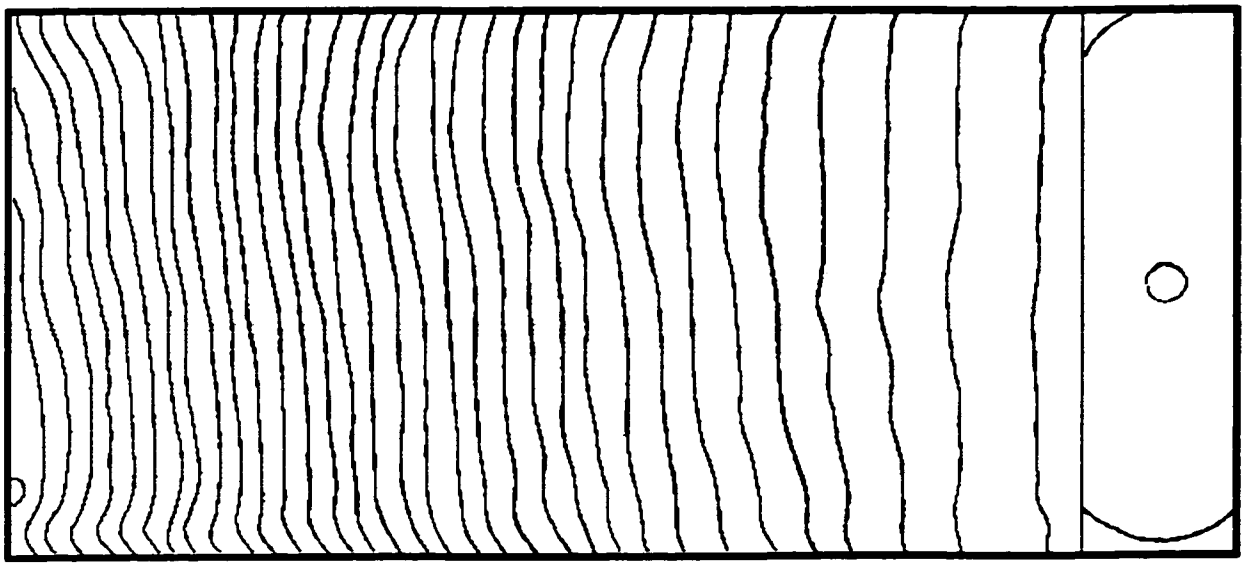

Figure B.3(a) - Fluid flow patterns for experiment (MOI3).
($\Delta t = 5s$, $T_{filling} = 168s$)

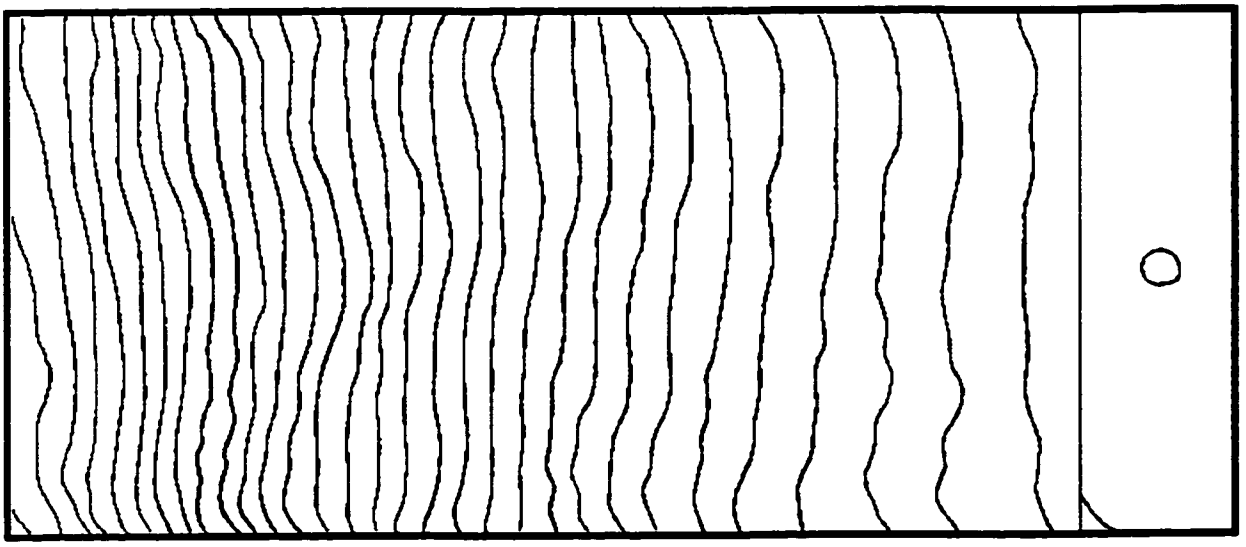

Figure B.3(b) - Fluid flow patterns for experiment (MOIX3).
($\Delta t = 5s$, $T_{filling} = 154s$)

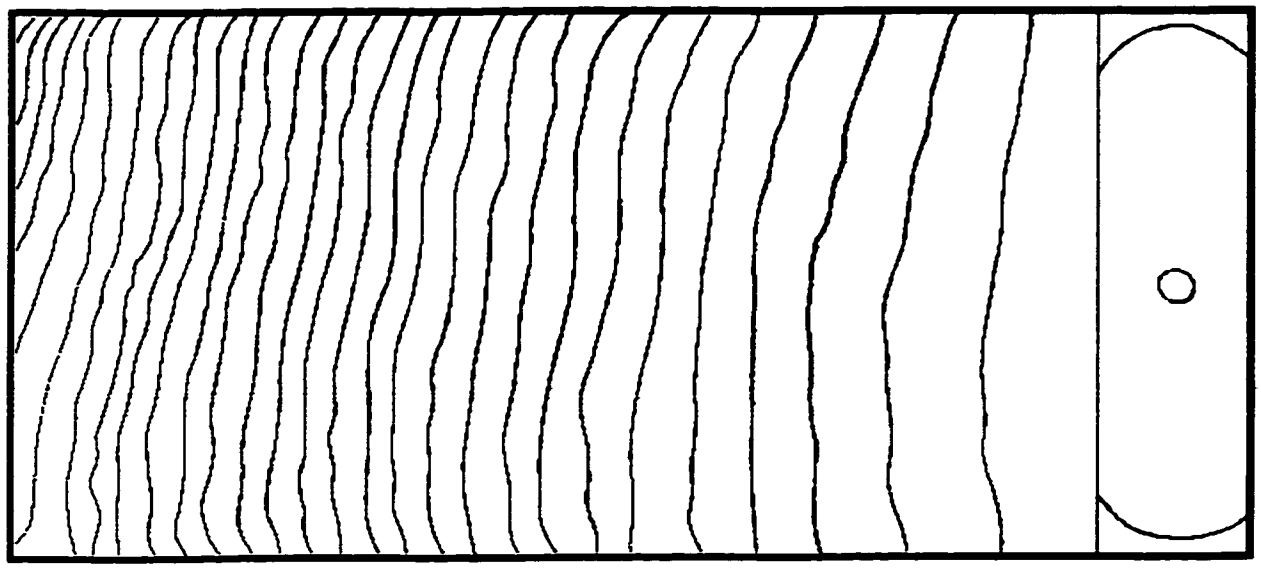

Figure B.4(a) - Fluid flow patterns for experiment (MOII1).
($\Delta t = 5s$, $T_{filling} = 154s$)

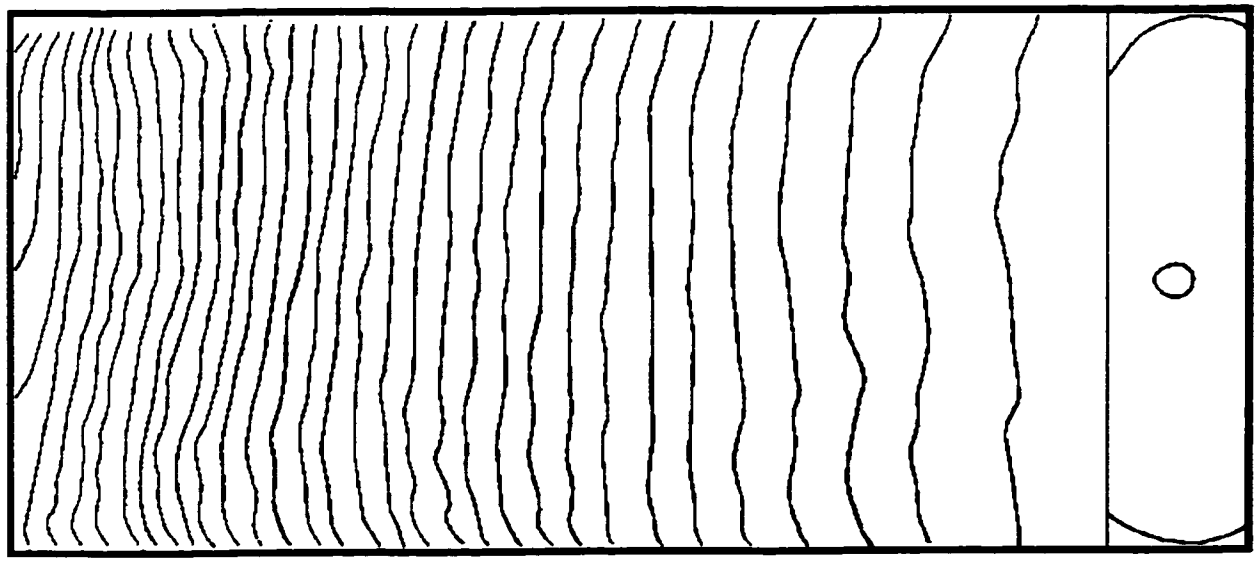

Figure B.4(b) - Fluid flow patterns for experiment (MOIIX1).
($\Delta t = 5s$, $T_{filling} = 170s$)

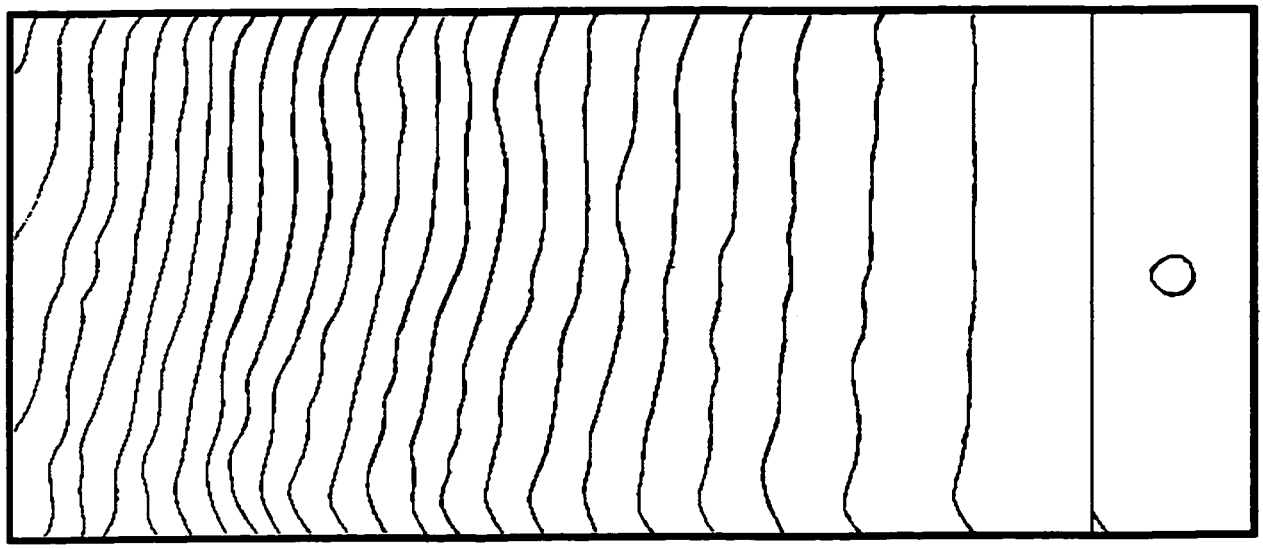

Figure B.5(a) - Fluid flow patterns for experiment (MOII2).
(Δt = 10s, $T_{filling}$ = 245s)

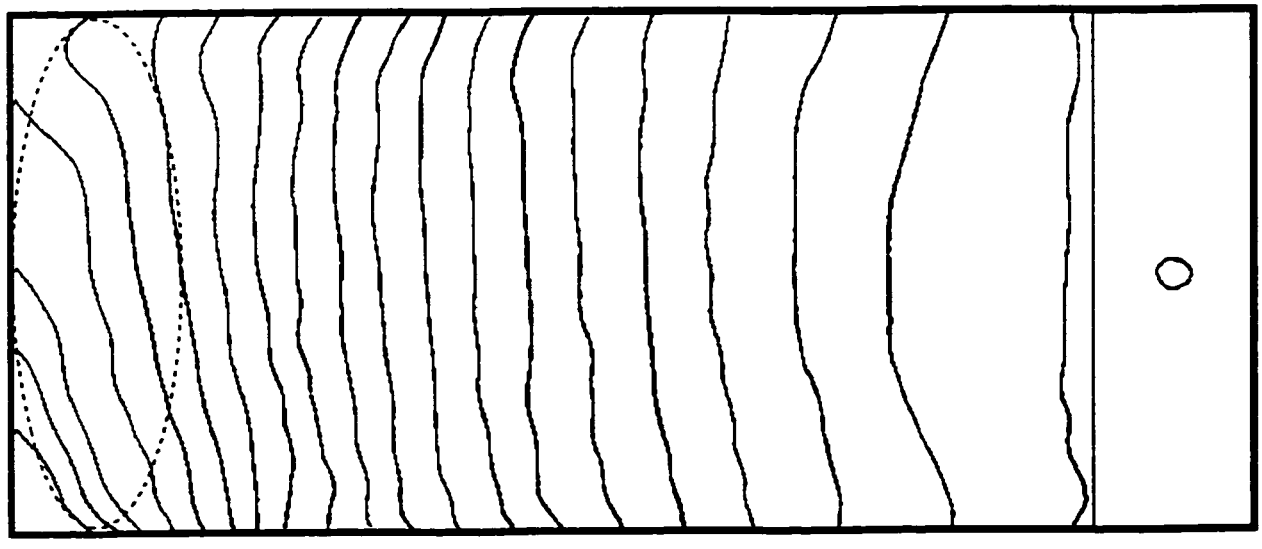

Figure B.5(b) - Fluid flow patterns for experiment (MOIIX2).
(Δt = 10s, $T_{filling}$ = 211s)

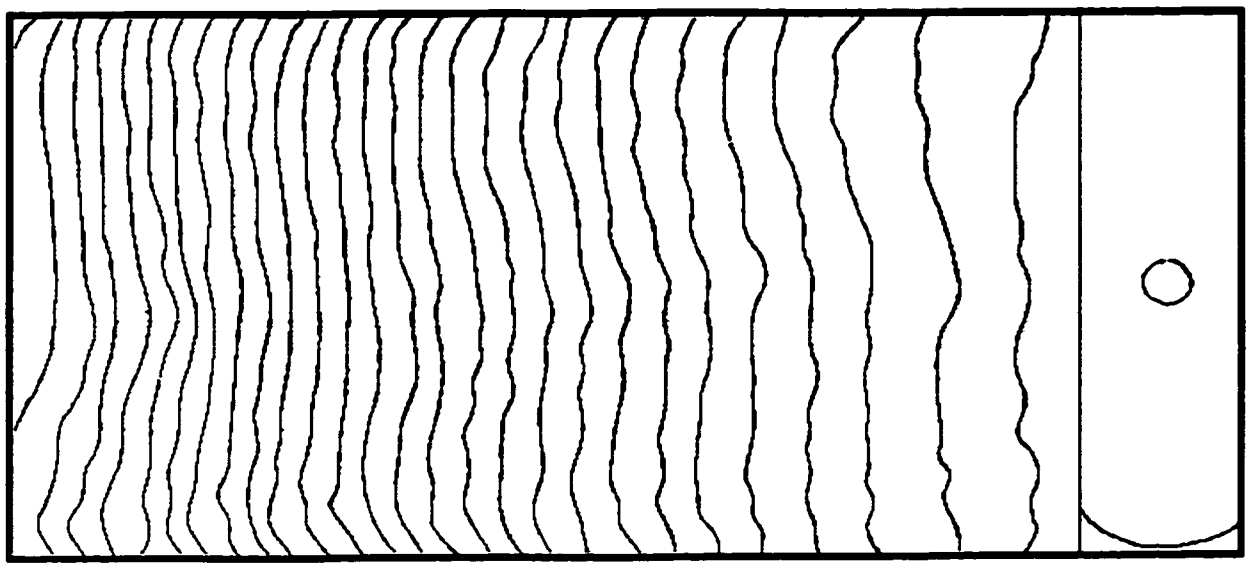

Figure B.6(a) - Fluid flow patterns for experiment (MOII3).
(Δt = 15s, $T_{filling}$ = 421s)

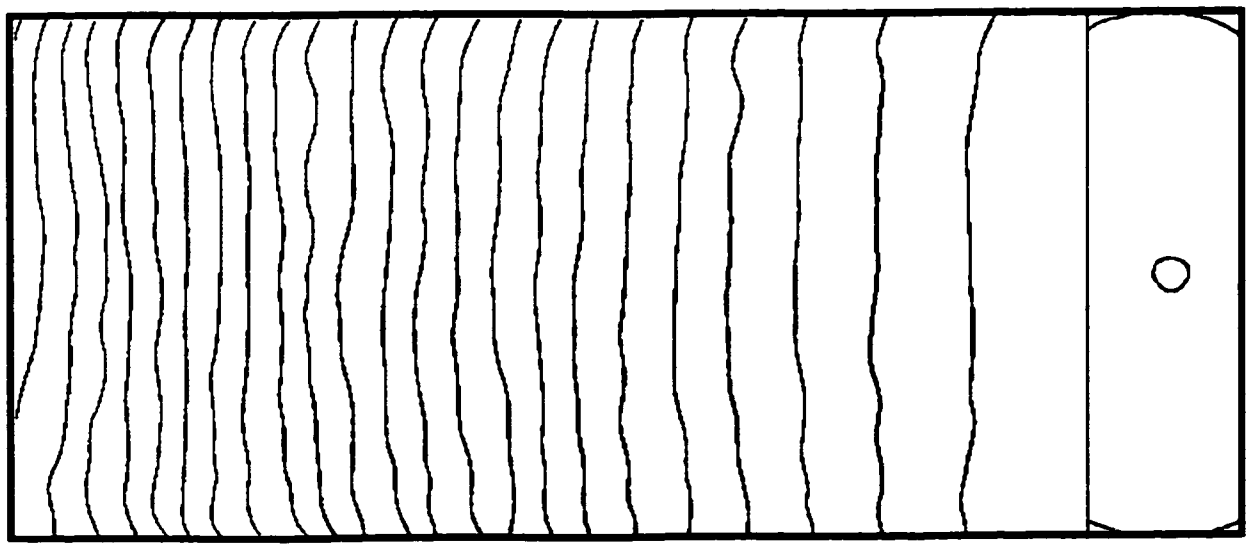

Figure B.6(b) - Fluid flow patterns for experiment (MOIIX3).
(Δt = 15s, $T_{filling}$ = 359s)

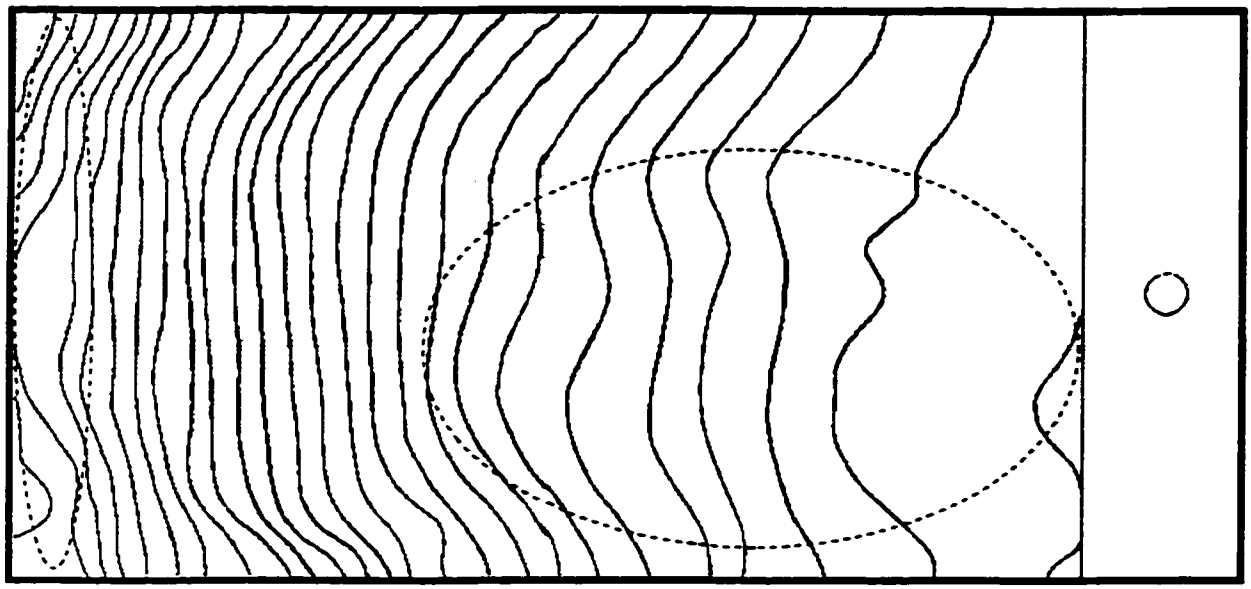

Figure B.7(a) - Fluid flow patterns for experiment (RWR1).
(Δt = 8s, $T_{filling}$ = 217s)

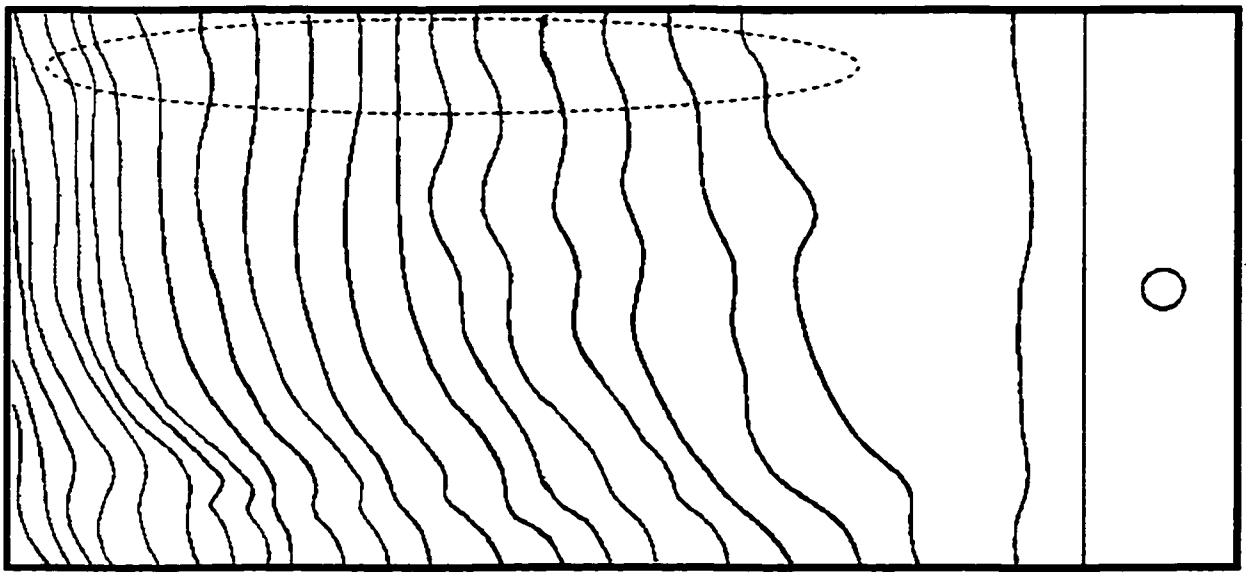

Figure B.7(b) - Fluid flow patterns for experiment (RWRX1).
(Δt = 8s, $T_{filling}$ = 171s)

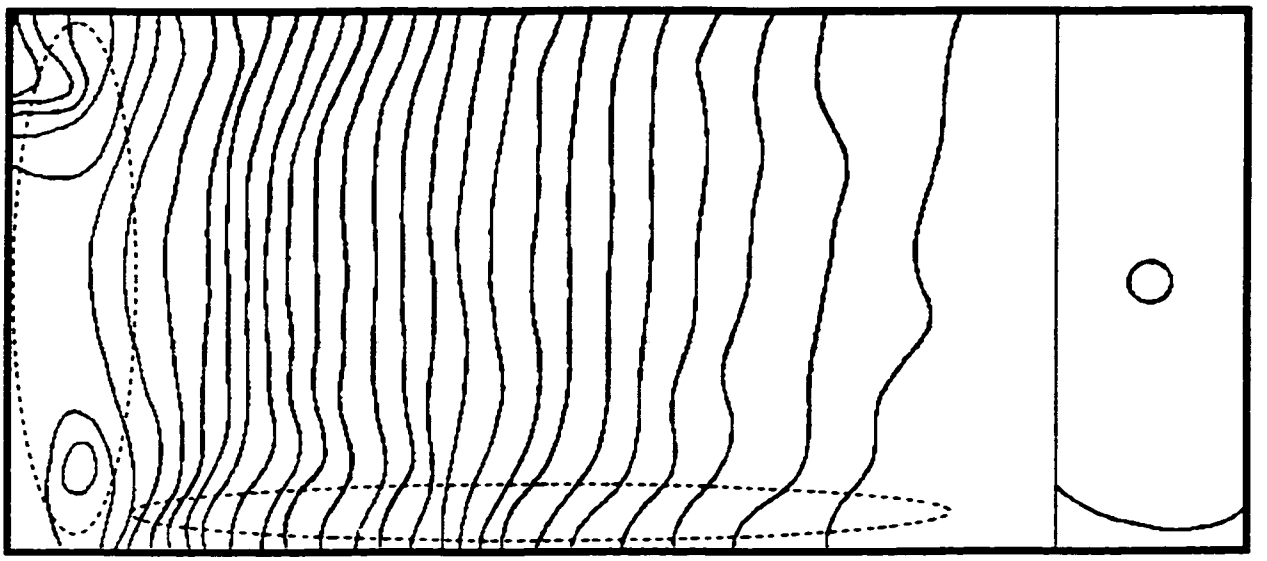

Figure B.8(a) - Fluid flow patterns for experiment (RWR2).
(Δt = 10s, $T_{filling}$ = 289s)

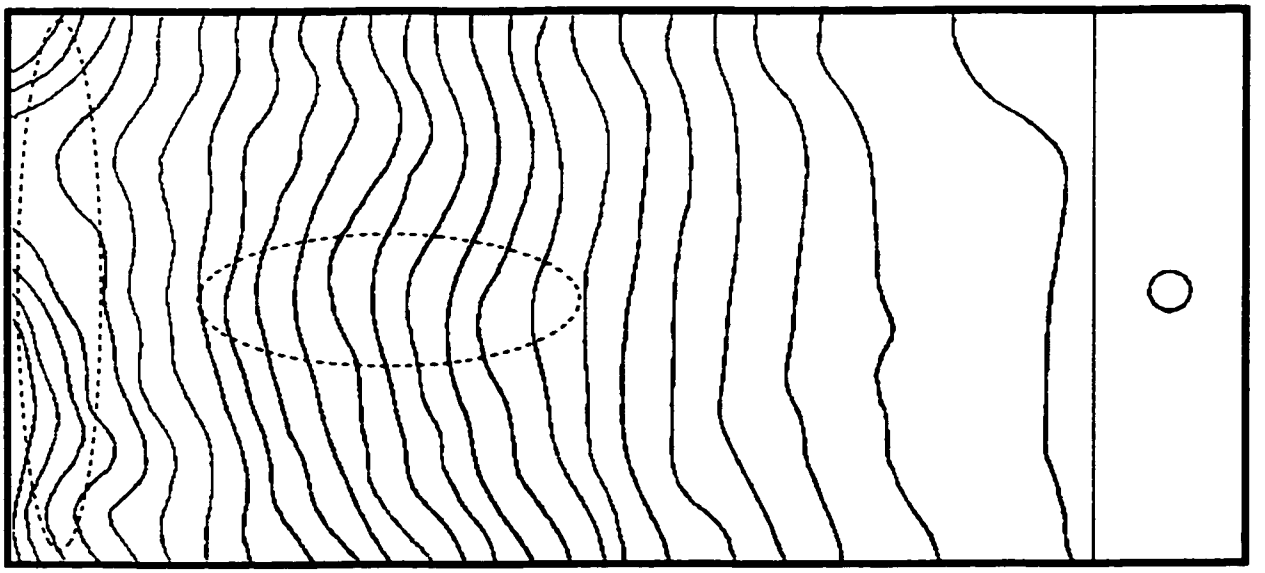

Figure B.8(b) - Fluid flow patterns for experiment (RWRX2).
(Δt = 10s, $T_{filling}$ = 242s)

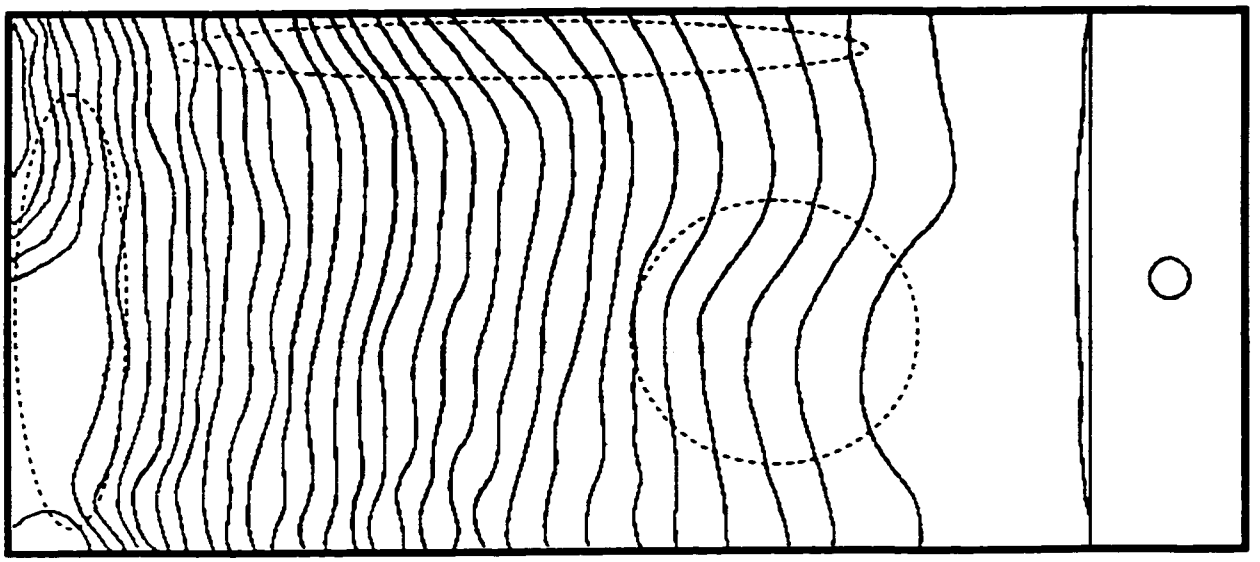

Figure B.9(a) - Fluid flow patterns for experiment (RWR3).
($\Delta t = 20s$, $T_{filling} = 647s$)

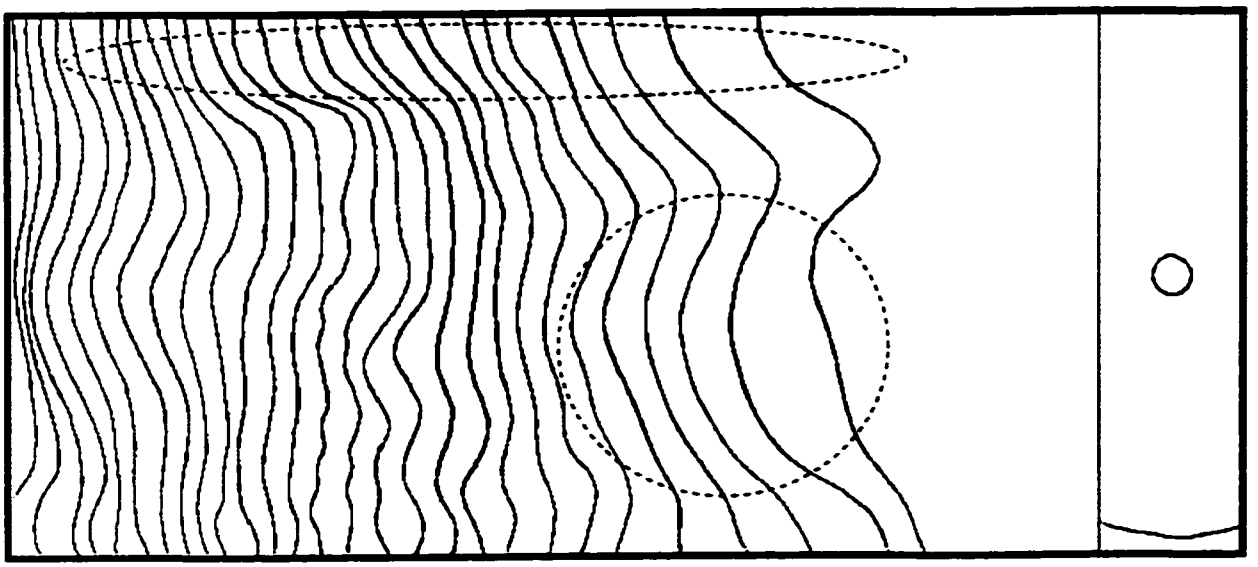

Figure B.9(b) - Fluid flow patterns for experiment (RWRX3).
($\Delta t = 20s$, $T_{filling} = 579s$)

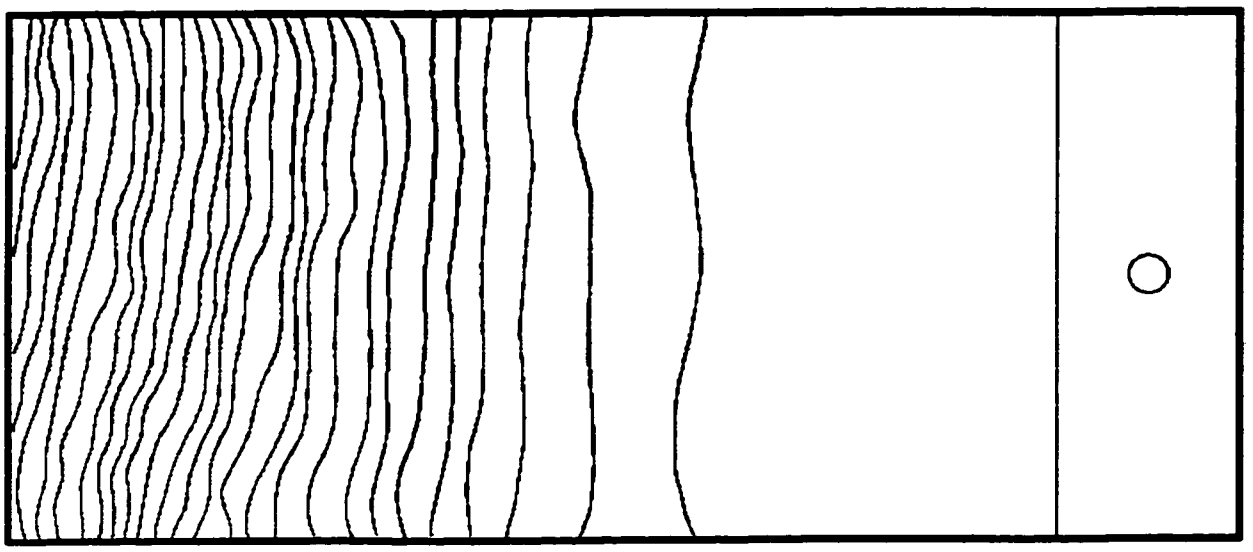

Figure B.10(a) - Fluid flow patterns for experiment (RM1).
($\Delta t = 45s$, $T_{filling} = 1256s$)

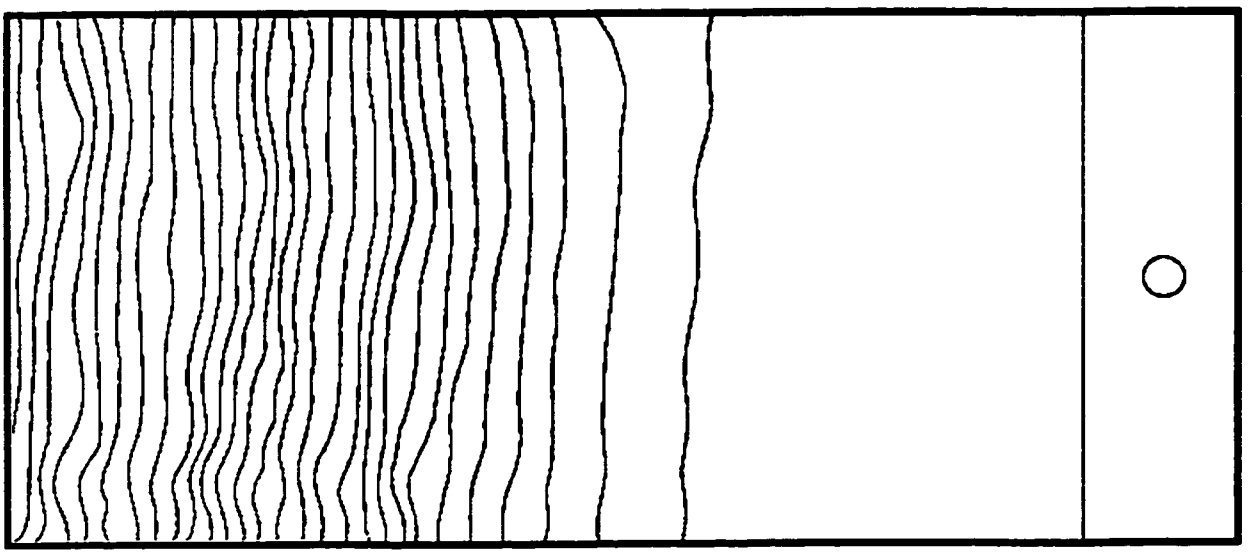

Figure B.10(b)- Fluid flow patterns for experiment (RMX1).
($\Delta t = 45s$, $T_{filling} = 1302s$)

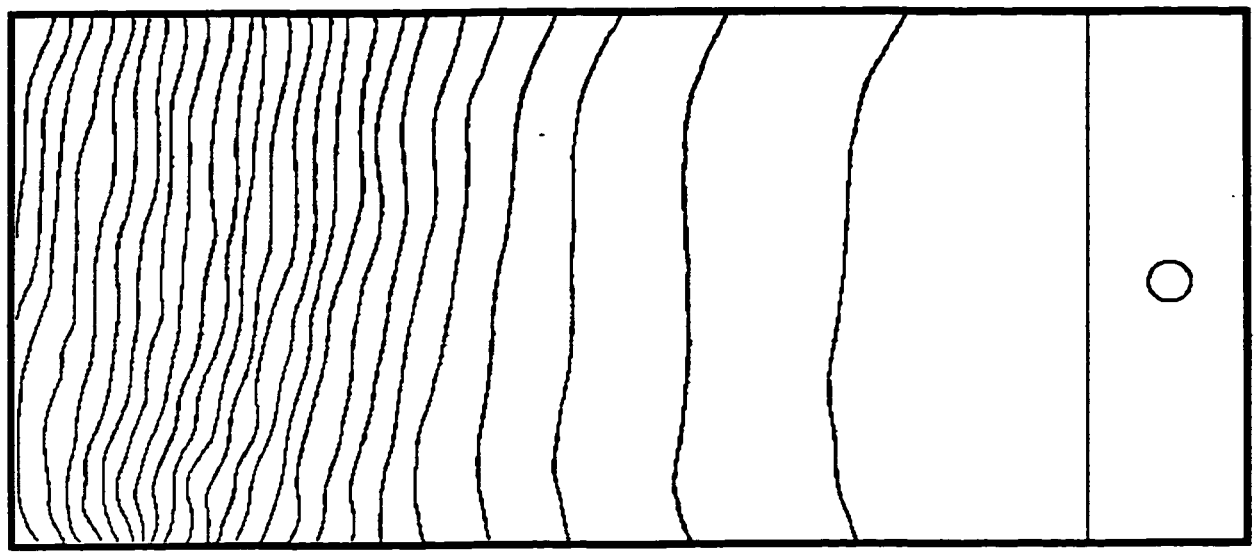

Figure B.11(a) - Fluid flow patterns for experiment (RM2).
($\Delta t = 30s$, $T_{filling} = 772s$)

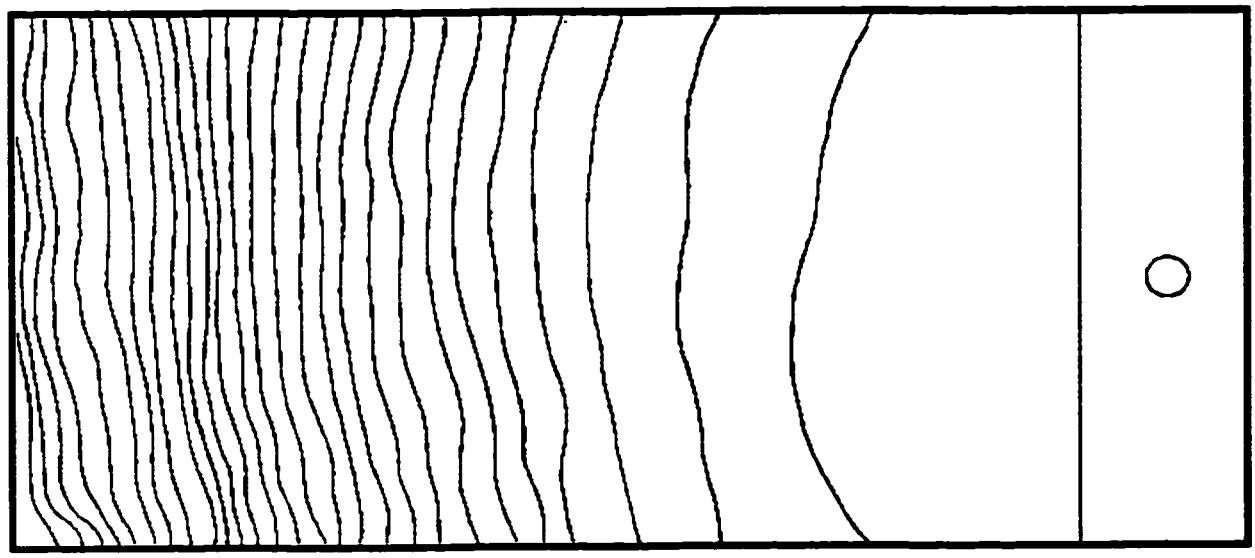

Figure B.11(b) - Fluid flow patterns for experiment (RMX2).
($\Delta t = 30s$, $T_{filling} = 831s$)

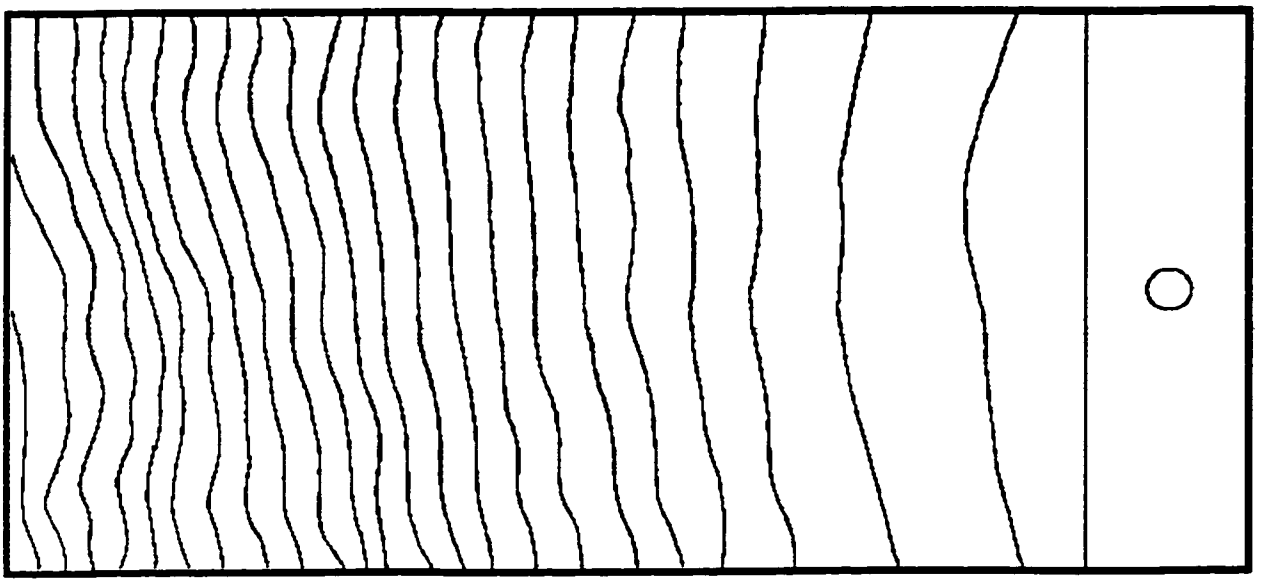

Figure B.12(a) - Fluid flow patterns for experiment (RM3).
($\Delta t = 35s$, $T_{filling} = 820s$)

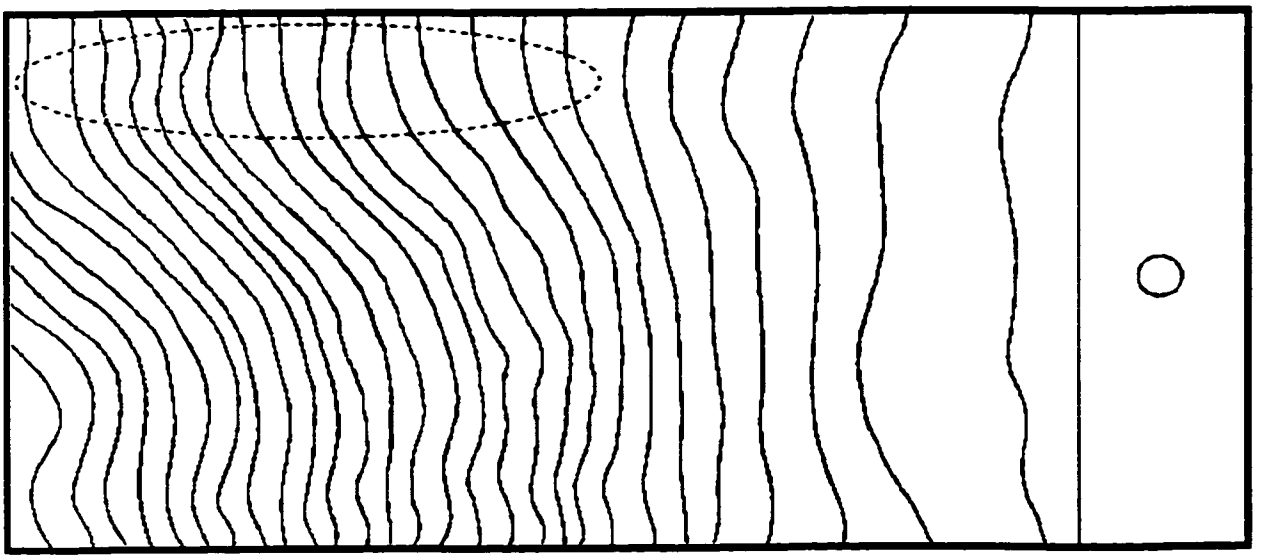

Figure B.12(b) - Fluid flow patterns for experiment (RMX3).
($\Delta t = 35s$, $T_{filling} = 985s$)

APPENDIX C
Fluid Flow Front Position and Velocity

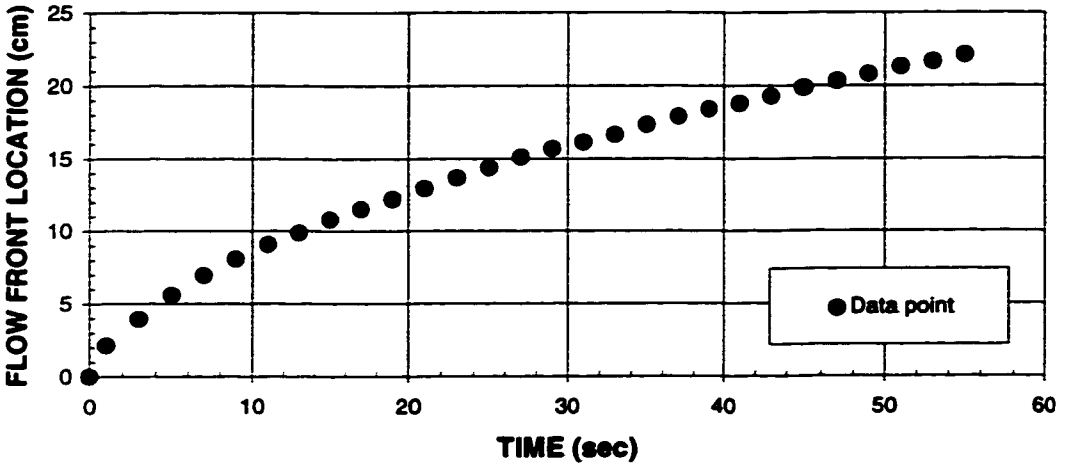

Figure C.1(a) - Flow front propagation for experiment MOI1.

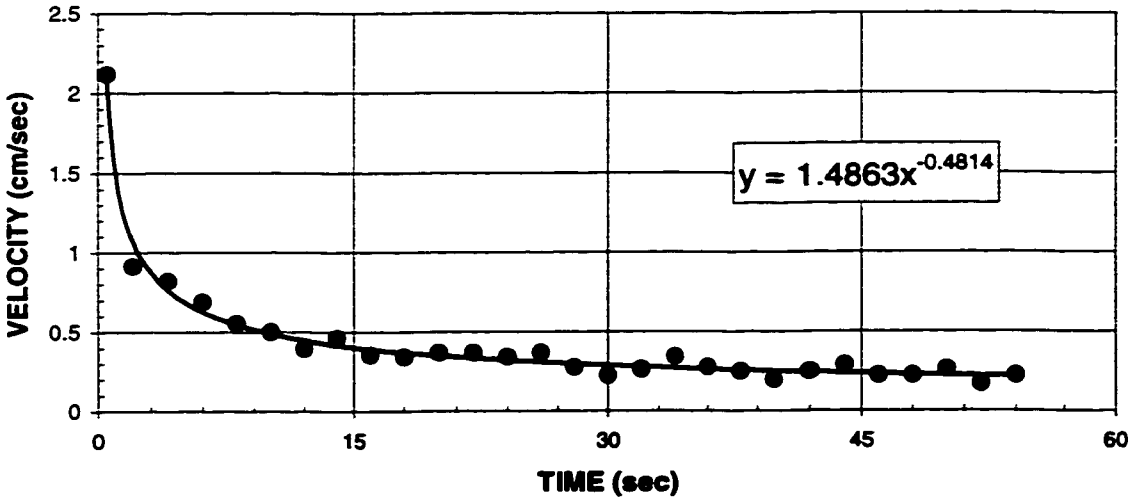

Figure C.1(b) - Flow front velocity as a function of time for experiment MOI1.

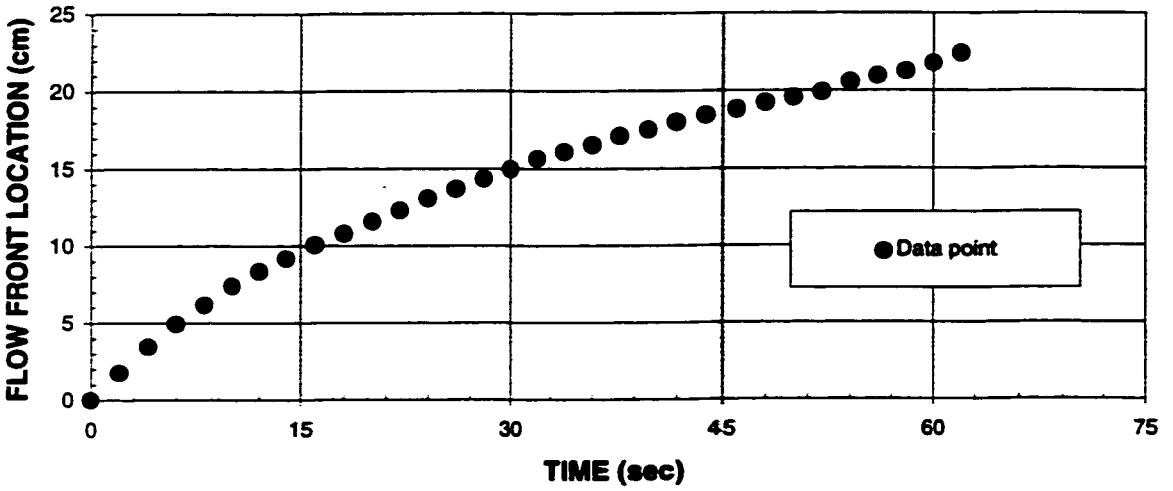

Figure C.2(a) - Flow front propagation for experiment MOIX1.

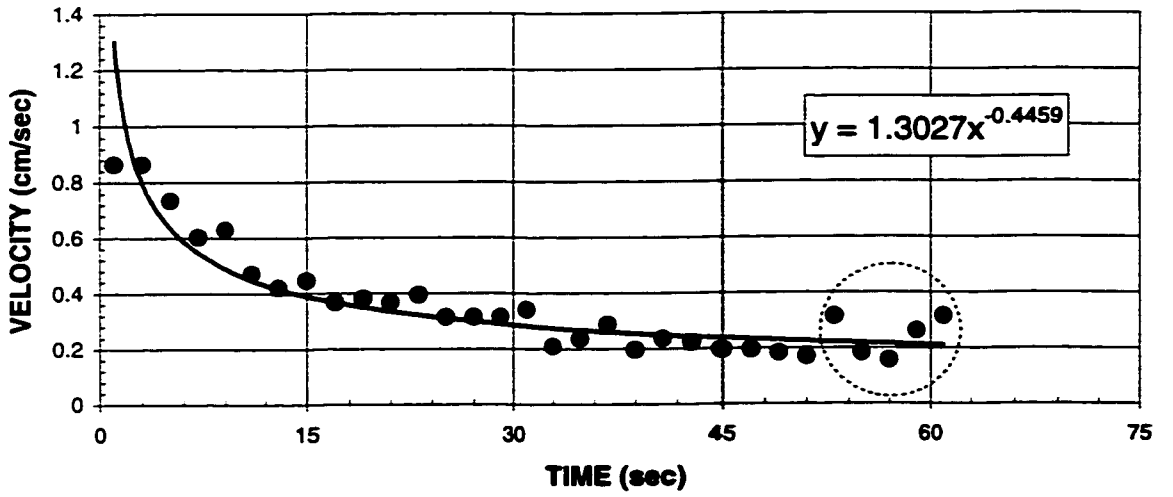

Figure C.2(b) - Flow front velocity as a function of time for experiment MOIX1.

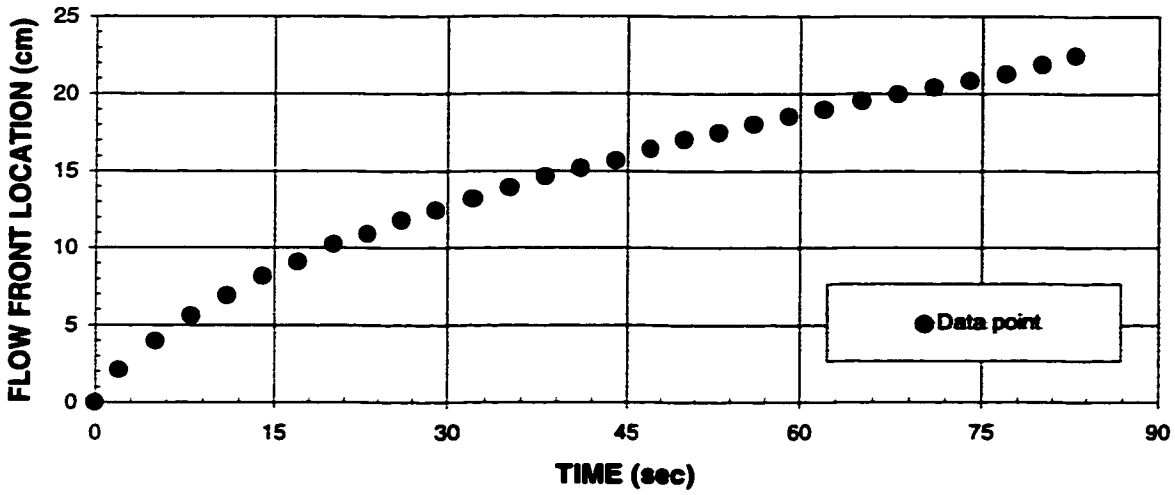

Figure C.3(a) - Flow front propagation for experiment MOI2.

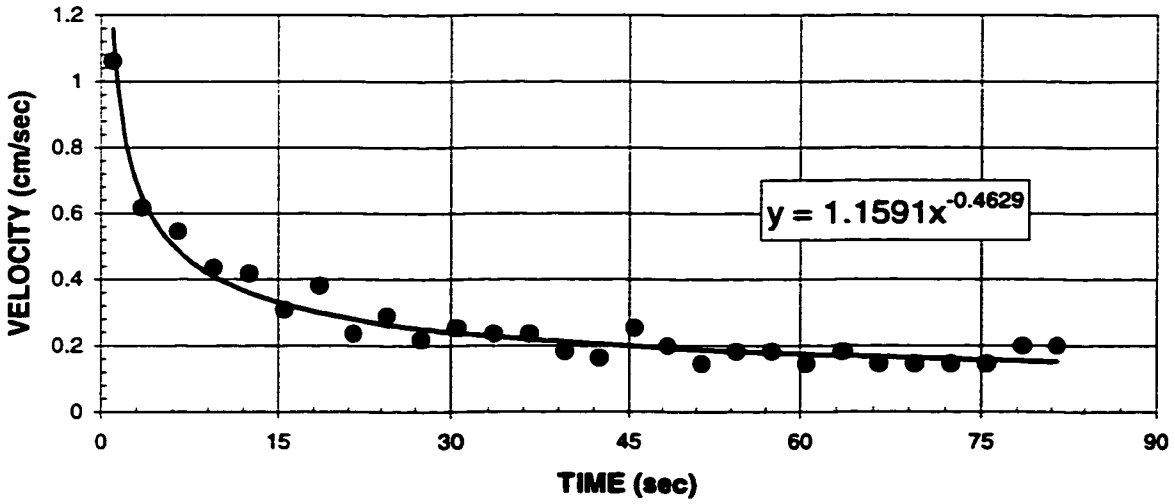

Figure C.3(b) - Flow front velocity as a function of time for experiment MOI2.

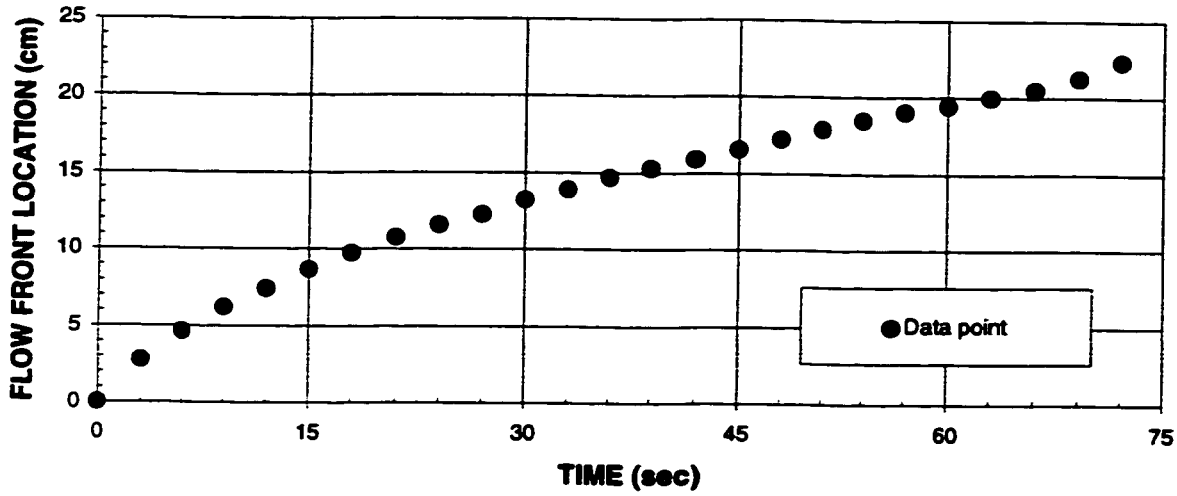

Figure C.4(a) - Flow front propagation for experiment MOIX2.

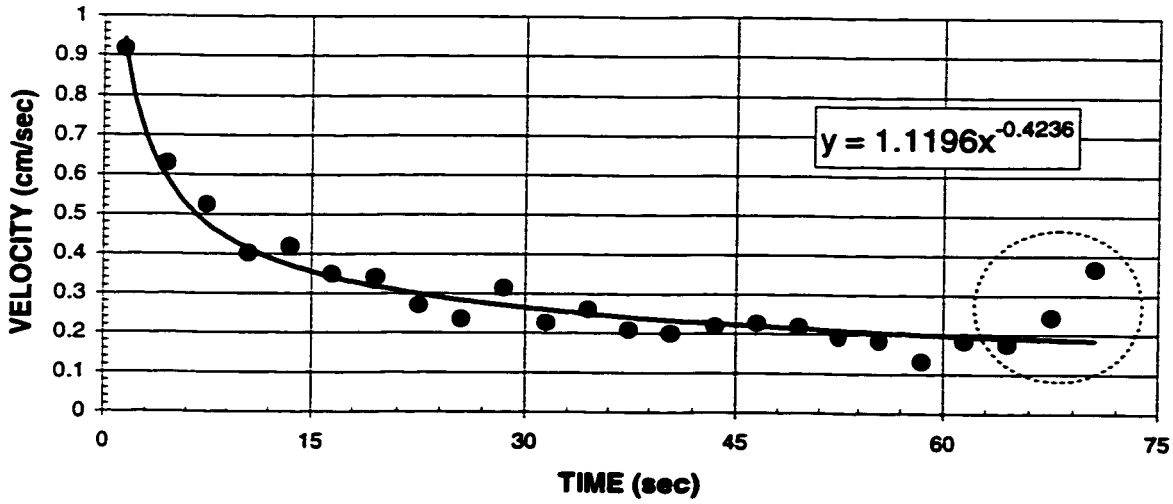

Figure C.4(b) - Flow front velocity as a function of time for experiment MOIX2.

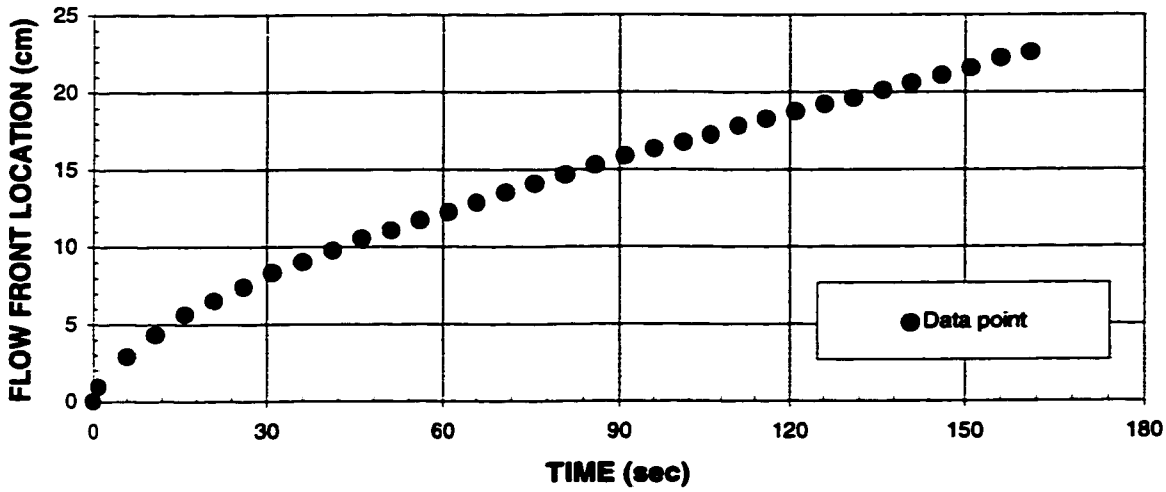

Figure C.5(a) - Flow front propagation for experiment MOI3.

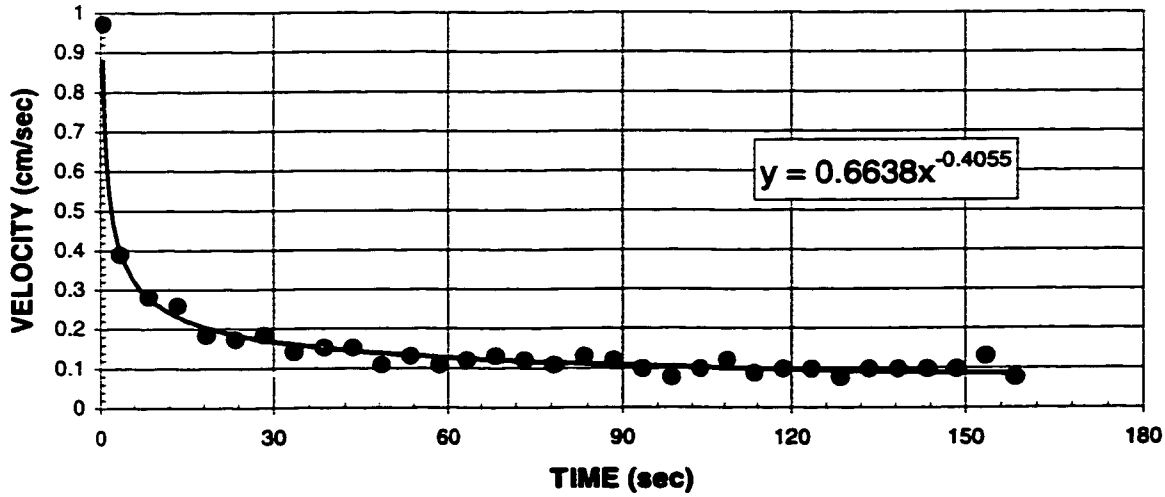

Figure C.5(b) - Flow front velocity as a function of time for experiment MOI3.

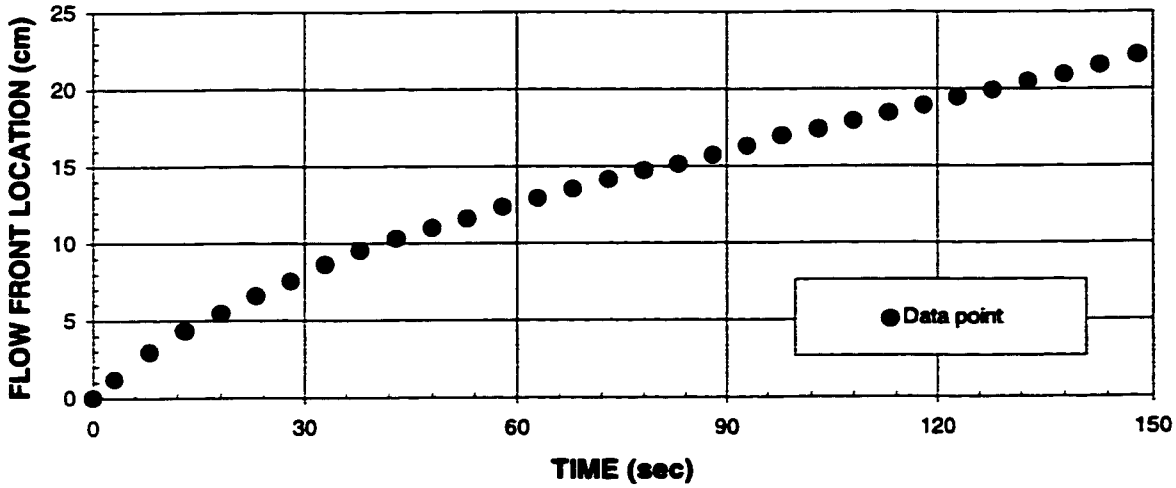

Figure C.6(a) - Flow front propagation for experiment MOIX3.

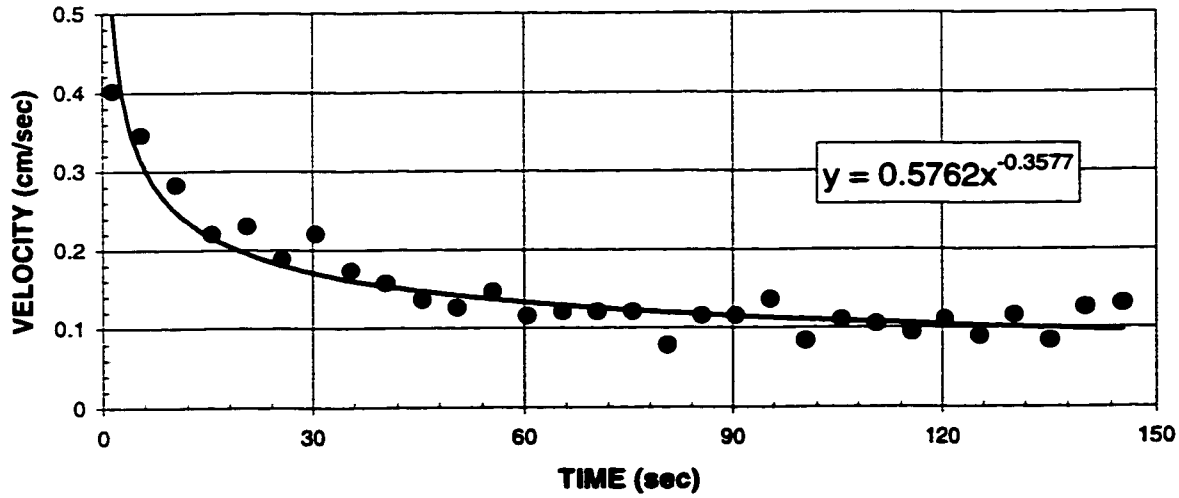

Figure C.6(b) - Flow front velocity as a function of time for experiment MOIX3.

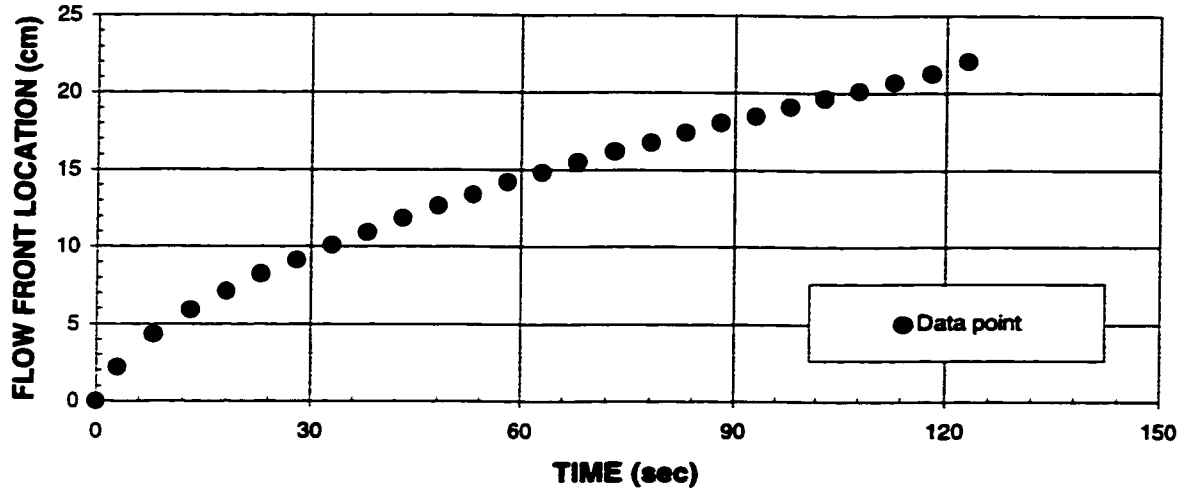

Figure C.7(a) - Flow front propagation for experiment MOII1.

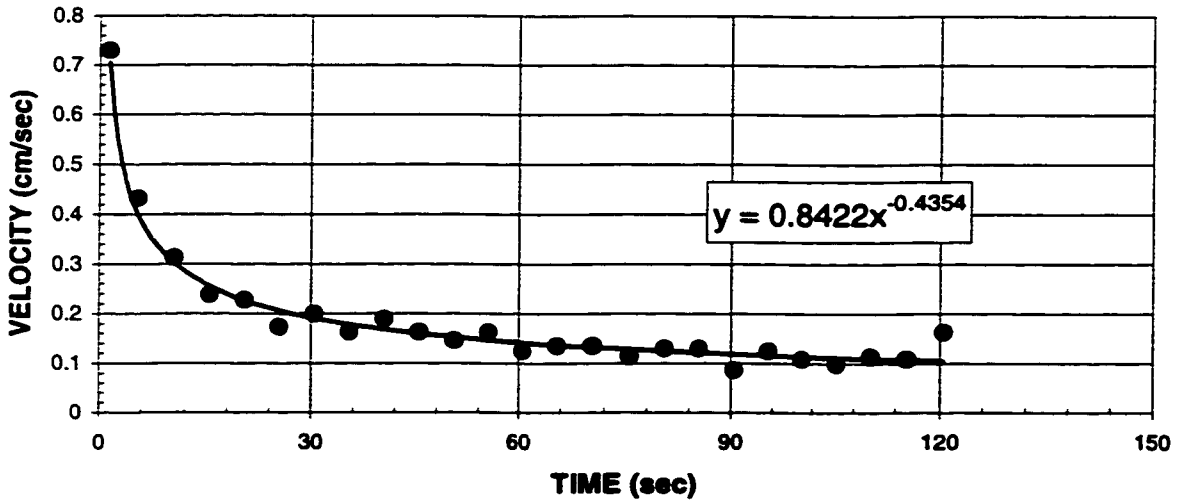

Figure C.7(b) - Flow front velocity as a function of time for experiment MOII1.

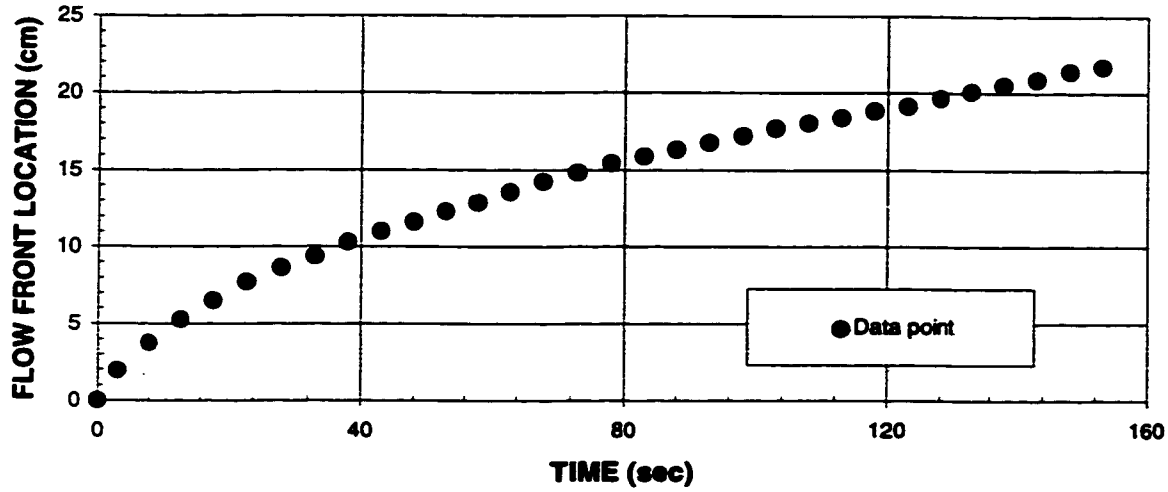

Figure C.8(a) - Flow front propagation for experiment MOIIX1.

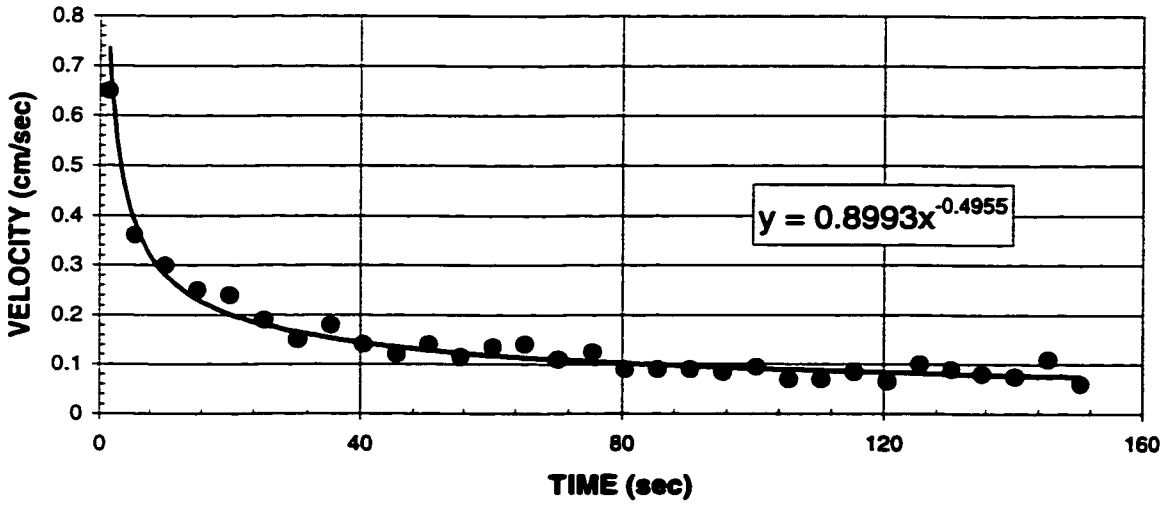

Figure C.8(b) - Flow front velocity as a function of time for experiment MOIIX1.

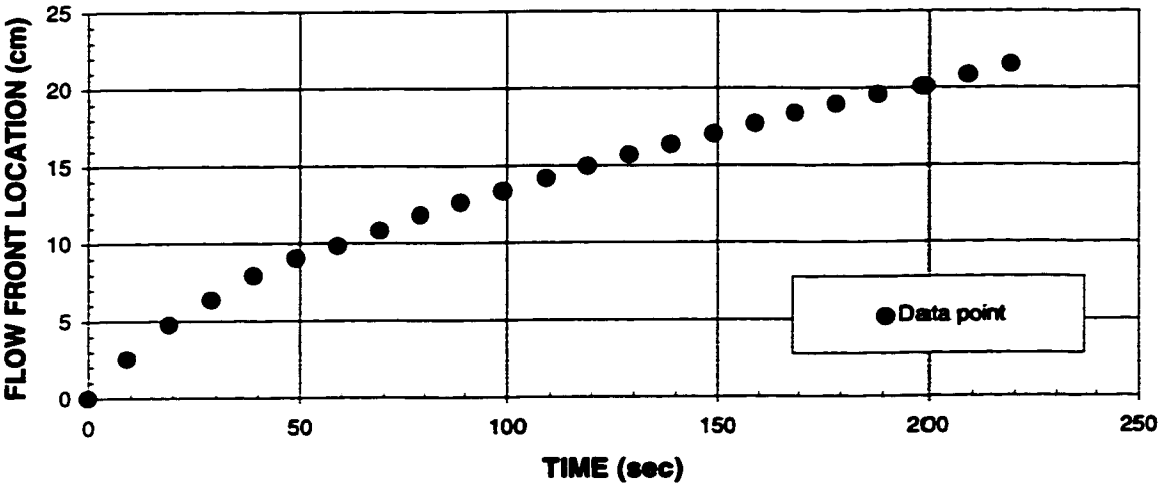

Figure C.9(a) - Flow front propagation for experiment MOII2.

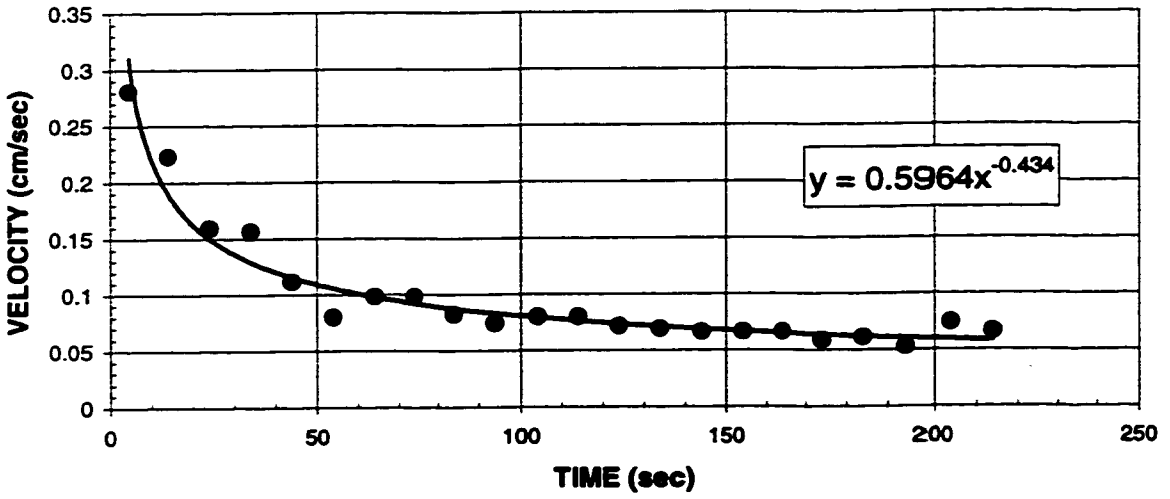

Figure C.9(b) - Flow front velocity as a function of time for experiment MOII2.

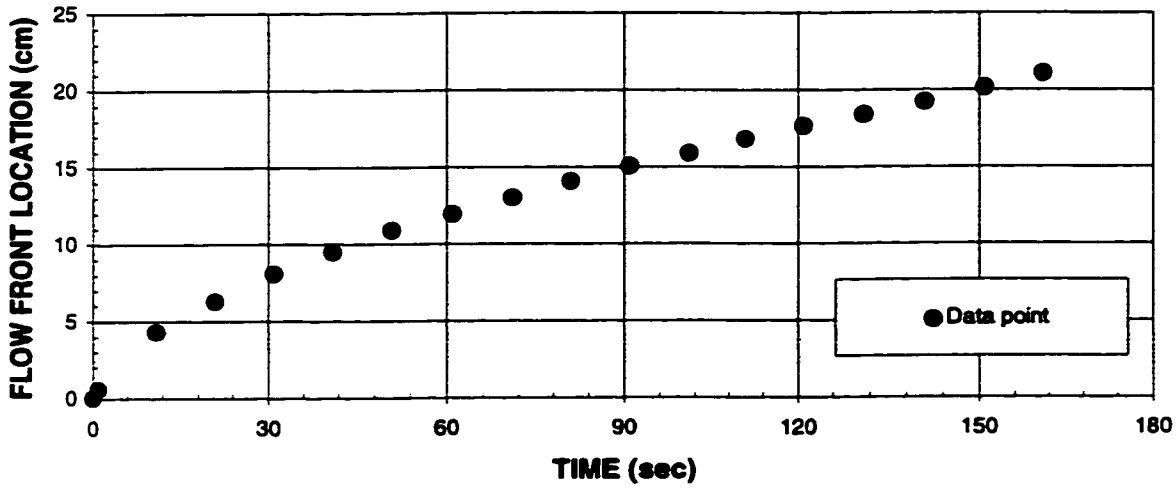

Figure C.10(a) - Flow front propagation for experiment MOIIX2.

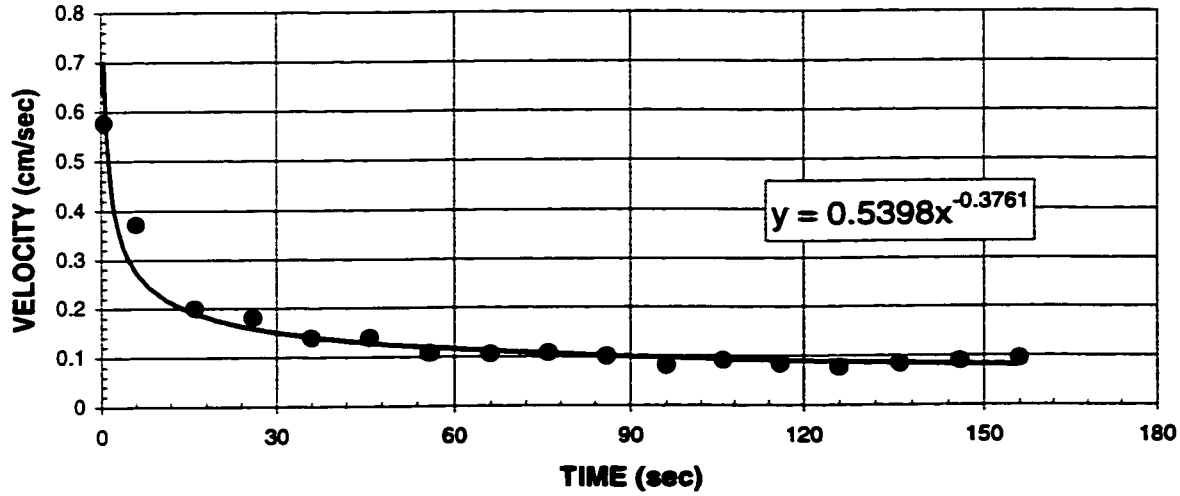

Figure C.10(b) - Flow front velocity as a function of time for experiment MOIIX2.

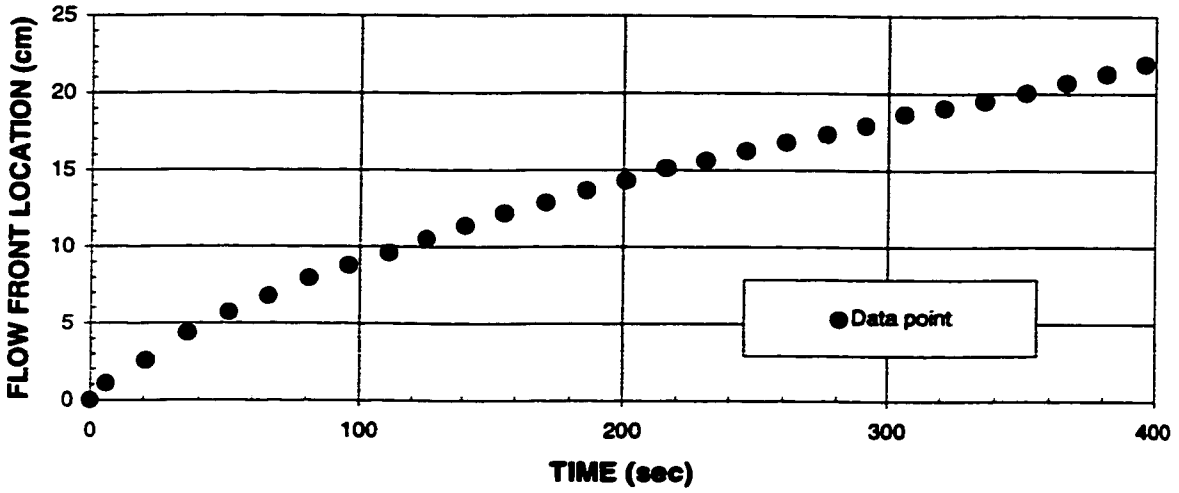

Figure C.11(a) - Flow front propagation for experiment MOII3.

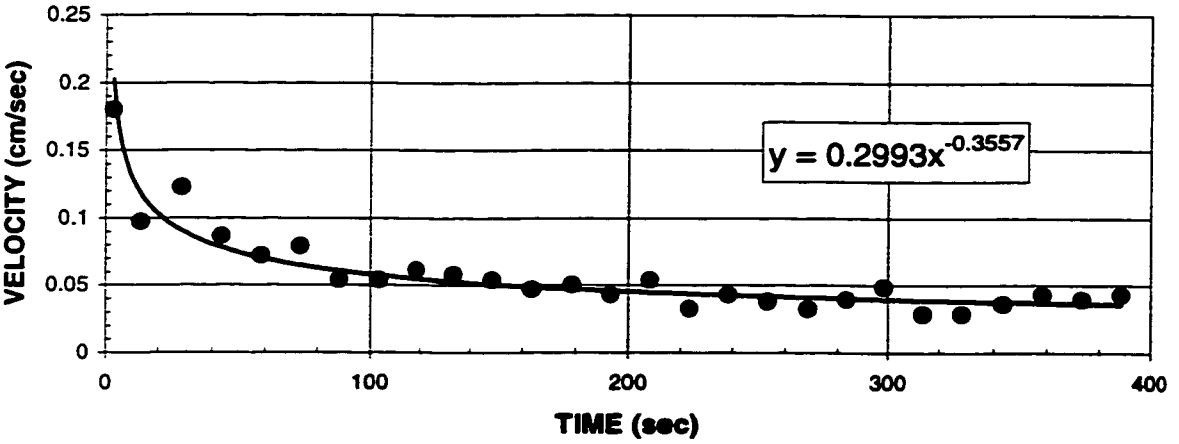

Figure C.11(b) - Flow front velocity as a function of time for experiment MOII3.

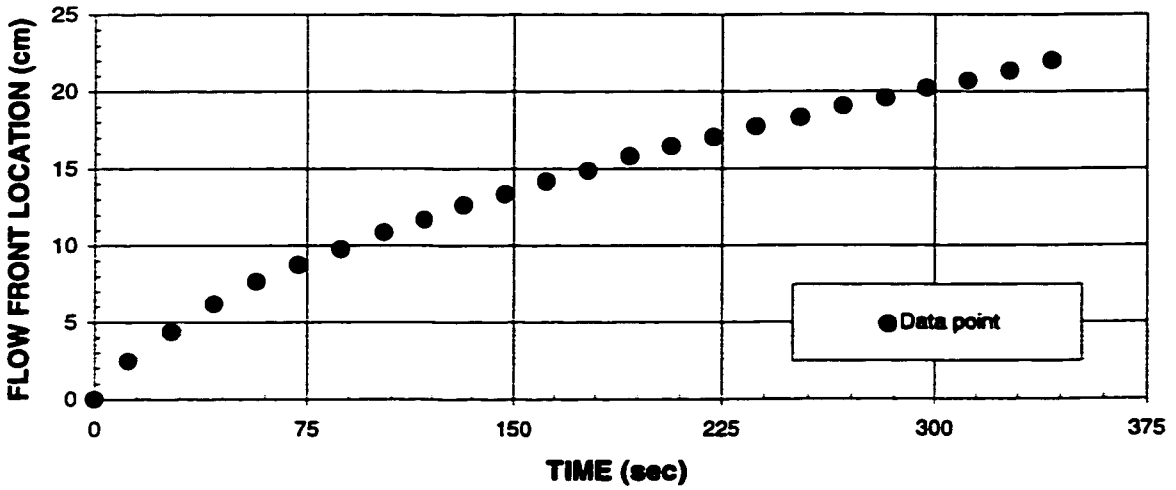

Figure C.12(a) - Flow front propagation for experiment MOIIX3.

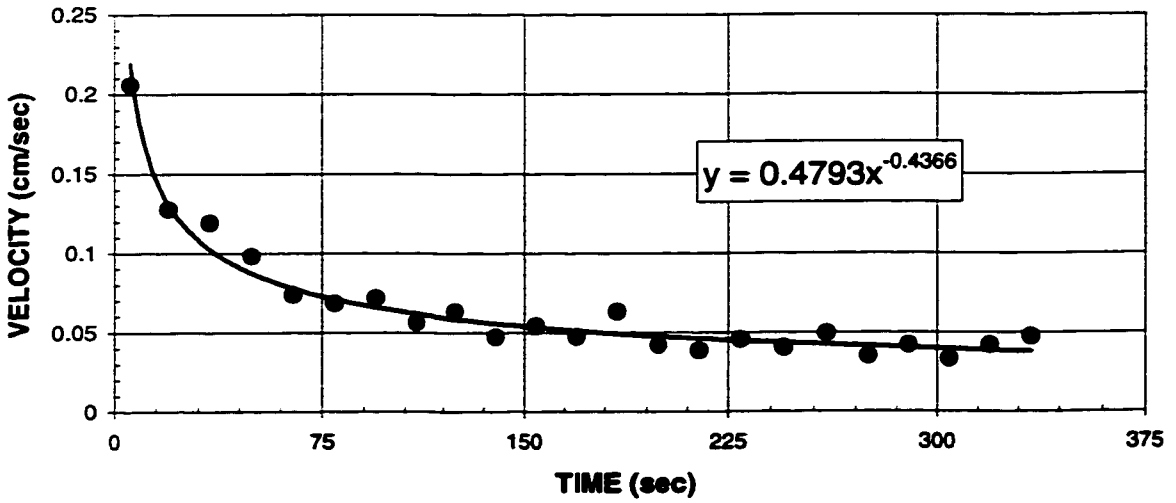

Figure C.12(b) - Flow front velocity as a function of time for experiment MOIIX3.

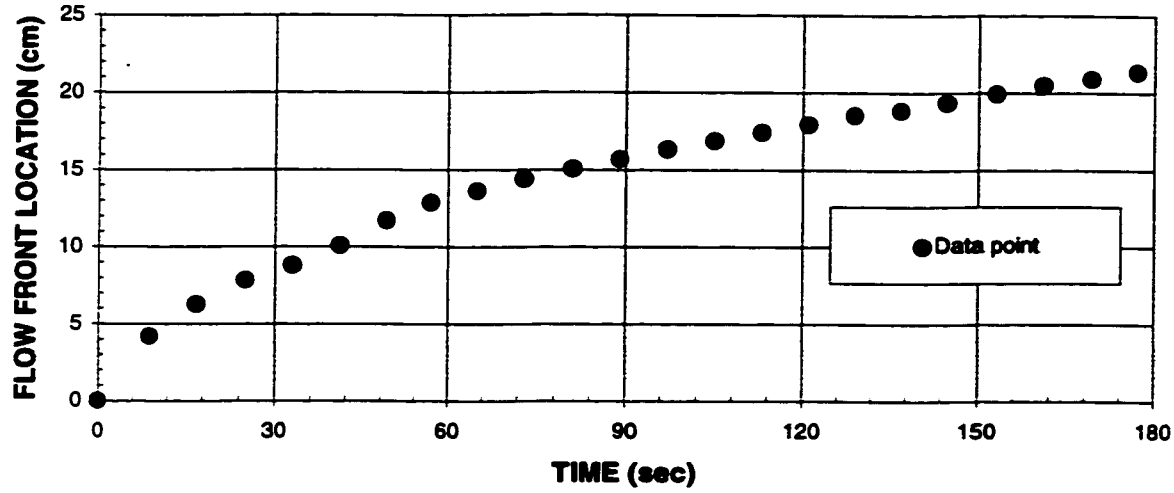

Figure C.13(a) - Flow front propagation for experiment RWR1.

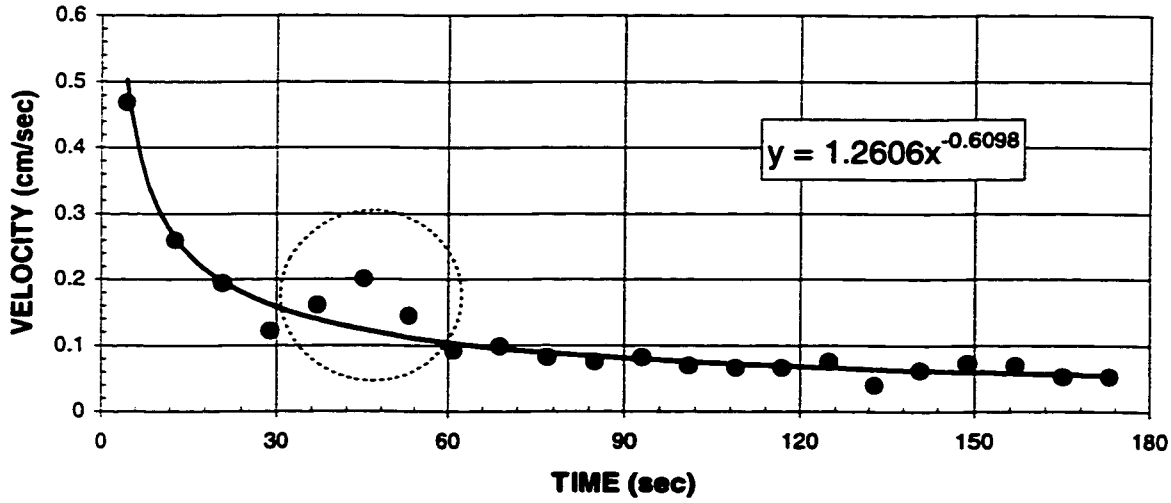

Figure C.13(b) - Flow front velocity as a function of time for experiment RWR1.

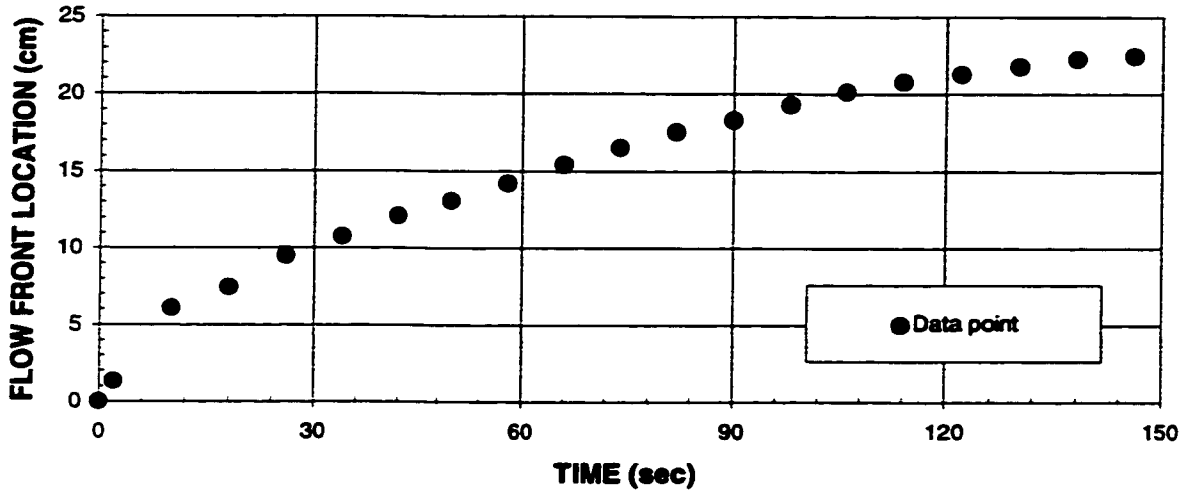

Figure C.14(a) - Flow front propagation for experiment RWRX1.

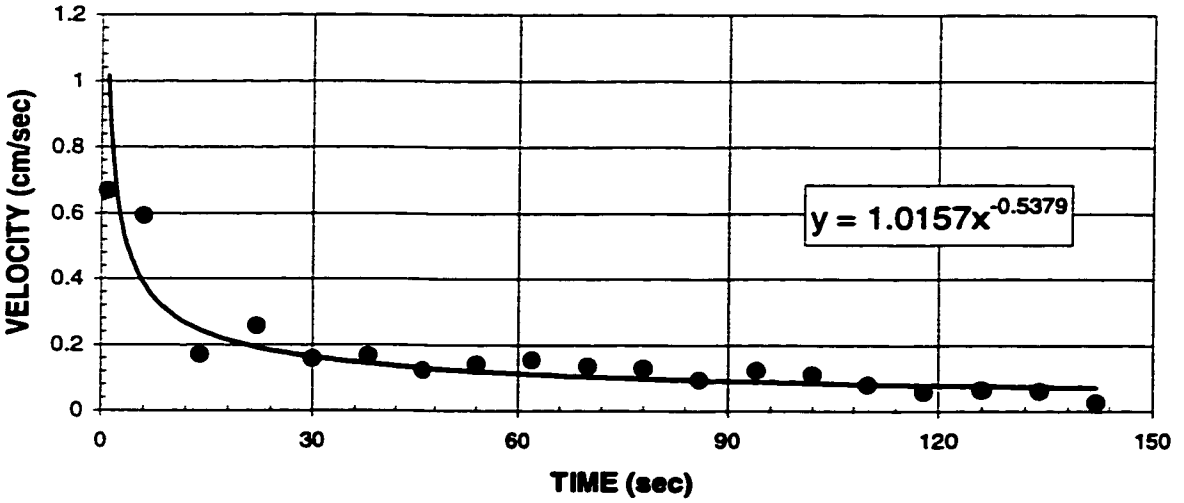

Figure C.14(b) - Flow front velocity as a function of time for experiment RWRX1.

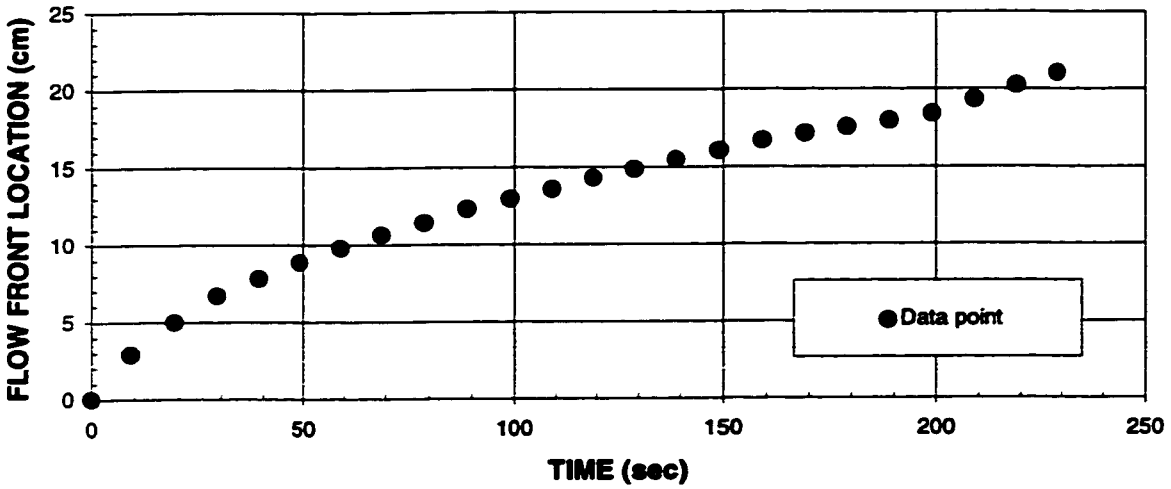

Figure C.15(a) - Flow front propagation for experiment RWR2.

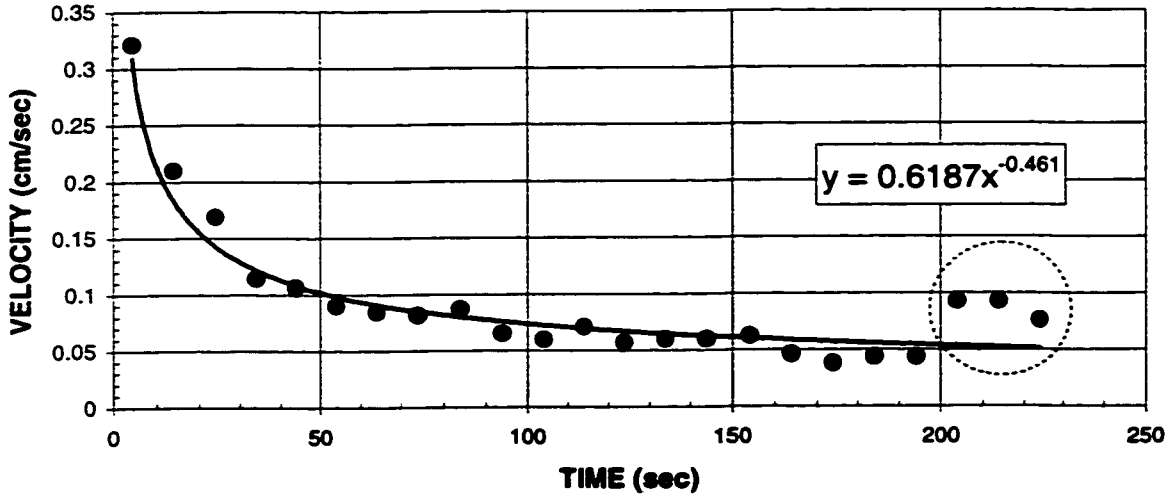

Figure C.15(b) - Flow front velocity as a function of time for experiment RWR2.

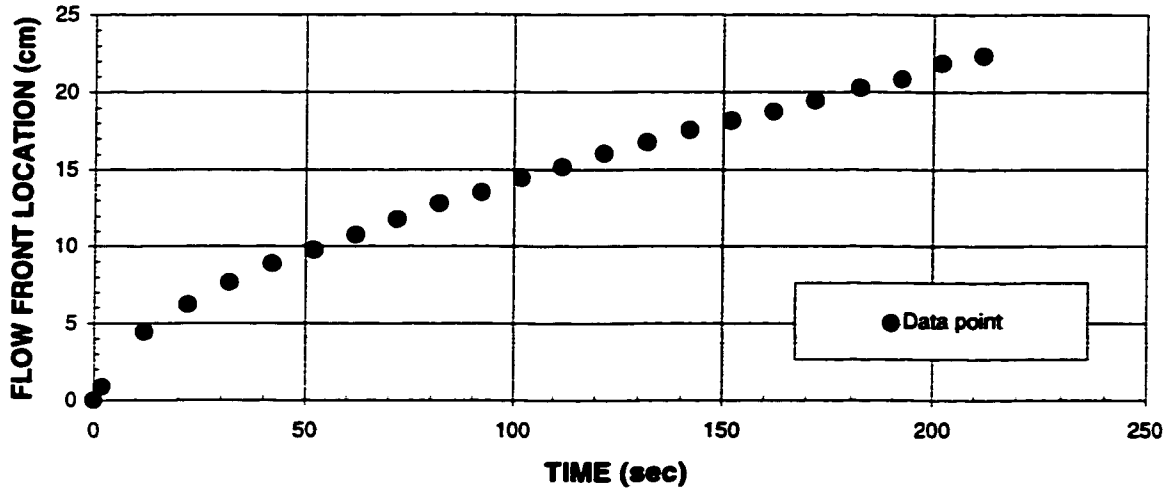

Figure C.16(a) - Flow front propagation for experiment RWRX2.

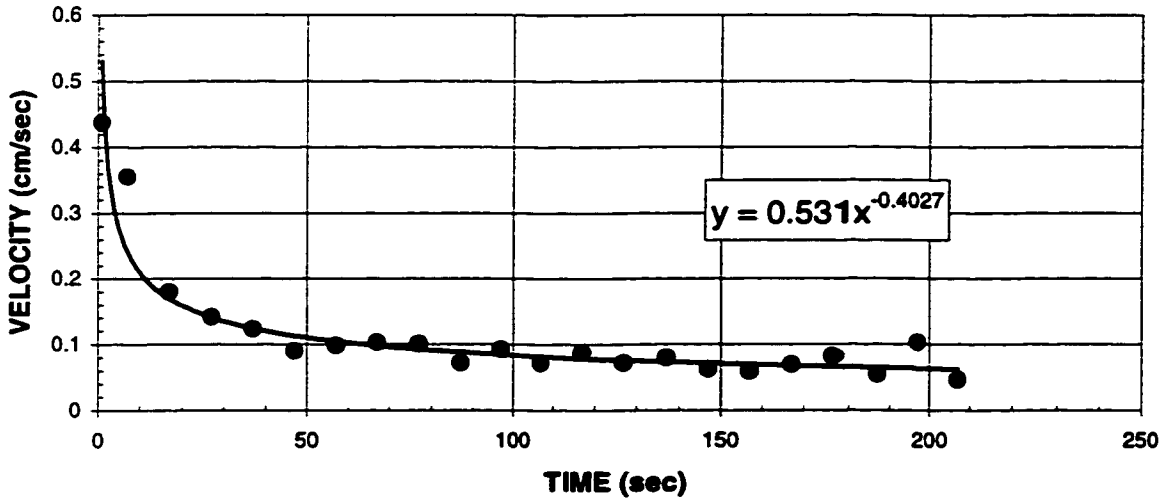

Figure C.16(b) - Flow front velocity as a function of time for experiment RWRX2.

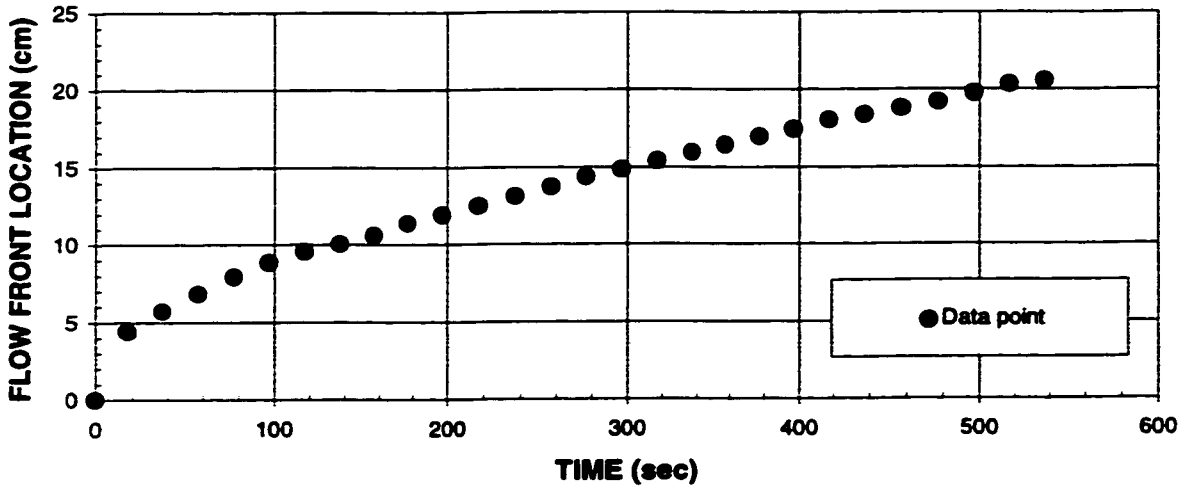

Figure C.17(a) - Flow front propagation for experiment RWR3.

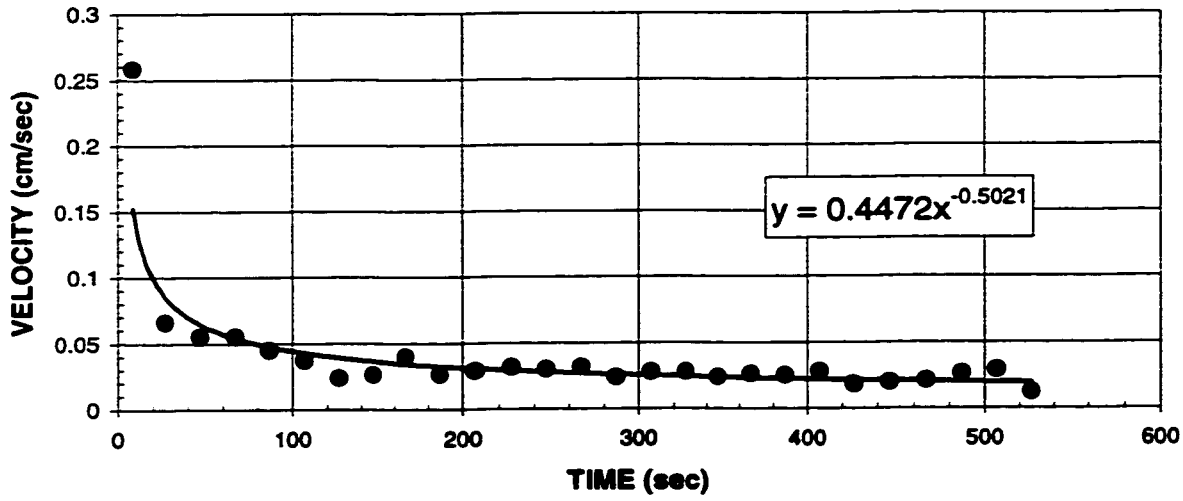

Figure C.17(b) - Flow front velocity as a function of time for experiment RWR3.

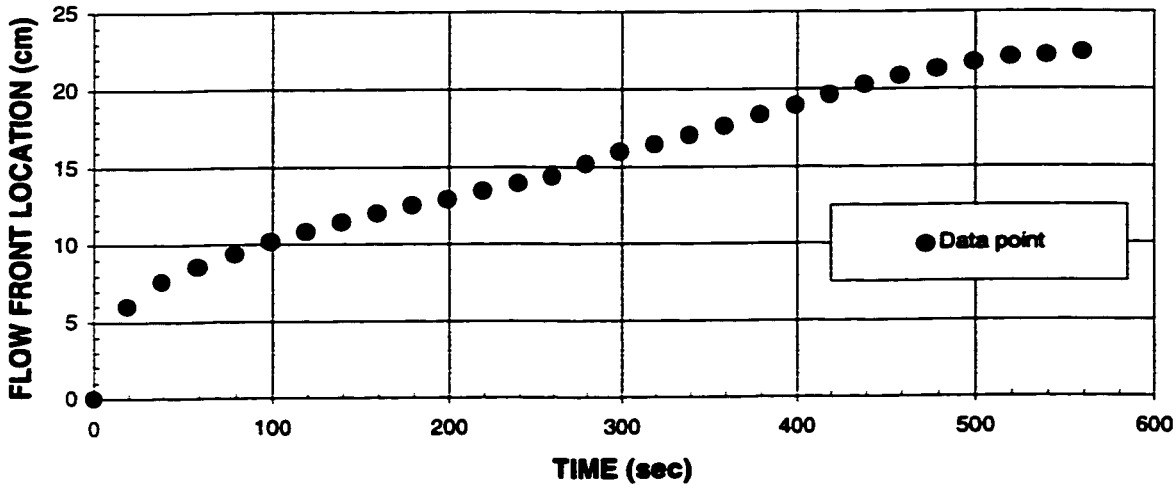

Figure C.18(a) - Flow front propagation for experiment RWRX3.

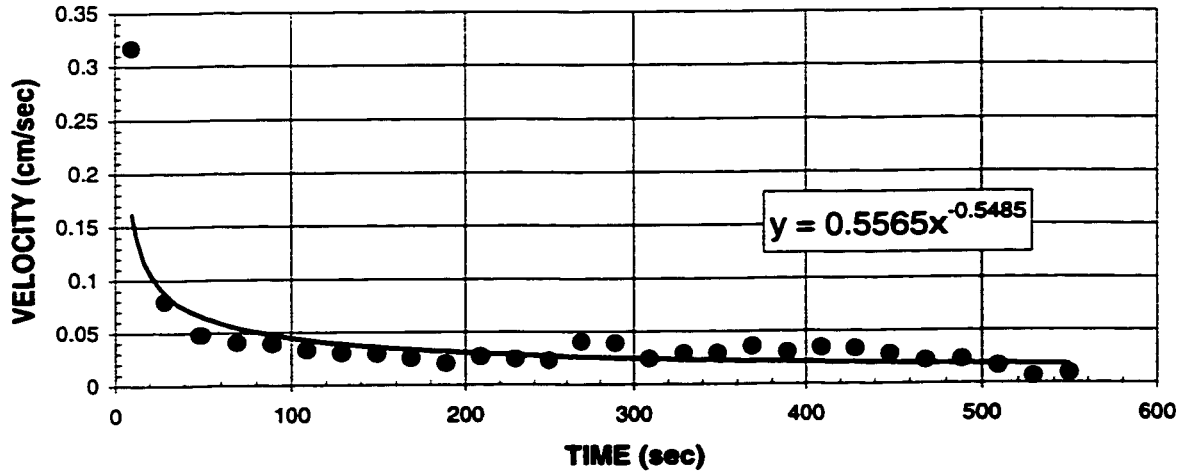

Figure C.18(b) - Flow front velocity as a function of time for experiment RWRX3.

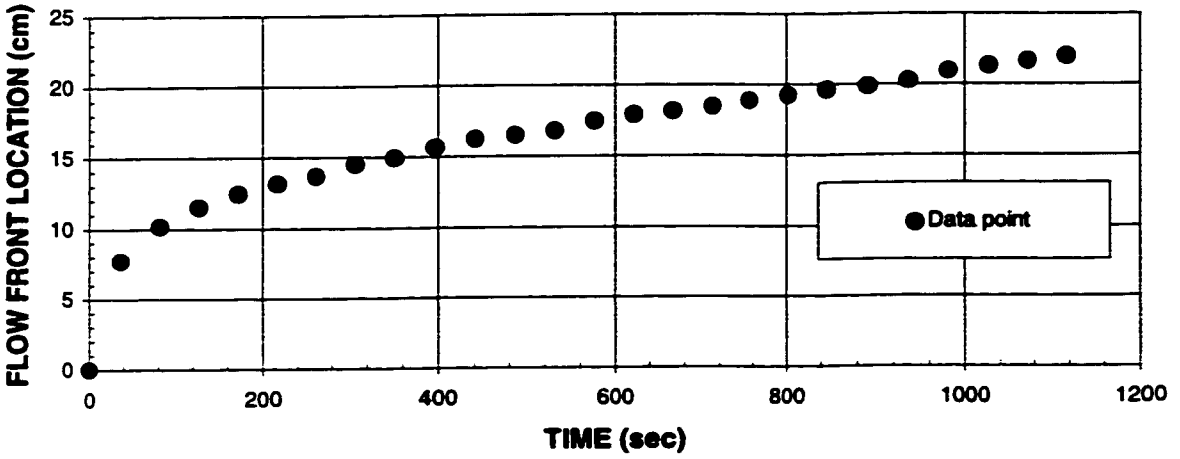

Figure C.19(a) - Flow front propagation for experiment RM1.

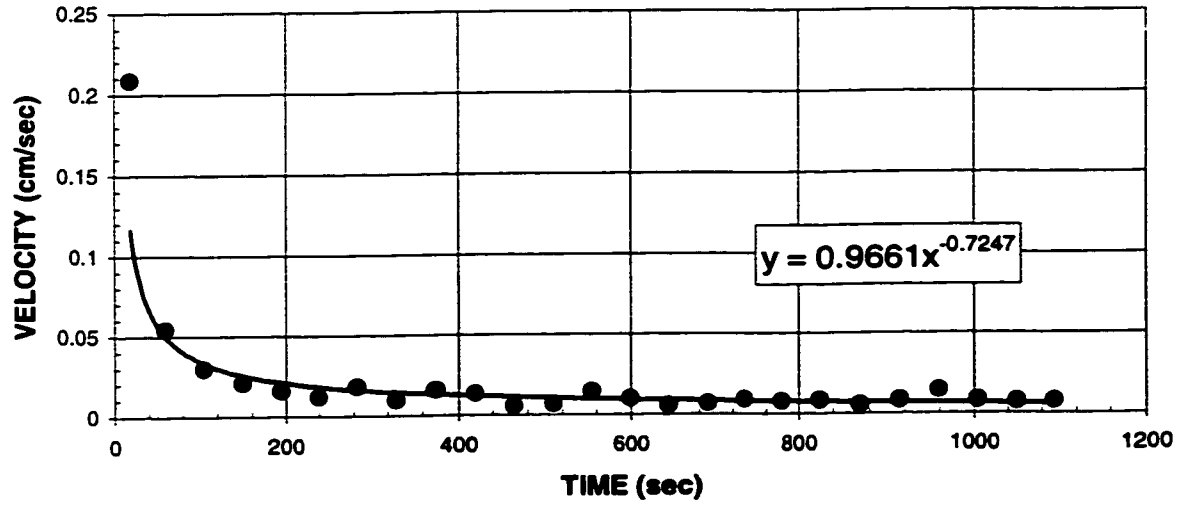

Figure C.19(b) - Flow front velocity as a function of time for experiment RM1.

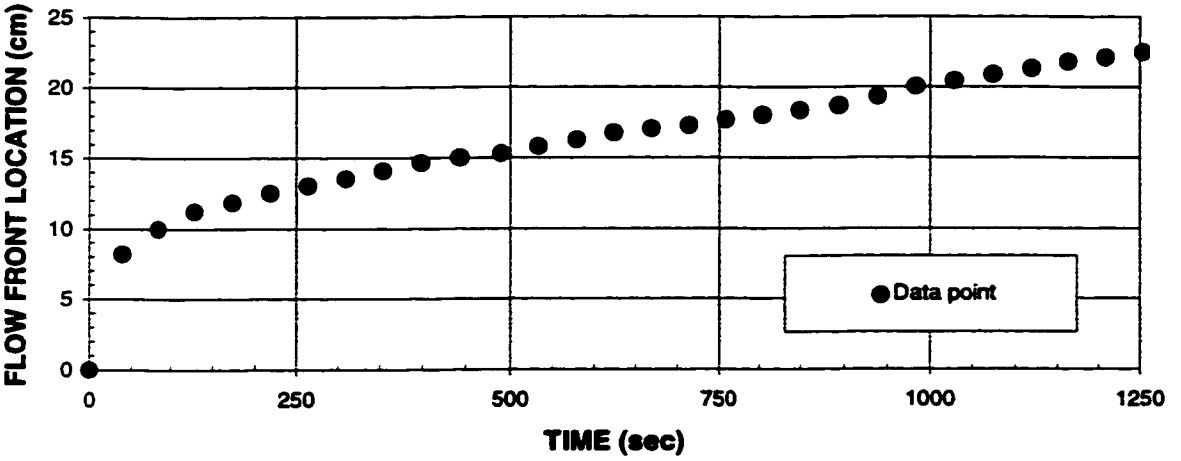

Figure C.20(a) - Flow front propagation for experiment RMX1.

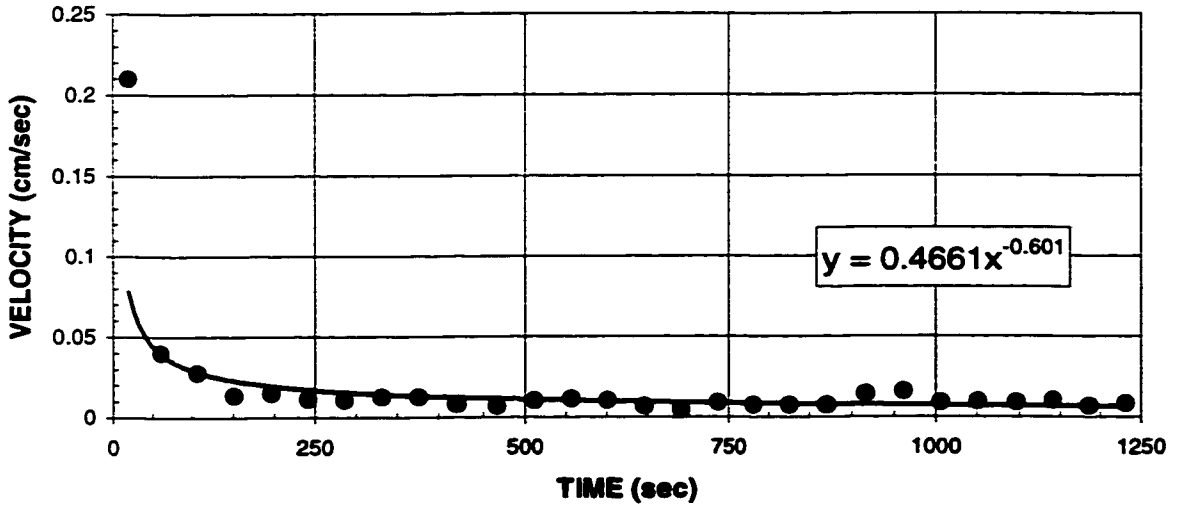

Figure C.20(b) - Flow front velocity as a function of time for experiment RMX1.

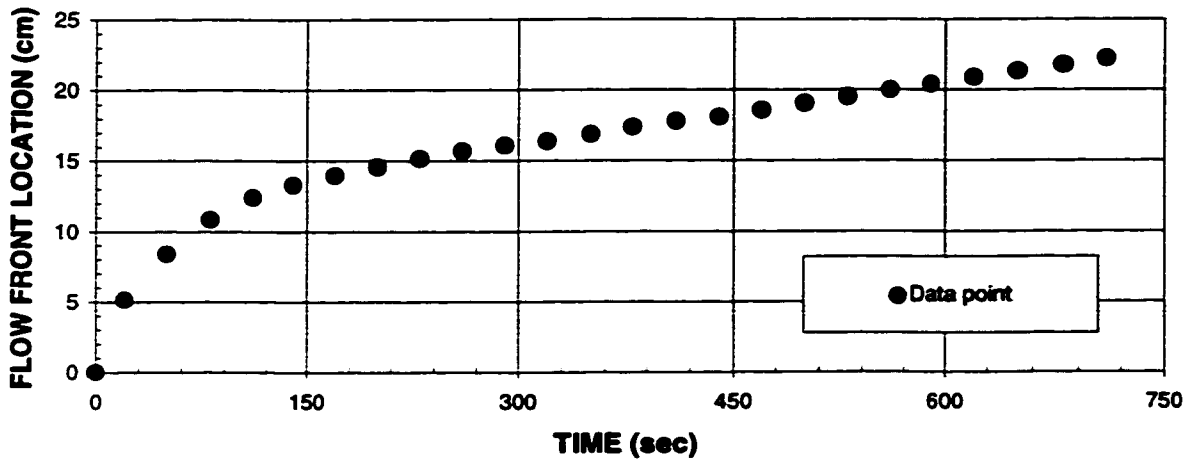

Figure C.21(a) - Flow front propagation for experiment RM2.

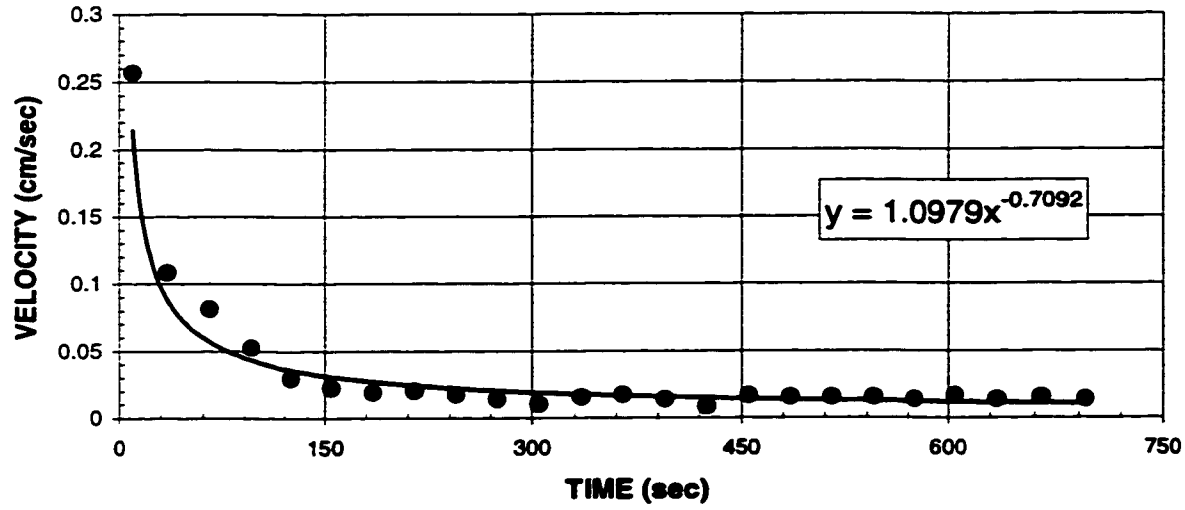

Figure C.21(b) - Flow front velocity as a function of time for experiment RM2.

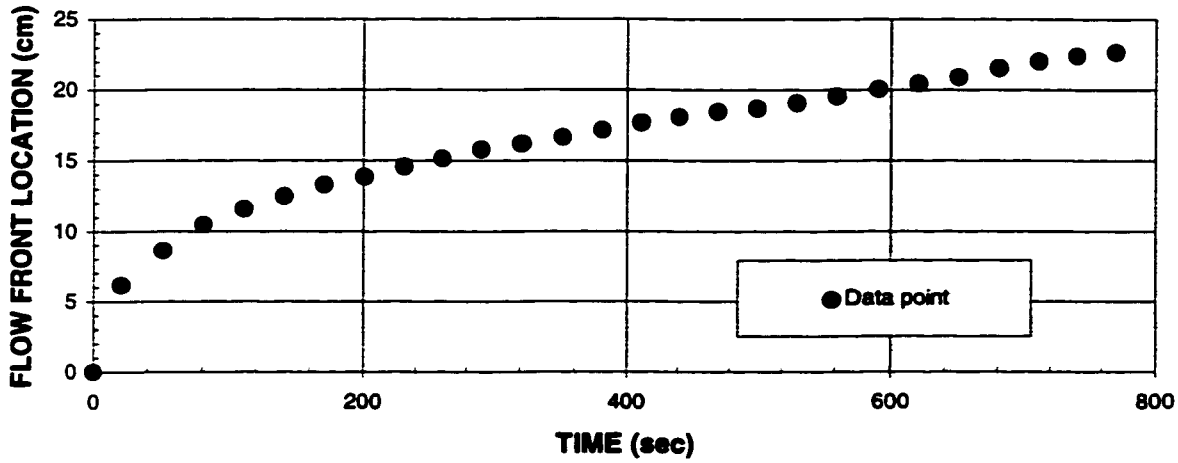

Figure C.22(a) - Flow front propagation for experiment RMX2.

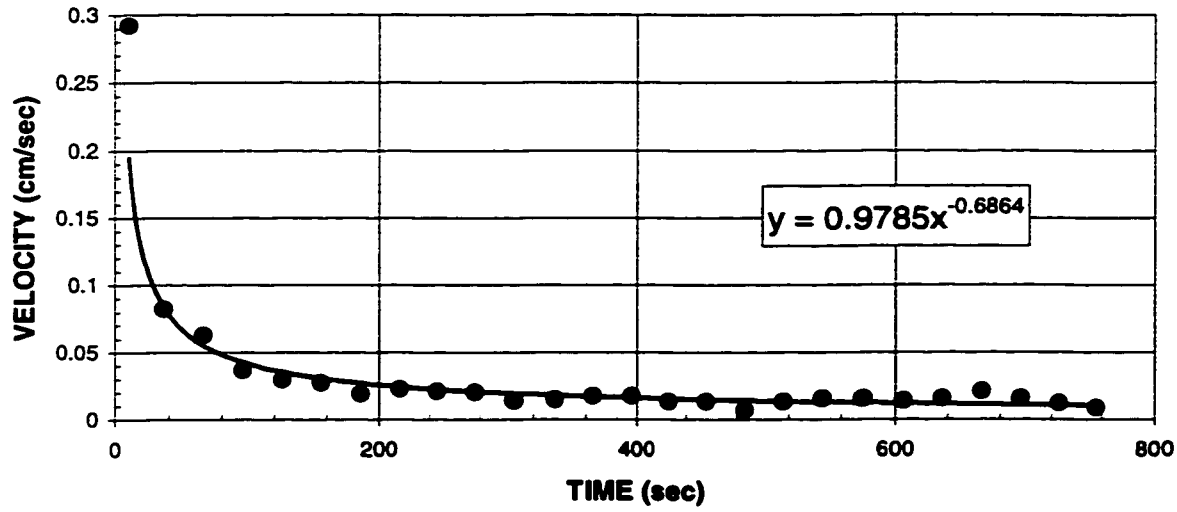

Figure C.22(b) - Flow front velocity as a function of time for experiment RMX2.

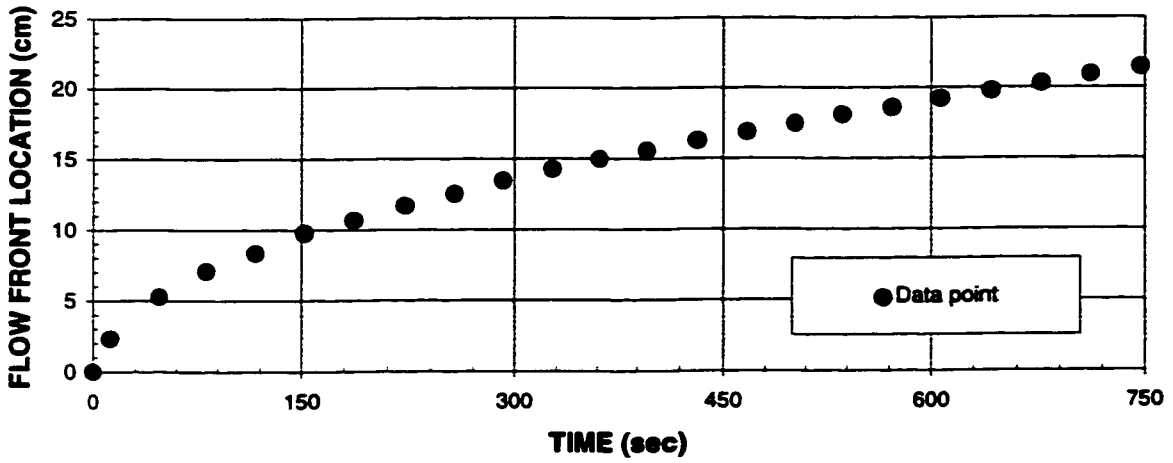

Figure C.23(a) - Flow front propagation for experiment RM3.

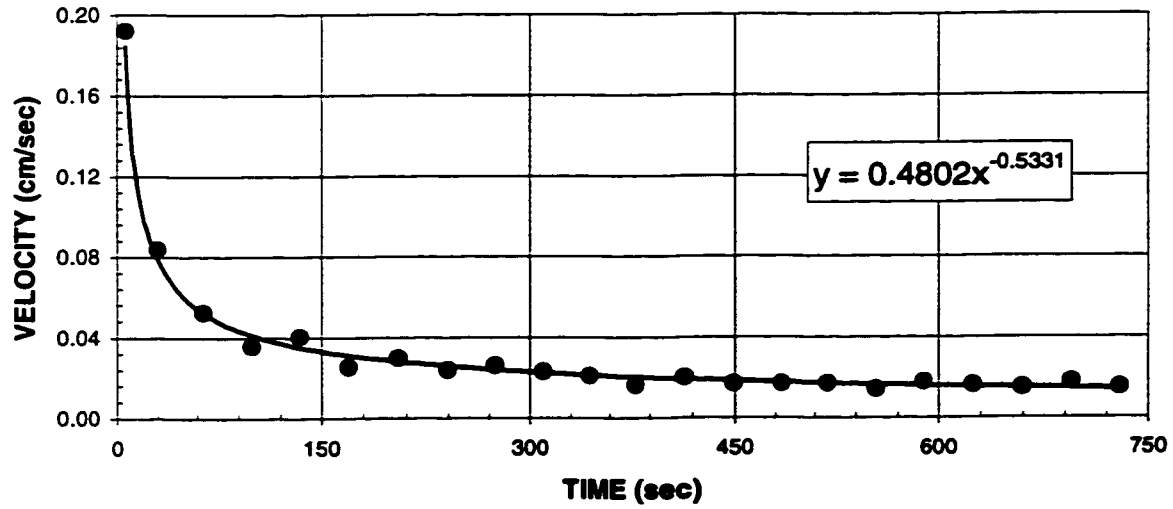

Figure C.23(b) - Flow front velocity as a function of time for experiment RM3.

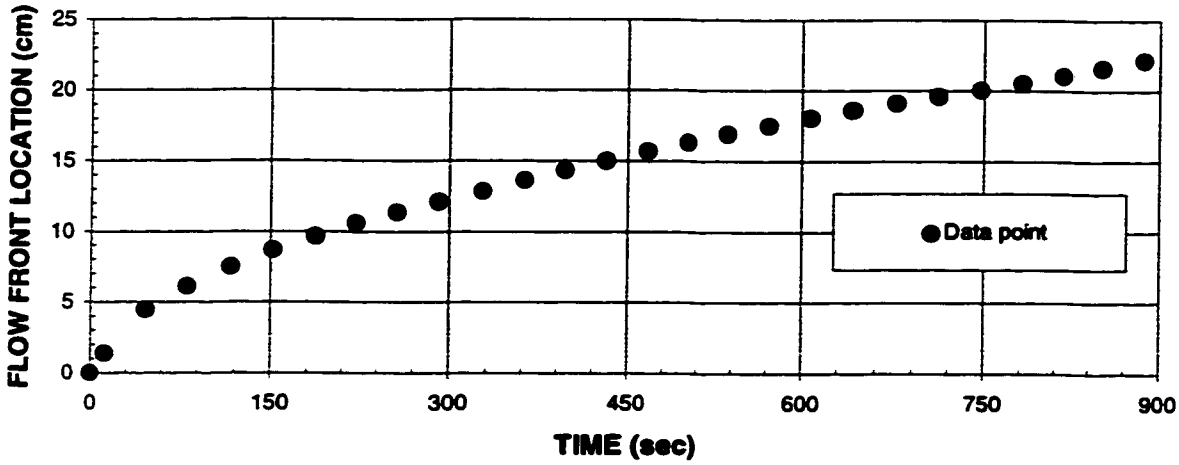

Figure C.24(a) - Flow front propagation for experiment RMX3.

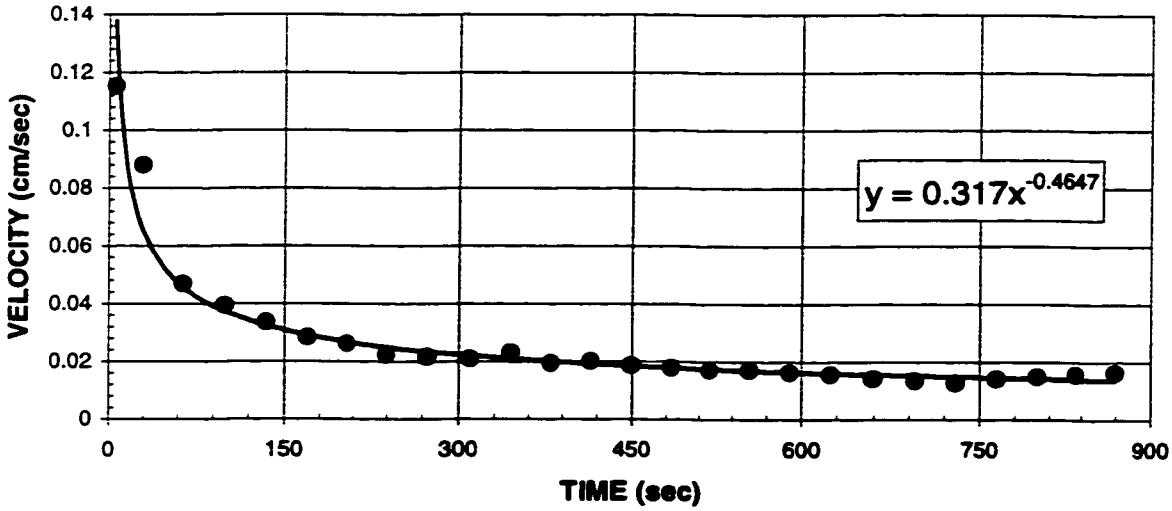

Figure C.24(b) - Flow front velocity as a function of time for experiment RMX3.